Ministère de l'Enseignement Supérieur et de la Recherche Scientifique

Université Aboubekr BELKAID-Tlemcen

Faculté de Technologie

Thèse

Pour l'obtention du Doctorat de science en Génie Mécanique

Spécialité : Energétique : Dynamiques des Transferts

Sujet de la thèse :

Study of thermodiffusion in multi-component mixtures in porous media

Présentée par :

Zakaria AOUF

Soutenue devant le jury composé de :

KORTI A. Nabil	Pr	Univ. Aboubekr Belkaid Tlemcen	Président
SELADJI Chakib	Pr	Univ. Aboubekr Belkaid Tlemcen	Directeur
BENZENINE Hamidou	MCA	Univ. Ain Temouchent	Examinateur
BENOSMAN Ahmed Soufiane	Pr	ESSA de Tlemcen	Examinateur
SAIM Rachid	Pr	Univ. Aboubekr Belkaid Tlemcen	Invité

2021/2022

Dedication

To my dear Father

To my great Mother

for their countless generosity…

To all my family…

Acknowledgments

First and foremost, I thank Allah for everything, for granting me the strength and patience to reach this station, in the long path of study.

I would love to thank my parents for their support, patience and prayer for success. I hope to appease them and make them satisfied.

This thesis work was carried out with the supervision of Pr. Chakib SELADJI. I would like to express here all my gratitude for the confidence and for the freedom of initiative that he has granted me. His professional and human qualities push me to go further.

My acknowledgments addressed to the jury members Pr. KORTI A. Nabil, Dr. BENZENINE Hamidou, and Pr. BENOSMAN Ahmed Soufiane for the honor they provided in agreeing to review this work.

Fingerprint traces in this work, by the orientations and the suggestions of Dr. Redha Rabhi and in particular of Pr. ALLOUI Zineddine cannot be unnoticed; May their good find here the expression of my gratitude

For all the people who contributed from near or far, in the realization of this work, I will say from the depth of my heart: Thank you!

Finally, special thanks are reserved for all my family, especially my parents and my wife for their patience, their support and their encouragement.

Aouf Zakaria

ملخص

غالبًا ما تتم مصادفة انتقال الحرارة والمادة في وسط مسامي غير متجانس في عدة مجالات طبيعية وصناعية، بما في ذلك البتروكيماويات والبيولوجيا والجيولوجيا والمعادن والهندسة البترولية. قياس ومراقبة فصل مكونات مزيج في أوساط مسامية غير متجانسة أو بها صدع يمكن أن يكشف عن العديد من الظواهر المتضاربة. في دراستنا، تم تحليل تأثير الكسر المنفرد على الحمل الحراري المتداخل مع تأثير Soret في تجويف مسامي عمودي ثنائي الأبعاد، مشبع بمزيج ثنائي تم تسخينه وتغذيته من الجهة اليمنى.

المعاملات الرئيسية الموضوعة للاشكالية المطروحة هي: R_T معامل Rayleigh الحراري، Le معامل Lewis ، N نسبة الطفو، Sp معامل Soret، ومعامل شكل التجويف A . اعتمادًا على خصائص الكسر (النفاذية ، الموضع ، والسمك)، يتم تحليل التدفق الحراري-المادي.

أظهرت النتائج الرئيسية لهذه الدراسة أن الصدع يمكن أن يؤثر بشكل كبير على التدفق الجاذبي-الحراري وقد يلعب دورًا إيجابيًا في الفصل الناجم عن تأثير Soret ، خاصةً عندما تكون السماحية k أقل من السماحية المثالية k_{opt}. ومع ذلك ، عندما تكون السماحية k أكبر أو تساوي k_{opt}، يؤثر الصدع سلبًا على عملية الفصل. علاوة على ذلك، فإن الصدع المائل إلى الجدار البارد يسبب انفصالًا كبيرًا مقارنةً بالحالة عندما يتم إمالة الصدع إلى الحائط الساخن بنفس الزاوية. نتيجة لذلك، يمكن تحسين عملية الفصل بشكل كبير.

الكلمات المفتاحية: تأثير Soret، انتشار حراري، وسائط مسامية، صدع، غير متجانس، فصل.

Abstract

Heat and mass transfer in heterogeneous porous medium is often encountered in natural as well as industrial fields, involving petrochemical, biology, geology, metallurgy, and petroleum engineering. Measuring and controlling species separation in heterogeneous or fractured porous media could reveal many conflicting phenomena. In our investigation, the effect of a single discrete fracture on the thermo-solutal convection coupled with Soret effect in a two-dimensional vertical porous medium cavity, saturated by a binary mixture, heated and salted from the right-end have been analyzed.

Key parameters considered for the described problem are the thermal Rayleigh number, $\mathbf{R_T}$, the Lewis number **Le**, the buoyancy ratio **N**, the Soret parameter **Sp** and the aspect ratio of the cavity **A**. Depending on the fracture characteristics (permeability, position, and thickness), the thermo-solutal convection flow is analyzed.

The main results of this study show that the fracture can greatly affect the behavior of the thermo-gravitational flow and might play a positive role to the separation caused by the Soret effect, especially when the permeability **k** is below the optimal permeability $\mathbf{k_{opt}}$. However, when the permeability **k** is greater or equal to the optimal $\mathbf{k_{opt}}$, the fracture affects negatively the separation process. Furthermore, the fracture tilted to the cold wall causes a large separation compared to the case when the fracture is tilted to the hot wall with the same angle. As a result, the separation process could be greatly improved.

Keywords : Soret effect, thermodiffusion, porous media, fracture, heteroginious, separation.

Résumé

Les transferts de chaleur et de masse en milieu poreux hétérogène sont souvent rencontrés dans les domaines naturels et industriels, impliquant la pétrochimie, la biologie, la géologie, la métallurgie et le génie pétrolier. Mesurer et contrôler la séparation des espèces dans des milieux poreux hétérogènes ou fracturés pourrait révéler de nombreux phénomènes contradictoires. Dans notre étude, nous avons analysé l'effet d'une fracture discrète sur la convection thermosolutal, associé à l'effet Soret, dans une cavité poreuse verticale bidimensionnel, saturée par un mélange binaire, chauffée et alimentée du côté droit.

Les paramètres clés pris en compte pour le problème décrit sont le nombre de Rayleigh thermique, $\mathbf{R_T}$, le nombre de Lewis **Le**, le coefficient de flottabilité **N**, le paramètre de Soret **Sp** et le facteur de forme de la cavité **A**. En fonction des caractéristiques de fracture (perméabilité, position et épaisseur), le flux de convection thermosolutal est analysé.

Les principaux résultats de cette étude montrent que la fracture peut grandement affecter le comportement du flux thermo-gravitationnel et peut jouer un rôle positif dans la séparation provoquée par l'effet Soret, notamment lorsque la perméabilité k est inférieure à la perméabilité optimale kopt. Cependant, lorsque la perméabilité k est supérieure ou égale au kopt optimal, la fracture affecte négativement le processus de séparation. En outre, la fracture inclinée à la paroi froide provoque une séparation importante par rapport au cas où la fracture est inclinée à la paroi chaude avec le même angle. En conséquence, le processus de séparation pourrait être grandement amélioré.

Mots clés : Effet Soret, thermodiffusion, milieux poreux, fracture, hétérogène, séparation.

Contents

Chapter II: Fundamental theory

Chapter III: Numerical Solution

Chapter IV: Results and discussion

List of Figures

List of Tables

Nomenclature

Variables		
A	Aspect ratio	/
a	The ratio of the fracture's Rayleigh number to the porous medium's Rayleigh number	/
c	Mass fraction of the reference component	/
C	Concentration of the solute	$Kg.m^{-3}$
c_a	The acceleration coefficient tensor	/
c_F	Dimensionless form-drag constant	/
c_P	Heat capacity of the mixture at constant pressure	$J.\ Kg^{-1}.\ K^{-1}$
D	Molecular diffusion Coefficient	$m^2.s^{-1}$
Da	Darcy number	m^2
D_T	Thermodiffusion coefficient	$m^2.s^{-1}.K^{-1}$
D_P	Pressure diffusion coefficient	$m^2.s^{-1}.\ Pa^{-1}$
$\vec{g}$	Gravity acceleration vector	$m.s^{-2}$
H_i	The partial molar enthalpy of component i	$J.mol^{-1}$
$\vec{J}$	Mass diffusion flux	$Kg.m^{-2}.s^{-1}$
k	Intrinsic permeability of porous medium	m^2 or mD
k_k	Kozeny constant	/
k_{Ti}	Thermodiffusion ratio of Component i	/
L_c	Characteristic length	m
M_i	Molecular weight of component i	$Kg.mol^{-1}$
N	The buoyancy parameter	/

Nu	Nusselt number	/
P	The intrinsic fluid Pressure	Pa
Q_i	The heat of transport of component i	$J.mol^{-1}$
Q_i^*	The net heat of transport of component i	$J.mol^{-1}$
q	The heat flux	$W.m^{-2}.s^{-1}$
q"	The heat production per unit volume	W/m^3
Sp	Soret coefficient	/
T	Temperature	K
t	Time	s
u	Speed component in x direction	$m.s^{-1}$
U_i	Partial internal molar energy of component i	$J.mol^{-1}$
v	Speed component in the y direction	$m.s^{-1}$
$\vec{V}$	The fluid velocity vector (u, v)	$m.s^{-1}$
V_i	The partial molar volume of component i	$m^3.mol^{-1}$
x_i	The mole fraction of component i	/
L_e	Lewis number	/
S	Separation parameter	/
Sh	Sherwood number	/
R	Universal gas constant	$J{\cdot}K^{-1}{\cdot}mol^{-1}$
Re	Reynolds number	/
R_T	Thermal Rayleigh number	/
w_{Hi}	The activation energy of component i	$J.mol^{-1}$

Greek Symbols

α	Thermal diffusivity	$m^2.s^{-1}$
α_T	Thermodiffusion factor	/

β_c	Solute volume expansion coefficient	/
β_T	Thermal volume expansion coefficient	K^{-1}
δ	Thermodiffusion ratio	/
δ_D, δ_m, δ_T	Thermodiffusion characteristic time	s
ε	Porosity of the porous medium	/
ε_A	Accessible Porosity of the porous medium	/
η	The ratio of the fracture's porosity to the porous medium's porosity	/
θ	The inclination of the fracture	deg
λ	Thermal conductivity	$W.m^{-1}.K^{-1}$
λ_s	Thermal conductivity of the solid phase	$W.m^{-1}.K^{-1}$
μ	Dynamic viscosity	$kg.\ m^{-1}.\ s^{-1}$
μ_i	The chemical potential of component i	$J.mol^{-1}$
ν	Kinematic viscosity	$m^2.\ s^{-1}$
ρ	Density of the mixture	$kg.m^{-3}$
σ	heat capacity ratio	/
τ	Tortuosity of the porous medium	/
τ_i	The ratio of vaporization energy ΔU_i^{vap} to viscous flow energy ΔU_i^{visc}	/
φ	The separation ratio	/
ψ	Dimensionless stream function defined by $u = \frac{\partial \psi'}{\partial y},\ v = \frac{\partial \psi'}{\partial x'}$	/
ω_i	The volume fraction of molecule i	/

Subscripts

D	Related to Darcy	/
e	Effective	/
i	Related to component i	/

F	Fracture	/
f	Fluid mixture	/
opt	optimal	/
pm	Porous medium	/
s	solid phase of the porous medium	/
$'$	parameter with dimension (Real)	/
$\bar{}$	Mean	/

Superscripts

F	Related to Firoozabadi Model	/
H	Related to Hasse Model	/
k	Related to Kampers Model	/
0	a reference state	/

Introduction

The study presented in this thesis is part of a macroscopic analysis of the phenomena of heat, mass, and momentum transfer, for a binary mixture presented in a heterogeneous or anisotropic porous media.

Thermosolutal convection, also known as double-diffusive convection is a mixing process driven by the interaction of two fluid components of different molecular diffusivities diffuses at different rates [1]. Double diffusive convection in saturated porous medium has been widely studied because of its many fundamental and industrial applications, such as in the use of geothermal energy, modeling of petroleum reservoirs, thermal insulation of buildings, waste disposal. Nuclear and chemical catalytic converters. Reviews of recent studies are given by Nield and Bejan [2], Ingham and pop [3] Vafai [4], and Mojtabi et al. [5]

When a fluid mixture (liquid or gas) of several constituents is subjected to a temperature gradient, their species will separate spontaneously after a characteristic time, following a preferential direction of separation. Usually, the heaviest component migrates toward the coldest area. This was independently discovered by Carl Ludwig [6] and Charles Soret [7]. In recognition of these two researchers, this phenomenon is called Soret or Ludwig-Soret effect, also it is known as the Thermodiffusion effect.

This coupled phenomenon of mass diffusion induced by a temperature gradient is observed in mixtures of mobile particles where the different particle types exhibit different responses to the force of a temperature gradient. This physical process occurs when a thermal gradient is applied to a mixture. In terrestrial conditions, the force of gravity strongly affect heat and mass transfer. Thus, the Soret effect is always accompanied by the forces of natural convection or forces of double-diffusive convection. The coupling between thermosolutal convection and the Soret effect is known as thermogravitation diffusion, Costesèque et al [8].

Thermodiffusion most often applies to many natural and industrial areas such as: Industrial processes of separation; Geological applications; petroleum engineering application; Biological Application; high temperature/ high pressure application. We will address them in detail later.

study objectives

In this, present study; we propose to analyze the thermosolutal double diffusive convection coupled with the Soret effect for a binary fluid in a rectangular cavity, entirely occupied by a heterogeneous porous matrix. Particular attention will be paid in this work to fractured porous media, where the fracture is considered as a porous media characterized by distinct permeabilities.

Our objectives are outlined in these three main points:

- Study components' behaviors of a fluid subjected to the influence of Soret effect coupled with thermosolutal convection in a heterogeneous porous medium.
- Evaluate and quantify the importance of Soret effect on the separation of constituents.
- Determine the optimum properties of the porous medium/fracture corresponding to maximum separation of the mixture components.

Thesis organization

In order to carry on the study in a structured way, the following work plan has been adopted:

First, and before tackling the main part of this work, a bibliographical synthesis of theoretical, experimental and numerical works relating to thermosolutal convection in heterogeneous porous medium, with and without the Soret effect is brought to light, for various configurations and for various boundary conditions.

The first chapter is devoted for a general presentation on the basic concepts characterizing the studied phenomena (thermosolutal convection / thermodiffusion), and the environment in which develops (porous mediums / Fracture). Generality on the transport phenomena in porous mediums, modeling of the Soret effect, the physical model chosen, the governing equations as well as the associated boundary conditions are the subject of the second chapter.

The mathematical equations system obtained in the second chapter is solved by the finite difference method. A FORTRAN source code was adapted to produce the numerical results. The discretization of mathematical equations and the numerical resolution procedure, together with the presentation of our computational code, take place in the third chapter.

We collocate in chapter four the main results obtained numerically for this study. Comments, interpretations, and analyses of the various results are presented on the basis of the distributions of certain physical quantities. Finally, we end this work with a general conclusion that summarizes the main obtained results.

Bibliographic Analysis

In this section, we carry out a bibliographical review on thermodiffusion and thermosolutal convection, in confined porous medium saturated by a fluid mixture.

A mass fraction gradient is spontaneously created when a liquid or gas mixture is subjected to a temperature difference. This separation of components refers as the thermodiffusion effect [9], where generally the heavier or larger molecular species concentrate near the colder surface.

The Discovery of the thermodiffusion process is attributed to Ludwig; he filled in 1856 a U-shaped tube with a sodium sulfate solution, heated one arm with boiling water, and cooled the other one with melting ice. After a week, he observed a crystallization on the cold side, and more importantly a decrease of the salt concentration on the warm side. Years later, C. Soret [7] more rigorously identified this effect in various salt solutions [10].

For gases, Enskog in 1911, and Chapman in 1916 independently, predicted the thermodiffusion in ideal gas mixture theoretically using Boltzmann equation and

introduced the thermal diffusion coefficient, D_T. The approach which Chapman used differs from that of Enskog, the theory was proved experimentally by Chapman and Dootson in 1917 [11], [12].

A historical database of experimental and theoretical works has been presented by [13], including technical hitches of performing experiments on ground condition as well as in microgravity environment.

The coupling of Soret effect with natural convection or thermosolutal convection magnifies the primary separation coming from the Soret effect. This is known as the thermogravitation phenomena. [14] Were the first to carry out with significant success a process for isotopes separation in a vertical cavity, they invented the Thermo-gravitational column (TGC). Furry, Jones and Onsager [15], developed the thermodiffusion theory, known as (FJO theory), and even devoted an in-depth study for gases separation [16], which extended for liquids by De Groot (1942). However, the developed TGC was declined due to the operating features and so researchers are encouraged to combine the TGC technique with other reparative mechanisms and modified cell designs [17]. Lorenz and Emery [18] projected the idea of filling the thermo-gravitational cells with a porous medium, in order to reduce convection currents, which allows working with large dimension cells. In this regard, many works have recently been carried out to buttress these phenomena. The tilting effect of the Thermogravitational column has been studied by many researchers, [19] and [20] for instance. It is noticed that the separation can be significantly increased with tilted cavity. El Hajjar et al. [21], studied with the same configuration the stability of the mono-cellular flow, they demonstrated that the separation in this configuration is superior, as well as that the critical Rayleigh value is greater than that of maximum separation.

Lee et al. [22] investigated the effect of various forms of non-uniform basic temperature gradients on thermo-gravitational convection in an isotropic porous layer using non-equilibrium models. Two-field temperature models were used for

the energy equation and the Forchheimer-extended Darcy model to describe the flow. It is found that the linear temperature profile provides a reinforcement of stability, compared with the non-uniform temperature gradients.

Abahri, et al. [23] studied the thermo-gravitational separation of a binary liquid mixture in a horizontal porous annulus space heated isothermally from the inner cylinder. Theoretical and numerical results reveal that the separation can be increased for small values of Rayleigh number. Grigor'ev & Rivin [24] used the thermo-gravitational column to determine thermo-diffusion factors of organic liquids mixture. A comparison of the calculated values of the Soret coefficient and the experimental data obtained has been presented with a satisfactory agreement. In terms of the separation ratio, the cross-diffusion, and Lewis and Rayleigh numbers, Mutschler, et al. [25] suggests two analytical models describe the thermo-gravitational separation of N-component mixtures in a vertical cavity filled by a porous medium. Their theoretical model support strongly the experimental results. Recently, Mojtabi, et al. [26] studied the influence of the thickness and the nature of the bounding horizontal plates on the separation of a binary mixture in a horizontal porous cavity. Authors found that the ratio of the plate to the porous layer thickness and the ratio of their thermal conductivity greatly affect the species separation. Direct numerical simulations confirmed the analytical results. Kozlova & Ryzhkov [27] studied the transient separation of multicomponent mixture in a cylindrical thermo-gravitational column. The evaluation of separation in vertical direction is solved analytically and compared with two-dimensional numerical simulation of binary and ternary mixture, where a good agreement is observed. Hashemipour, et al. [28] performed an experimental and numerical study to separate toluene/n-heptane mixture by TGC. Good concordance can be seen between **experimental** and numerical results. The separation factor can reach 1.17 when the optimal conditions are achieved (feed flow rate, cut, Temperature gradient). In a packed thermo-gravitational cell, maximum separation is associated with an optimal permeability of porous medium as it was a subject of interest to several researchers [29]; [30].

Thermo-solutal convection in vertical porous cavity can be driven either by double diffusion (the solute gradient is induced by the solute boundary condition), or by cross diffusion (the solute gradient is induced by thermal boundary condition via Soret effect) [31]. However, in many practical applications, the thermosolutal convection is driven by both double diffusive convection and Soret effect [32]. In this wise, Amahmid, et al. [33] studied the double diffusive convection in a vertical cavity subjected to horizontal gradient of heat and mass. They focused on the situation in which thermal and solute buoyancy forces are oppose to each other and found that multiple steady state solutions are possible. Ben Niche, et al. [34] studied the unsteady double diffusive natural convection in a square cavity heated and cooled along the vertical walls, the focus was to identify the flow regime for thermal and solute dominated flows, and they found that Soret coefficient had great effect on the flow structure.

Er-Raki, et al. [35] studied the Soret effect on double diffusive boundary layer flowing in a vertical porous layer. Based on the parallel flow approximation[1], an analytical solution was developed which allows a detailed parametric study of the governing parameters effect on the convective flow and on heat and mass transfer characteristics. These analytical results were compared with the numerical solution.

Bhadauria [36] studied double-diffusive convection in an anisotropic porous layer with an internal heat source, heated and salted from below. A generalized Darcy model was used for the momentum equation. Linear and nonlinear stability analyses have been investigated for both steady and unsteady cases. The effects of internal Rayleigh number, anisotropy parameters, concentration Rayleigh number, and Vadasz number on stationery, oscillatory, and weak nonlinear convection have been presented graphically, and the effects of various parameters on heat and mass transfers have been discussed.

[1] The flow is considered unidirectional, and the horizontal velocity component is neglected.

Raju, [37] investigated the effect of temperature dependent viscosity on Ferro-thermohaline convection saturating an anisotropic porous medium, where the cavity is heated from below and salted from above. Using the computational Galerking technic, he found that permeability of the porous medium, anisotropy effect and temperature dependent viscosity stabilizes the system. Alloui, et al. [32], studied analytically and numerically the combined effects of Soret and thermosolutal convection, in a vertical rectangular cavity filled with a binary mixture. Neumann-type boundary conditions for temperature and solute were applied to the vertical walls of the cavity, while the horizontal walls are assumed impermeable and insulated. Depending on the fundamental parameters of the problem, they find a good agreement between the analytical study based on the parallel flow approximation, and the numerical study.

Jiang, et al., [38] examined numerically the effect of natural convection on the Soret effect in a vertical cavity heated laterally. They used the mathematical model of Shukla and Firoozabadi to calculate the molecular diffusion, the thermo-diffusion, and the pressure diffusion coefficients as functions of temperature, pressure, and other physical properties of the binary mixture at each point of the grid. As a function of separation factor, their results indicate that as permeability increases, separation increases until it peaks at 10 md, then decreases. Jiang, [39] examined using the same mathematical model the effect of medium's heterogeneity in a stratified porous vertical cavity. They found that the Soret effect is strongly dependent on heterogeneity of the medium; the authors announced that the separation in heterogeneous porous medium is always greater than in homogeneous one. Their declaration is further elaborated in the results section. Jaber [40] thereafter studied the effect of the permeability in a fractured porous medium cavity filled with a ternary mixture with the consideration of likely thermo-diffusion effect. The system was set at 10 md for the permeability of the porous medium, while the permeability of the fracture was varied from 10 to 1000 md (1millidarcy = 1md = 0.986923×10^{-15}

m^2). The outcome showed an increasing of the flow field in the fracture, which affects the behavior of each component.

Limited studies considered the Soret effect while investigating the thermosolutal convection phenomenon in heterogeneous porous media. This study has the objective of investigating the role of an inclined discrete fracture on thermosolutal convection coupled with the Soret effect. The porous medium is isotropic, comprised of a discrete fracture, and saturated by a binary fluid, where the fracture is also filled with another porous medium. Depending on its permeability, the fracture could either promote the mass transfer or act as a barrier reducing the flow circulation. More precisely, the influence of the fracture characteristics (permeability, positioning, and thickness) on the fluid flow and heat and mass transfer is examined in terms of the separation parameter (S), [41]. The separation parameter is defined as the deference of the maximum concentration in the hot wall and the minimum concentration in the cold wall [42].

Chapter I

Soret Effect in Porous Media

I.1. Introduction

This first chapter will briefly present the phenomenon of interest and the medium where it takes place. We will present generalities about double diffusion convection, thermodiffusion or Soret effect, the porous medium characteristics, and fractures.

I.2. Naturel, Force and mixed convection

The term convection is used to define movements derive from thermal agitation due to differences between the density of fluid molecules. Natural convection refers to agitations induced in the fluid by forces (volume or surface) acting inside the studied volume. The movements generated are due to local variations in the density of the fluid as a function of temperature and/or concentration. Forced convection concerns the convective movements that appear under the action of an external source, such as a pump or the movement of an object in the fluid, i.e., the movements induced by a pressure difference are forced convection movements. Where the flow persists even in the absence of a temperature gradient. When convection is due to the coupled effects mentioned above, we then speak of mixed convection [43].

I.3. Presentation of the Soret effect

In an initially homogeneous solution of at least two components, a thermal gradient leads to a transfer of material within the mixture. This results in the formation of a concentration gradient, and a fluid inhomogeneity, this is what called Soret effect [43]. “Thermodiffusion or the Soret effect is the separation of the components of a mixture toward the hot/cold regions of a domain that is characterized by a non-uniform temperature distribution” [44].

Fig. I-1 represents the principle of thermodiffusion for a binary fluid, between two chambers under different temperature, the heaviest constituent generally moves towards the cold zones. By considering the thermodynamics of irreversible processes, De Groot and Mazur (1984) demonstrated that energy and mass fluxes are dependent on both concentration and temperature gradients. Table.1 represent the coupling between force and flux of heat and mass and resulting phenomena.

Table -1: coupling between force and flux of heat and mass, Paszkuta [45]

Flux \ Force	∇T	∇C
Heat	Conduction (Fourier's Law)	Dufour effect
Mass	Soret Effect	Diffusion (Fick's Law)

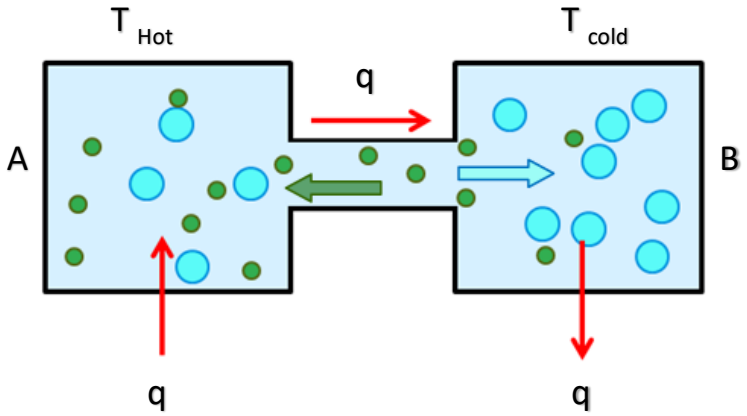

Figure 1: Representative diagram of thermodiffusion (the Soret effect)

Heat flux generated by the temperature gradient (conduction) and mass flux generated by concentration gradient (diffusion) and considered primary transport phenomena. While, it is worth mentioning that the Dufour and Soret effects are of orders of magnitude smaller than the effects described by the laws of Fourier and Fick, which is why they have been neglected in many studies.

I.3.1. Relevance of the Soret effect

Thermodiffusion has an impact on the behavior of several natural activities; likewise, it has also been shown to be exploited in many industrial processes. Srinivasan and Saghir [44] in their book presented a detailed presentation of Soret effect applications; readers can also find wide-ranging thermodiffusion applications in [46]. In order to give a simple

inclusive idea about the different application domains, table I-2 recapitulate the most thermodiffusion application from the two previous references.

Regarding the building's insulation, it has been found that the contribution of thermodiffusion on the mass flux of moisture through insulating materials can exceed 30% as reported by [47].

Table I-2: Thermodiffusion applications, recapitulated from [44], and [46].

Domain of Application	Studies (for instance)	Ref.
Natural activities	Convection in stars (Spiegel, 1972)	[44]
	Physics of solar pond (Weinberger, 1964)	
	Salinity gradient in ocean (Schmitt, 1994)	
	timing of abrupt climate changes (Severinghaus, et al., 1998)	[46]
Industrial application	Separation of polymers (Janca, 2006) (Kita, et al., 2004) (Kohler, et al., 1995) (Schimpf & Giddings, 1987)	[44]
	Separation of colloidal materials (Janca,2003) (Van Batten, et al., 1997)	
	Separation of charged particles (Pasti, et al., 2007)	
	Separation of isotopes in gas and liquid (Furry, et al., 1939) (Chapman, 1919)	
	Freezing process of food (Pham, 2006)	
	Separation of hydrocarbon oil mixtures (Kramers & Broeder, 1948)	[46]
	Separation of Isomers (Jones & Milberger, 1953)	
Geological applications	Oil reservoir components distribution (Montel, et al., 2007)	[44]
	Magma dynamics and molten rocks (Wahl, 1946)	[46]
	mineral concentration and crystallization in deep aquifers, (Oldenburg & Pruess, 1998)	

Petroleum Engineering Applications	wax deposition in pipelines (Banki, et al., 2008)	[46]
	carbon dioxide injection in fractured reservoirs. (Hoteit & Firoozabadi, 2009)	
	improved oil recovery, (Darvish, 2007)	
biological applications	Separation of bacteria (Janca, et al., 2007) (Kasparkova, et al., 2007)	[44]
	Biological mechanism of transport (Bonner & , 1984)	
	Trapping of DNA (Braun & Libchaber, 2002)	
	determination of biomolecular binding curves (Baaske, et al., 2010)	
	To powerful screening methods for biomolecules and colloids. (Wiegand, 2004)	[46]
	complementing well established methods, such as electrophoresis and optical tweezers (Delville, et al., 1999)	
	water transfer through wood (Peralta & Skaar, 1993)	
	To improve the ability to influence biological systems such as plants (Astumian, 2007)	
	measure stomatal[2] aperture in plant leaves (Spanner, 1956)	
	thermal diffusion may have played a role in the origin of life (Gaeta, et al., 1975)	
High temperature/ high presser applications	organic and inorganic synthesis and destruction of hazardous waste butenhoff (Butenhoff, et al., 1996)	[46]
	combustion, (Gomez & Rosner, 1993) ;soot formation, (Rosner, et al., 2000) ; corrosion, and vapor deposition (Rosner & Arias-Zugastia, 2007)	

The Soret effect can be an important factor of predicting both the initial state and the actual composition of a reservoir [48]. Ghorayeb, et al. [49] showed that thermal diffusion generated by geothermal temperature gradients; predominate -in some cases- Fickian and pressure diffusion. In such a situation, the density gradient of the reservoir could be

[2] Stomata are microscopic pores on plant leaves that regulate gas exchange in plants [46]

reversed, where a denser fluid floats on top of a lighter mixture. However, thermodiffusion as a separation method suffers from slow rates and high energy requirements; therefore, [50] considered the industrial use of thermal diffusion as a separating method would only be used when it is the only choice and when heat-energy is abundant [51].

I.3.2. Thermodiffusion coefficients

On account of the Soret effect, a mixture subjected to a thermal gradient will induce a concentration gradient. However, the Fickian diffusion process begins to restore the uniformity of the mixture. Hence, in the absence of a pressure gradient, the net mass flux of a species is a result of a competition between Fickian diffusion and thermodiffusion.

For a binary mixture, the mass flow of a species is written as [44]:

$$J = -\rho \left(D\nabla C + D_T\, c(1-c)\, \nabla T\right) \qquad \text{(I-1)}$$

Where:

$\boldsymbol{D_T}$ is the thermodiffusion coefficient with units $m^2s^{-1}K^{-1}$.

$\boldsymbol{D}$ is the molecular diffusion coefficient with units m^2s^{-1}.

$\boldsymbol{\rho}$ is the mixture density.

$\boldsymbol{c}$ is the mass fraction of the reference species.

$\boldsymbol{T}$ is the temperature in Kelvin.

At equilibrium, when the net flux vanishes (J = 0), the previous equation can be rearranged to define **the Soret coefficient $\boldsymbol{S_P}$** with unit K^{-1} as follow:

$$S_P = \frac{D_T}{D} = -\frac{\nabla C}{c(1-c)\,\nabla T} \qquad \text{(I-2)}$$

Also, we define **the thermodiffusion factor $\boldsymbol{\alpha_T}$**, *a* dimensionless parameter defined as:

$$\alpha_T = T\,\frac{D_T}{D} \qquad \text{(I-3)}$$

Another closely related dimensionless parameter is **the thermodiffusion ratio $\boldsymbol{\delta}$** that is defined as :

$$\boldsymbol{\delta} = \alpha_T x_1 x_2 \tag{I-4}$$

Where:

$\boldsymbol{x_1, x_2}$ Is the mole fractions of the two components in a binary mixture.

We notice that, many authors use a different form of eq. (I-1). They use a different thermal diffusion coefficient $\boldsymbol{D_T^*}$. The relationship between the two diffusion coefficients is:

$$\boldsymbol{D_T^*} = c\,(1-c)\,\boldsymbol{D_T} \tag{I-5}$$

I.3.3. The characteristic time

As with any diffusive phenomenon, De Groot, [9], showed that it was also possible, to associate to the thermodiffusion a characteristic time δ_D, corresponding to the attainment of the stationary state, and defined as:

$$\delta_D = \frac{d^2}{\pi^2 D} \tag{I-6}$$

Where:

d: The distance between the two walls of different temperatures.

D: Molecular diffusion coefficient

Moreover, it is interesting to note that numerous improvements have been achieved to the perception of the laws describing the characteristic times δ_D, δ_m, δ_T corresponds to the attainment of the stationary state, the establishment of the mole fraction gradient, and the establishment or relaxation of the thermal gradient respectively, [52].

Eq. (I-7) present the characteristic time correspond to the establishing of the mole fraction gradient, while the characteristic time correspond to the establishing or relaxation of the thermal gradient is described in eq. (I-8).

$$\delta_m = e^{-\frac{t}{\delta_D}} \tag{I-7}$$

$$\delta_T = \frac{D^2}{a} \tag{I-8}$$

Where thermal diffusivity a, is defined as:

$$a = \frac{\lambda}{\rho Cp} \tag{I-9}$$

Cp: The heat capacity of the mixture at constant pressure.

I.3.4. Experimental methods

Several experimental methods have been used ether to measure the thermodiffusion coefficients in a binary fluid mixture, or to realize a separation process built-on the thermodiffusion phenomena. For a detailed view of all the techniques that exist and the pros and cons of each, the reader may consult [53], and [10]. Following are some widely use methods:

a) The two-bulb method

The two-bulb technique is the most used method for determining diffusion coefficients, (Yabsley and Dunlop 1976), and thermodiffusion coefficients of gases mixture, (Grew and Ibbs 1952) in [54].

A two-bulb cell consists of two chambers at the same pressure connected by a small volume tube. The two chambers are filled with fluid mixtures of different compositions. Initially, a uniform composition is attained by diffusion through the tube. Exposing the bulbs to different temperatures, (uniform on each bulb) generates a temperature gradient through the tube, which allows the occurrence of the thermodiffusion phenomenon, thus a composition gradient. Experimental studies of thermodiffusion are generally based on determining the separation that can be found from the change in composition that occurs in a single ampoule.

Fig. I-2 shows a sketch of a two-bulb experimental set-up used by Davarzani [54] for the diffusion and thermal diffusion tests.

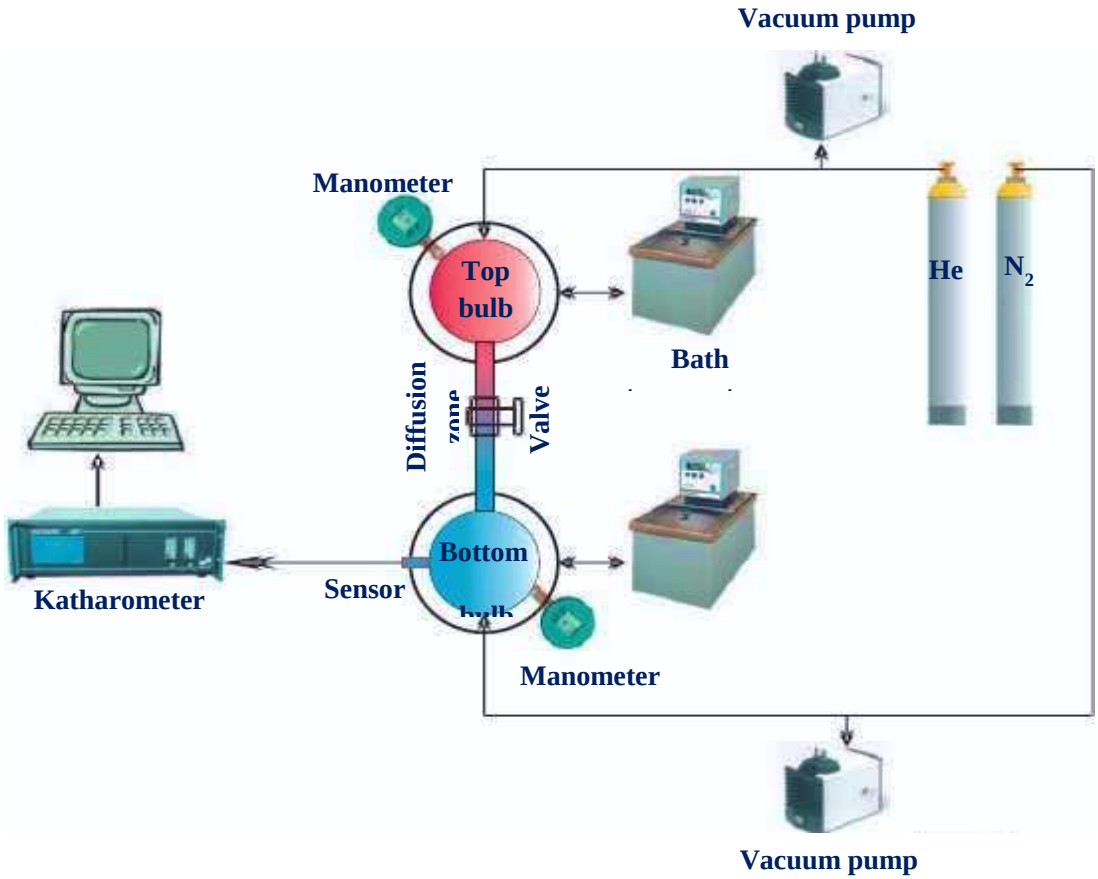

Figure I-2: A sketch of a two-bulb experimental set-up used by Davarzani [54]

In the literature, to determine the thermodiffusion coefficient numerous measurements were made using a two-bulb method. For instance, for a Helium-Argon system, the reader could consider the works done by Ibbs, 1925; Puschner, 1937; Atkins, 1939; grew, 1947; Saxena, 1959; and [55].

b) The Thermogravitational Column

The thermogravitational column consists of two vertical plates separated by a narrow space under a horizontal or vertical thermal gradient [56], Fargue, et al., 2004 in [54]. It is used either for the separation of mixtures or for measuring thermodiffusion coefficients (see Fig. I-3).

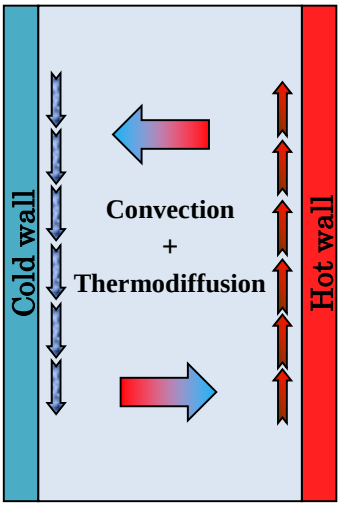

Figure I-3: Principle of Thermogravitational Cell with a horizontal temperature gradient [54]

Thermogravitational column was designed by Clusius and Dickel (1938), and theoretically revealed by Furry et al. [57], then was validated by many experiments. The thermogravitational column uses a thermal gradient to produce a mass flow by thermodiffusion and a convection flow at once. The coupling of the two transport mechanisms causes the separation of the components; the optimal coupling ratio leads to a maximum separation. The rate of separation in this system is the difference in concentration between the cold and the hot walls of the cell. The thickness of the column controls the balance between thermal diffusion and convection; small thickness disfavors convection and promotes the thermodiffusion effect. The optimal thickness in a free fluid is less than one millimeter for usual liquids [54]. In order to work with large dimension cells Lorenz and Emery [18] projected the idea of filling the thermo-gravitational cells with a porous medium, in order to reduce convection currents. It has also been found that the

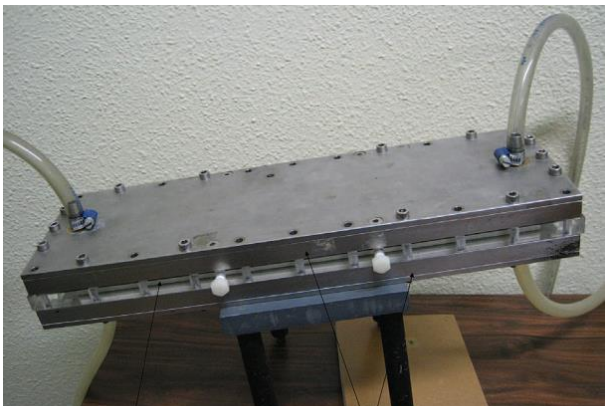

Figure I-4: An inclined thermogravitational cell used by [21]

separation in a Thermogravitational column can be substantially increased by inclining the column, for instance [21] Fig. I-4.

Recently, many researchers investigate vibrations effect, they find that vibrations can lead whether to increase or decrease heat and mass transfers in the thermogravitational column, benchmark results can be found in [58].

This study has the idea of filling the Thermogravitation column with an anisotropic porous media, introducing an inclined discrete fracture filled with another porous medium. Depending on its permeability, the fracture could either promote the mass transfer or act as a barrier reducing the flow circulation.

c) Thermal Field-Flow Fractionation

Thermal Flux Fractionation is a technique that relies on the thermodiffusion force (applying a temperature gradient) to characterize and separate polymers and particles. The separation of suspended particles is generally carried out in a solvent carrier. The particles of higher molecular weight migrate and compact more tightly next to the cold wall. Due to the parabolic velocity profile of the carrier, unlike the lower molecular weight particles (likely situated in the center of TFFF channel), large particles will have a less average velocity. The difference between the average velocities causes a spatial and temporal separation along the channel. The thermal flow fractionation system has unique characteristics making it more suitable for certain separations, (Caldwell, 1973) in [54]. The TFFF is an excellent technique for measuring Soret coefficients especially for

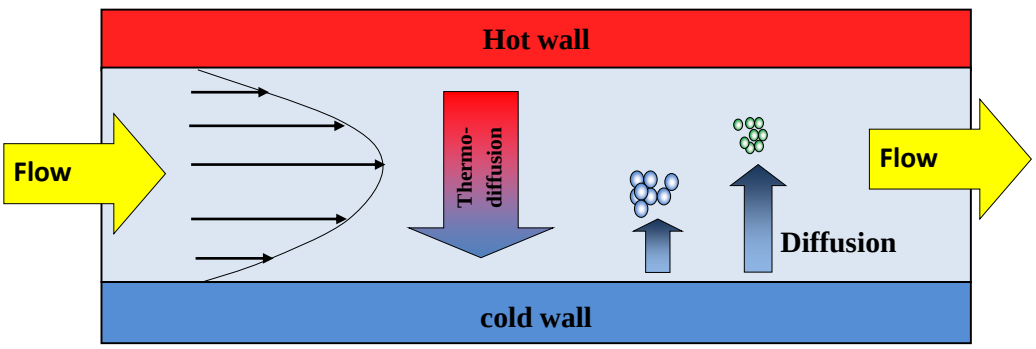

Figure I-5: Principle of Thermal Field-Flow Fractionation (TFFF) [54]

suspended particles and dissolved polymers, Schimpf 1998 (Davarzani 2010). A sketch of the system is shown in Fig. I-5.

d) Thermal Diffusion Forced Rayleigh Scattering method

The basic principle of a TDFRS is to generate a vertical intensity and thereby temperature grating inside an absorbing sample volume by the interference of two pulsed, high-power laser beams of equal wavelength and equal intensity. This is technically realized by splitting up one laser beam into two beams that intersect inside the sample cell. Due to the absorption of the laser light, the interference grating created by the intersection of two split laser beams is directly converted into a temperature gradient, which in turn create a concentration grating by the Soret effect. Both gratings contribute to a combined refractive index grating that is read out by diffraction of a third laser beam (Fig. I-6 and Fig. I-7).

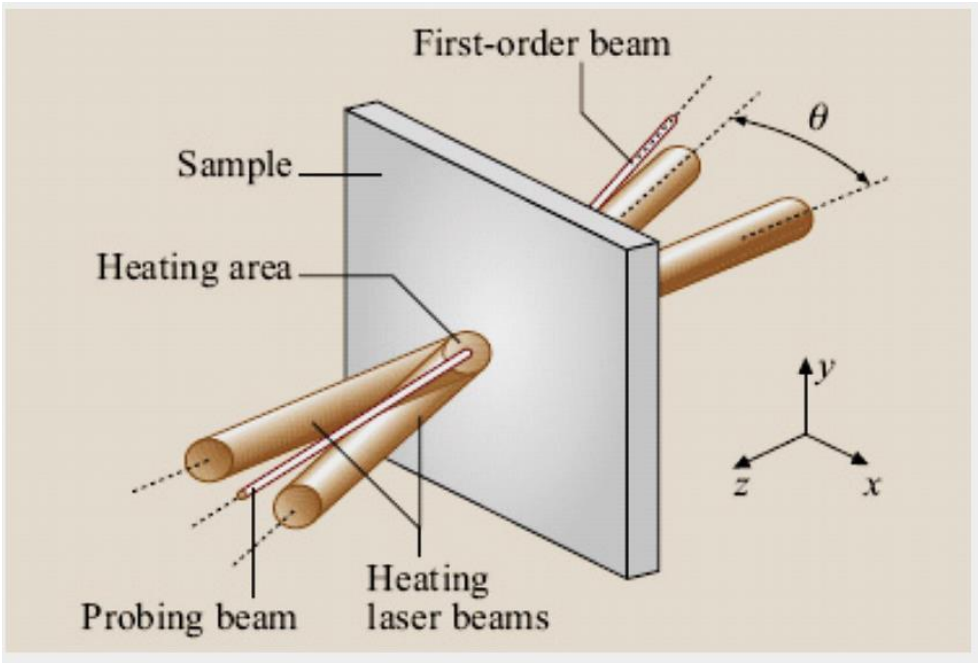

Figure I-6: Principle of forced Rayleigh scattering, (Tropea and Foss, 2007) in [54]

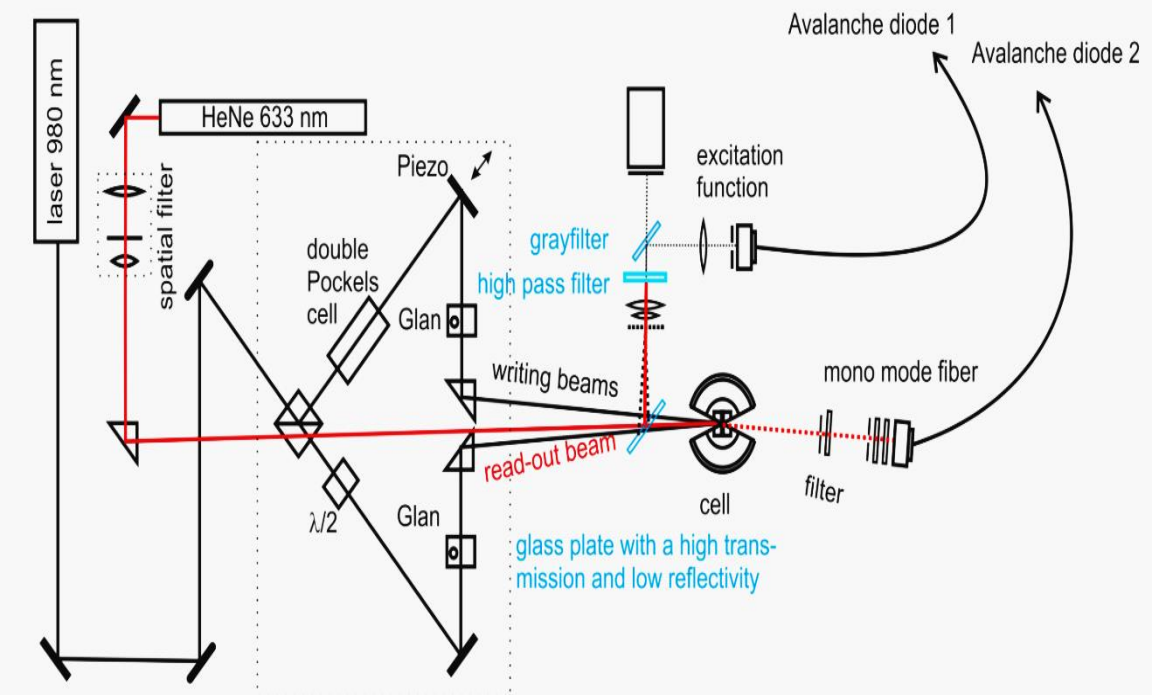

Figure I-7: Schematic drawing of an IR Thermal Diffusion Forced Rayleigh Scattering setup, used by Wang & Xuzhou, [80].

Analyzing the time dependent diffraction efficiency, three transport coefficients can be obtained (the thermal diffusivity α, the diffusion coefficient D, and the thermal diffusion coefficient D_T) [54].

I.3.5. Soret coefficient sign and behavior

It is worth mentioning that the Soret coefficient sign could changes repeatedly at certain temperatures and/or compositions, as observed in polar systems. For instance, Wiegand group, have been carried out systematic studies of polymers in water, alcohol, or water/alcohol mixtures, they reported concentration-induced sign changes. With the fact that polyethylene oxide has a positive Soret coefficient in pure water and in water-rich water/ethanol mixtures, the sign becomes negative at higher ethanol content, and the polymer migrates toward the warm side (Gans, et al., 2003) in [10]. For the same system, Kita, et al., have been also reported temperature-induced sign changes [10].

The Soret effect is a multi-factor phenomenon. The main factors that affect thermodiffusion behavior are molecular masses, sizes and moments of inertia, these first three contributions are easily accessible particle properties. Three other contributions stem from chemical interactions, which are solvent-solute, solute–solute, and solvent–solvent parameters interactions, generally these parameters contribute separately, but in very limited cases, those contributions could be additive [59]. These parameters are illustrated in Fig. I-8.

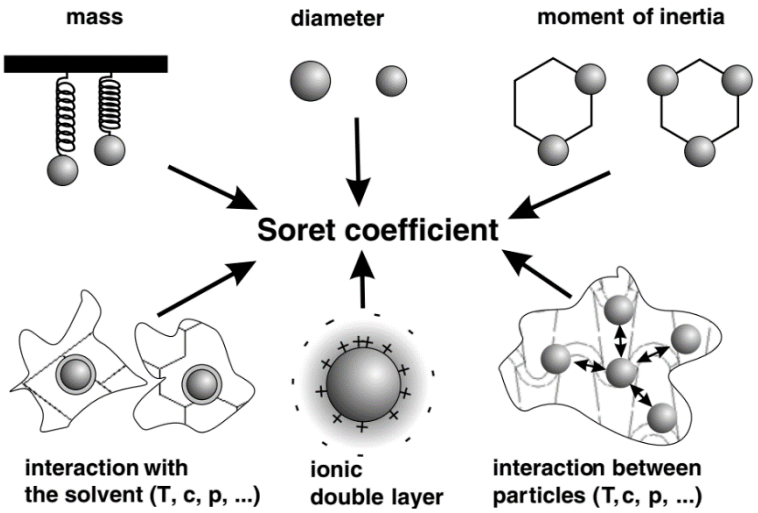

Figure I-8: The main features determining thermodiffusion behavior (Wiegand, 2004)

Despite the significant advancements that have been made, is not easily to characterize the Soret effect by a single simple model. However, due to the discovery of additivity laws[3], the modern progress in studying thermal diffusion is allowing for a convenient classification of the phenomenon, its interpretation, and even a proper estimation and prediction of the thermodiffusion parameters [10].

I.4. Porous medium properties

A porous medium is a continuous medium (either cohesive or not), internally presents a fraction of volume accessible to a fluid. This fraction of non-solid volume is made up of

[3] Integral laws: relate to the general behavior of the substances in a temperature field according to their thermophobicities, and the specific laws relate to the additivity of the particular contributions (Köhler & Morozov, 2016).

caverns, crevices, pores, etc. A porous medium containing either blind or open pores. The more the pores are interconnected, the more allows the fluid to flow.

I.4.1. *porosity of a porous medium*

The porosity of a porous medium is the volume fraction of its voids, denoted ε. While the origin of porosity in artificiale porous materials is usually known and understood, the same is not necessarily true about natural porous media, which has to be determined.

$$\varepsilon = \frac{total\ volume\ of\ pores}{total\ volume\ of\ the\ porous\ medium} \tag{I-10}$$

We define the accessible porosity ε_A, which depends on that part of the void space that can be reached from its external surface, it can be calculated by Eq. (I-11), [60].

$$\varepsilon_A = 1 - \frac{V_1}{V_3} - \frac{V_2}{V_3}\frac{P_2}{P_2 - P_1} \tag{I-11}$$

Where V_1 is the volume of the container in which the porous system is enclosed, V_2 the volume of the evacuated container, V_3 is the volume of the porous sample, and P_1 and P_2 are the initial and final pressures of the medium respectively.

We present in Table I-3 the total porosity range of several classes of porous materials obtained from [60].

Table I-3: Porosity ranges for several classes of porous media [60].

Porous medium	$\boldsymbol{\varepsilon}$ (%)
Black slate powder	57-66
Silica powder	37-49
Random packing of spheres	36-43
Sand	37-50
Sandstone	8-38
Limestone (dolomite)	4-10
Coal	2-12
Concrete	2-7

Porosity is obviously an essential descriptive element of the porous medium, however, two porous media having the same porosity can have very different properties.

I.4.2. permeability of a porous medium

The permeability of a porous medium reflects a measure of how easily a fluid can flow through it under a pressure gradient. The permeability k depends only on the porosity and the geometry of the solid matrix. Several evaluations of the permeability k depending on porosity and characteristic size of the porous matrix pore-scale were proposed. We cite some selected relations determining the permeability, the reader could see [61] for more relations.

The relation of Kozeny (1927) -Carman (1937), gives an estimate of the permeability k(mD) for an unconsolidated porous medium made up of identical elements of simple geometry [62]:

$$k = \frac{d^2\varepsilon^2}{36k_k(1-\varepsilon)^2} \tag{I-12}$$

d: Designates a characteristic dimension of the elements constituting the porous matrix (the diameter of a sphere, or the rib of a cube...)

k_k: A Kozeny constant, depending on the shape of the grains ($3.6 < k_k < 5$), in particular $k_k = 4.84$ for spherical grains.

Ergun [63], establishes an expression similar to that of Kozeny-Carman by considering the unidirectional flow of an incompressible fluid within a porous column made up of spherical particles, of diameter d (microns), and subjected to a pressure gradient:

$$k = \frac{d^2\varepsilon^2}{150(1-\varepsilon)^2} \tag{I-13}$$

Which corresponds to a value of Kozeny's constant, $k_k = 4.16$.

Modeling of the pores by capillary cracks of width w, and distant d, leads to a permeability:

$$k = \frac{w^3}{12(w+d)} = \frac{w^2}{12}\varepsilon \tag{I-14}$$

Modeling the porous matrix as a bundle of parallel capillary tubes leads to the following expression for permeability:

$$k = \varepsilon\frac{d^2}{32}, \qquad \varepsilon = \frac{n(\pi d^2)}{4} \tag{I-15}$$

n: the number of capillaries per unit area perpendicular to the direction of flow, and d: the diameter of the capillaries.

For Fractures, another relation is proposed to calculate the permeability [61]:

$$k = \frac{0.5444 \times 10^8 \times w^3}{h} \tag{I-16}$$

With: k = permeability (Darcy) h = fracture width (inches) w = fracture aperture (inches).

We present in table I-4 the permeability values for different porous materials, taken from [2].

Table I-4: Permeability range for certain porous media, [2]

Porous Material	Permeability κ (m^2)
slate	$4.9 \times 10^{-14} - 4.4 \times 10^{-13}$
Brick	$4.8 \times 10^{-15} - 1.2 \times 10^{-13}$
Concrete	$1.0 \times 10^{-13} - 2.3 \times 10^{-11}$
Leather	$9.5 \times 10^{-14} - 1.2 \times 10^{-13}$
Limestone	$2.0 \times 10^{-15} - 4.5 \times 10^{-14}$
Sand	$2.0 \times 10^{-11} - 1.8 \times 10^{-10}$
Sandstone	$5.0 \times 10^{-16} - 3.0 \times 10^{-12}$
Silica	$1.3 \times 10^{-14} - 5.1 \times 10^{-14}$

I.4.3. Tortuosity

The description of the geometry of the pores involves the concept of connectivity, corresponding to the complexity of a continuous path through the pore space. It is also necessary to take into account the "dead arms" which are numerous in low porous and very heterogeneous environments (Fig. I-9). To describe these different aspects, we introduce the parameter τ designating the tortuosity, which is defined as follows:

$$\tau = \left(\frac{L_C}{L}\right)^2 \qquad \text{(I-17)}$$

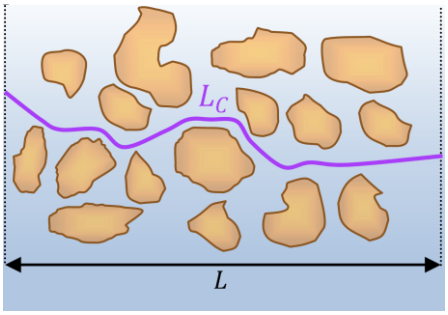

Figure I-9: The tortuosity of a porous medium

Where: L_C is the actual length of the fluid streamlines passing through a sample of length L of a porous medium, modeled as a network of parallel or wavy capillaries. This ratio also plays an important role in diffusion matters.

I.5. A Hierarchy of Heterogeneities and Length Scales

The study of any given phenomenon in a porous medium depends essentially on several length scales over which the effective properties of the medium may or may not be constants. A porous medium is considered homogeneous when its effective properties are independents of its linear size. The overall behavior of a porous medium depends on the rate of the transport processes (diffusion, conduction, and convection), the way the fluids distribute themselves in the medium, and the medium's morphology. Generally, the morphology of a porous medium plays the most important role compared to the other influencing factors [60].

In order to possess a complete description of a porous medium, we have to excavate every part of it. In practice, however, this is impossible for large natural porous mediums or reservoirs, for that matter, a description of such porous mediums is a combination of the deterministic components (measurable information) and indirect inferences that, inevitability, have stochastic or random elements in them. The statistical physics of disordered media has played an essential role in developing the stochastic component of description of porous media.

In general, the heterogeneities of a natural porous medium are described at mainly four distinct length scales that are as follows, (Haldorsen and Lake, 1984) in [60]:

1. The microscopic heterogeneities: at the level of the pores or grains, and are visible only through scanning electron microscopy or thin sections.

2. The macroscopic heterogeneities: at the level of core plugs that are collected in fields and analyzed. The property values are varying widely from core to core. However, in most theoretical studies, cores are assumed homogeneous and the average effective properties are assigned to them, notwithstanding their microscopic heterogeneities.

3. The megascopic or field-scale heterogeneities: at the level of the entire reservoir that may have large fractures and faults. They can be modeled as a collection of thousands, perhaps millions, of cores, oriented and organized in some order.

4. The gigascopic heterogeneities: encountered in landscapes that may contain many such reservoirs, along with mountains, rivers, and so on.

In practice, a porous medium may not contain all aforementioned heterogeneities. For instance, porous catalysts usually contain only microscopic heterogeneities, and packed beds may be heterogeneous at both the microscopic and macroscopic levels.

I.6. Representative Elementary Volume

When studying flows in porous media, two scales are necessary for the description of the phenomena [64].

• The pore scale, or microscopic, within which local sizes can vary widely. In general, this scale is associated with the average diameter of the pores, d.

• The scale of the porous medium, or macroscopic, characteristic of significant variations of these same quantities, defined as averages, over a certain volume of the porous medium. This macroscopic scale is associated with a geometric dimension of the medium L.

For large-scale porous media, the solid-fluid interface is so tortuous, which makes the problem mathematically intractable. Consequently, it becomes essential to pick out a macroscopic description at a length scale much larger than the dimension of individual pores. A revised approach that averages flow rates over dimensions much larger than the pore diameter greatly simplifies analysis. Here, a representative elementary volume (REV)

The macroscopic quantities, characterizing the porous medium, are therefore obtained by taking an average of corresponding microscopic quantities. The macroscopic field variables allow satisfying such equations as Fick's law of diffusion or Darcy's law of flow. The adopted REV has to be small enough in comparison to the overall extent of the porous medium so that it can be assigned a unique temperature, pressure, and fluid velocity, but large compared to the scale of their microscopic fluctuations. Thus, if l denotes the characteristic dimension of the REV, l must satisfy the following double inequality: $d < l < L$. A comparison of laboratory-scale, and REV-scale is shown in Fig. I-10, with REV-scale (of the order of a few hundred microns), laboratory-scale (tens of millimeters); d_p is the particle diameter (10–100µ). For more thoughts about the various changes of scales and their validity, the reader could see for instance [65].

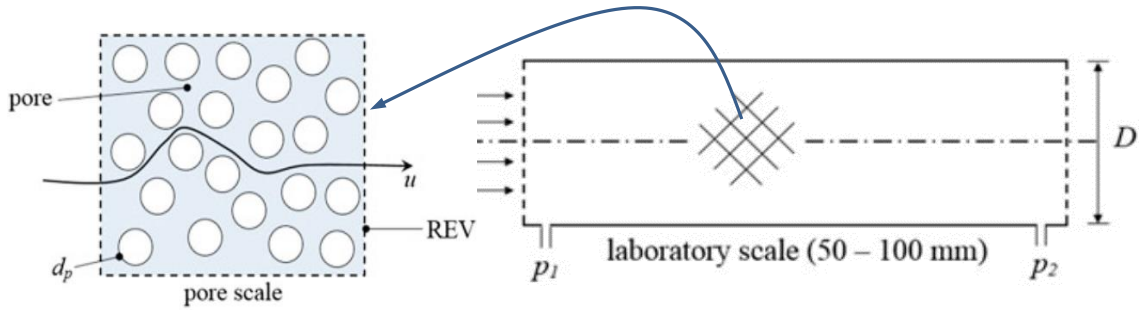

Figure I-10: A comparison of laboratory-, and REV- length scales [65]

I.7. Heterogeneity and Fracture modeling

A natural porous medium is likely to contain fractures and heterogeneities at certain length scale as explained earlier. Geologists often use precise terminology when they consider single fractures, which describe some of the features of these entities. Adler, et al., [66] presented in their book three major different kind of fracture according to their origin, we found that is convenient to cite theme by here:

1. A fault: is a fracture on which there has been an appreciable shear displacement of the material located on both sides; where the motion occurred parallel to the fracture plane, as shown in Fig. I-11a. A fault inevitably involves some crushed porous medium, except if it is filled by another mineral precipitation due to fluid circulation inside the fault zone.

2. A joint: is an open fracture in which there is an opening displacement normal to the fracture plane, as illustrated in Fig. I-11b. This kind of fracture includes bedding joints in sedimentary rocks and cooling joints in initially hot rock masses such as lavas.

3. A vein: is a mineralized impermeable fracture (see Fig. I-11c). Before its mineralization, the vein may or may not have encountered some shear displacement; however, some opening motion of the fracture necessarily occurred to create the free space.

Fissures, and cracks, are some other different employed terms, usually, they designate fractures of relatively small extensions [66].

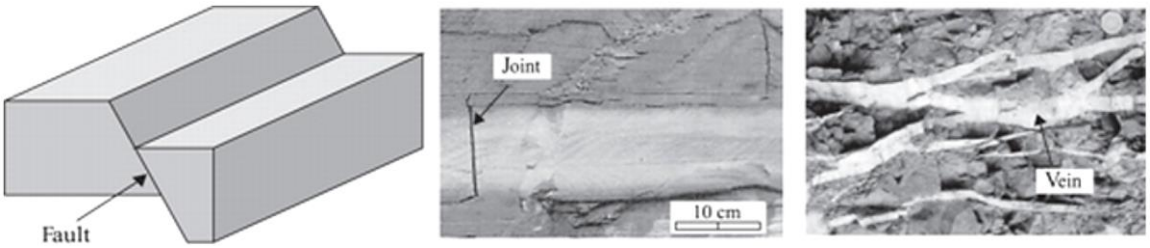

Figure I-11: Geological terminology of fractures: (a) a fault, (b) a joint, (c) veins (the scale is indicated by a coin in the upper right corner). (b) and (c) are from Ameen (1995), [66]

Several quite diverse studies investigate flow, dispersion, and displacement processes in porous and fractured media. In recent decades, analyses have been extended to include detailed structural properties of the media. Based on the physical phenomenon that is considered, these studies can be divided into two groups of models: the continuum models and discrete or network models.

I.7.1. Continuum models

Continuum models represent the classical engineering approach to describing materials of complex and irregular geometry, where several distinct length scales exist. The physical laws that govern flow and transport at the microscopic level are well expressed. Therefore, theoretically, it sounds possible to solve the differential conservation equations at the fluid-solid interface. However, practical and computationally, and economically feasible techniques, while available, are often not workable for solving such boundary-value problems due to the irregularity interface in typical porous media - even when knowing the detailed morphology of the porous medium.

We mean to point out that various models associated with the classical descriptions of the porous medium are continuum models. Due to their convenience and familiarity, continuum models have been vastly used in engineering. However, they do have some limitations, among them; they are not well- adequate for describing phenomena in which the connectivity of the pore space or the fracture network, or that of a fluid phase, plays a major role. Continuum models also collapse if there are correlations in the system with a range that is comparable with the linear size of the porous medium [60].

I.7.2. Discrete fracture models.

This class of models is free of the limitations of the continuum models. They describe phenomena at the microscopic level and have been extended recently to describe various phenomena at the macroscopic and even larger scales. Their main weakness, from a practical point of view, is the large computational effort required for a realistic discrete treatment of the pore space. Unlike continuum models, discrete fracture models are particularly useful when the effect of the pore space or fracture network connectivity is strong, or with long-range correlations [60]. A review of conceptual models and discretization approaches for flow in porous and fractured media is recently offered by [67].

I.8. Conclusion

In this chapter, the opportunity has been given to us to highlight various concepts and phenomena involved with thermosolutal convection in Porous and fractured media. Thus, we briefly present the various phenomenon having place under a thermal gradient including thermodiffusion, and the parameters characterizing the medium that host these physical phenomena (fractured porous medium). Generalities on transport phenomena in porous mediums, modelization of the Soret effect, the physical model chosen, the governing equations as well as the associated boundary conditions are assigned to the next chapter.

Chapter II

Fundamental theory

In this chapter, for information purposes, we will first look at the most important models used to determine the values of thermodiffusion factors. Then we will shift to the fundamental equations in porous media and the mathematical model used.

II.1. Theoritical models of thermodiffusion

For years, research has strived to determine reliable models for thermodiffusion coefficients. The most challenging problem is how to avoid the convection effects; this difficulty remains tough under the ground conditions. Therefore, the measurement conditions have to be precisely controlled. Several models have been proposed for binary mixture based on different theoretical approaches. These include the phenomenological theory of irreversible thermodynamics by Haase [68], the kinetic theory of irreversible thermodynamics by Rutherford & Roof [69], Shukla & Firoozabadi [70], the maximization of the partition function of two idealized bulbs by Kempers [71]. Partial molar properties derived from the equation of state are required for all the above models, which also affect the accuracy of the models [72]. The three most used models are defined by next:

II.1.1. Haase Model

The Hasse model [68] is based on the phenomenological approach. In the phenomenological approach, the equation of irreversible thermodynamics was used to derive an expression for the thermodiffusion factor, for binary systems in terms of the net heat of transport and chemical potential: as shown below:

$$\alpha_T = \frac{Q_2^* - Q_1^*}{x_1 \frac{\partial \mu_1}{\partial x_1}} \qquad \text{(II-1)}$$

Where: α_T the thermodiffusion factor in a binary mixture, x_1 is the mole fraction of component 1, μ_1 the chemical potential of component 1, $Q_i^* = Q_i - H_i$, the net heat of transport of the component, $i = 1,2$, H_i is the partial molar enthalpy of component i, and Q_i is the heat of transport of component i. The heat of transport is

interpreted as the difference between the energy required when a k-component molecule moves to its position in a temperature field and the energy given when its empty hole is filled with one of its neighboring molecules.

In the Hasse model [73], the net heat of transport is interpolated with the molar enthalpy in a conserved mass system. With this assumption, the net heat of transport is expressed in the following format with the thermostatic enthalpy values:

$$Q_2^* - Q_1^* = \frac{M_1 M_2}{M_1 x_1 + M_2 x_2}\left(\frac{H_2}{M_2} - \frac{H_1}{M_1}\right) \quad \text{(II-2)}$$

Where: H_i is the partial molar enthalpy of component i, M_i is the molecular weight of component i, $i = 1,2$.

The expression of the thermodiffusion factor in the Hasse model will then have the following form:

$$\alpha_T^H = \frac{M_1 H_2 - M_2 H_1}{(M_1 x_1 + M_2 x_2) x_1 \left(\frac{\partial \mu_1}{\partial x_1}\right)} \quad \text{(II-3)}$$

For ideal gas/liquid at a reference temperature, equation (II-3) gives:

$$Q_2^* - Q_1^* = \frac{M_1 M_2}{M_1 x_1 + M_2 x_2}\left(\frac{H_2}{M_2} - \frac{H_1}{M_1}\right) \quad \text{(II-4)}$$

Where R is the gas constant. Then the Hasse model can be re-written, with regard to a reference state, as follow:

$$\alpha_T^H = \frac{\alpha_T^0 RT(M_1 x_1 + M_2 x_2) + M_1(H_2 - H_2^0) - M_2(H_1 - H_1^0)}{(M_1 x_1 + M_2 x_2) x_1 \left(\frac{\partial \mu_1}{\partial x_1}\right)} \quad \text{(II-5)}$$

II.1.2. Kampers Model

The Kempers approach, [73] is based on a statistical description of a two-bulb system, which is similar to a system with a fixed volume at uniform pressure, without external forces. This assumption is equivalent to the following expression of the net heat of transport:

$$Q_2^* - Q_1^* = \frac{V_1 V_2}{V_1 x_1 + V_2 x_2}\left(\frac{H_2}{V_2} - \frac{H_1}{V_1}\right) \tag{II-6}$$

With V_i is the partial molar volume of the component $i = 1,2$, x_1 is the mole fraction of component 1, and H_i is the partial molar enthalpy of component i.

The thermodiffusion factor in the Kempers model is defined as:

$$\alpha_T^K = \frac{V_1 H_2 - V_2 H_1}{(V_1 x_1 + V_2 x_2) x_1 \left(\frac{\partial \mu_1}{\partial x_1}\right)} \tag{II-7}$$

II.1.3. Firoozabadi model

Firoozabadi et al. [70], [74], presented a model for binary mixtures of reservoir fluids, based on the thermodynamics of irreversible processes. In this model, the net heat of transport is related to the energy required to detach a molecule from its neighbors in the mixing region, and to the energy given up in that region where a molecule fills a hole. This energy is expressed in terms of the partial molar internal energy, and the ratio of the energy of vaporization to the energy of the viscous flow of the component. The net heat of transport is given by:

$$\begin{cases} Q_1^* = W_{H1} - \omega_1 \left(x_1 W_{H1} + x_2 W_{H2}\right) \\ Q_2^* = W_{H2} - \omega_2 \left(x_1 W_{H1} + x_2 W_{H2}\right) \end{cases} \tag{II-8}$$

where ω_i represents the volume fraction of molecules moving into a hole left by a molecule of type i in the mixture, which can be measured using molar fractions x_i $(i = 1,2)$ and partial molar volumes V_i $(i = 1,2)$:

$$\omega_1 = V_1/(x_1V_1 + x_2V_2)$$
$$\omega_2 = V_2/(x_1V_1 + x_2V_2) \quad \text{(II-9)}$$

The activation energy is given by:

$$\begin{cases} W_{H1} = -\dfrac{U_1}{\tau_1} \\ W_{H2} = -\dfrac{U_2}{\tau_2} \end{cases} \quad \text{(II-10)}$$

Where U_i is the partial internal molar energy of component i, and τ_i is the ratio of vaporization energy, ΔU_i^{Vap}, to viscous flow energy, ΔU_i^{Visc}.

$$\tau_i = \frac{\Delta U_i^{Vap}}{\Delta U_i^{Visc}} \quad \text{(II-11)}$$

Therefore, the thermodiffusion factor is defined in this model by:

$$\alpha_T^F = \frac{(U_1/\tau_1 - U_2/\tau_2)}{x_1\left(\frac{\partial \mu_1}{\partial x_1}\right)} + \frac{(V_2 - V_1)(x_1U_1/\tau_1 + x_2U_2/\tau_2)}{(V_1x_1 + V_2x_2)x_1\left(\frac{\partial \mu_1}{\partial x_1}\right)} \quad \text{(II-12)}$$

For a binary mixture, the net heat of transport for a component i in the mixture has been proposed by [74] as follows:

$$Q_i^* = -\frac{\Delta \overline{U}_i}{\tau_i} + \left(\sum_{j=1}^{n} \frac{x_j \Delta \overline{U}_j}{\tau_j}\right) \frac{V_i}{\sum_{j=1}^{n} x_j V_j} \quad \text{(II-13)}$$

Firoozabadi model was the first proposed for thermodiffusion in multicomponent mixtures. Among others, the performance of Firoozabadi model is, in general, much closer to the experimental data for different non-ideal mixtures. The implication of the non-equilibrium properties of the mixture in the model, as well as the equilibrium properties contribute to a better physical understanding of such a complex phenomenon as thermodiffusion , [73].

II.2. Fundamental equations in porous media

One way to obtain the laws governing the macroscopic variables for a discontinued medium is to apply the representative elementary volume (REV) method. This spatial approach leads to defining the macroscopic variables as an appropriate means, starting from standard equations that the fluid obeys over an area containing many pores. It is assumed that the result is independent of the size of the REV (see chapter I).

By introducing a Cartesian reference frame, and involving the REV approach, a continuum model for the porous medium is then created. Therefore, conservation laws can be applied.

II.2.1. Darcy Velocity Vs intrinsic Velocity

We mean by Darcy velocity the average fluid velocity taken over a volume element $\bar{V}$ of the medium, incorporating both solid and fluid material. This quantity is also known by seepage velocity, filtration velocity, superficial velocity and volumetric flux density. It is denoted $v_{seepage} = (u, v, w)$. However, the average fluid velocity taken with respect to a volume element v_f consisting of fluid only, is the intrinsic average velocity $v_{intrinsic}$. It is related to the seepage velocity (v_D) by the Dupuit–Forchheimer relationship $v_D = \varepsilon' \, v_{intrinsic}$, [2]. Where $\varepsilon'$is the porosity of the porous medium.

II.2.2. Continuity equation

Applying the conservation of mass on an elementary unit volume of the medium, and equating the rate of increases of fluid within that volume $\frac{\partial \, \varepsilon' \rho_f}{\partial t}$ to the mass flux into it $-\nabla.\left(\rho_f \overrightarrow{V_D}\right)$. The Continuity equation is written as fellow [2]:

$$\varepsilon' \frac{\partial \rho_f}{\partial t} + \nabla\left(\rho_f \overrightarrow{V_D}\right) = 0 \qquad \text{(II-14)}$$

Where ρ_f is the fluid density, and $\varepsilon'$is the porosity of the medium (independent of t).

For multicomponent mixture, the principle of mass conservation can be applied to each component in the mixture. In the absence of component generation, the continuity equation becomes:

$$\frac{\partial \rho_i}{\partial t} + \nabla.\left(\rho_i \vec{V}_i\right) = 0 \tag{II-15}$$

It should be noted that $\vec{V}_i$ is the intrinsic velocity of component i. where, subscript i refers to the i^{th} component.

Taking the sum of all the components, the equation becomes:

$$\frac{\partial \rho}{\partial t} + \nabla.\left(\sum \rho_i \vec{V}_i\right) = 0 \tag{II-16}$$

This is analogous to the equation:

$$\frac{\partial \rho}{\partial t} + \nabla.\left(\rho \vec{V}\right) = 0 \tag{II-17}$$

Where $\vec{V}$ is the mass average velocity, given by:

$$\vec{V} = \frac{1}{\rho}\sum \rho_i \vec{V}_i \tag{II-18}$$

The diffusive flux of the component i, can be expressed by:

$$j_i = \rho_i (V_i - \vec{V}) \tag{II-19}$$

The mass conservation equation thus becomes:

$$\frac{\partial \rho_i}{\partial t} + \nabla\left(\rho_i \vec{V}\right) = -\nabla j_i \tag{II-20}$$

For the case of a two-component mixture, if the migration of the first component is the only one of interest, then the subscript can be dropped. The mass conservation equation considering the entire porous medium can be obtained by multiplying the Eq. (II-20) by ε' as follow:

$$\varepsilon' \frac{\partial \rho_f}{\partial t} + \nabla(\rho_f \overrightarrow{V_D}) = -\nabla j_{pm} \quad \text{(II-21)}$$

Where $j_{pm} = \varepsilon' j$ is the diffusive mass flux in the porous medium, which is the rate of flow of mass across unit cross-sectional area of the medium. Considering Soret and Dufour effects, the mass conservation equation in the presense of thermal, solutal and pressure gradient appears as follow [2]:

$$\varepsilon' \frac{\partial \rho}{\partial t} + \nabla(\rho_f \overrightarrow{V_D}) = \varepsilon' \nabla(\mathrm{D}\nabla\vec{C} + \mathrm{D}_T \nabla\vec{T} + \mathrm{D}_p \nabla\vec{P}) \quad \text{(II-22)}$$

Where D, D_T and D_P are the mass diffusion coefficient, the thermodiffusion coefficient of the species, and the pressure diffusion coefficient respectively. Soret effect refers to the mass flux produced by a temperature gradient, and Dufour effect refers to the heat flux produced by a concentration gradient.

$$\vec{j} = -(\mathrm{D}\nabla\vec{C} + \mathrm{D}_T \nabla\vec{T} + \mathrm{D}_p \nabla\vec{P}) \quad \text{(II-23)}$$

II.2.3. Momentum equation

a) Darcy's equation

Darcy's experiments on hydrology (1856) revealed a proportionality between flow rate and the applied pressure difference; it can be expressed by [2]:

$$u = -\frac{K}{\mu}\frac{\partial P}{\partial x} \quad \text{(II-24)}$$

Where u is a unidirectional velocity, $\partial P/\partial x$ is the pressure gradient in the flow direction, and μ is the dynamic viscosity of the fluid. K is the intrinsic permeability of the medium, it can be either a second-order tensor for three dimensions' flow, or a scalar for isotropic porous medium. It should be noted that in Eq. (II-24), P denotes an intrinsic quantity, and that Darcy's equation is not a balance of forces averaged over a R.E.V. The Darcy's equation can be written in a simple form as follow:

$$\nabla P = -\frac{\mu}{K} V_D \quad \text{(II-25)}$$

Many early authors used an extension of Eq. (II-25), of the form [2]:

$$\rho_f \left[\frac{\partial V}{\partial t} + (\mathrm{V}.\nabla)\mathrm{V}\right] = -\nabla P - \frac{\mu}{K}\mathrm{V}_D \tag{II-26}$$

Where, V is the intrinsic velocity, and V_D is the seepage or Darcy velocity. Using Dupuit–Forchheimer relationship, Eq. (II-26) becomes:

$$\rho_f \left[\frac{1}{\varepsilon'}\frac{\partial \mathrm{V}_D}{\partial t} + \frac{1}{\varepsilon'^2}(\mathrm{V}_D.\nabla)\mathrm{V}_D\right] = -\nabla P - \frac{\mu}{K}\mathrm{V}_D \tag{II-27}$$

Where ρ_f is the fluid density, and ε' is the porosity of the medium. Eq. (II-27) was obtained by analogy with the Navier-Stocks equation. The term $(\mathrm{V}_D.\nabla)\mathrm{V}_D$ doesn't explain the physical meaning in some cases, it is identically zero for steady incompressible unidirectional flow no matter how large the fluid velocity. Since this term is small compared with the quadratic drag term (Forchheimer's Equation) it seems best to drop it in numerical work. Eq. (II-27) then becomes:

$$\frac{\rho_f}{\varepsilon'}\frac{\partial \mathrm{V}_D}{\partial t} = -\nabla P - \frac{\mu}{K}\mathrm{V}_D \tag{II-28}$$

The left-hand side of this equation represents the remaining inertial term. To avoid the inadequacy of this equation, it can be replaced by:

$$\rho_f \mathrm{c}_a \frac{\partial \mathrm{V}_D}{\partial t} = -\nabla P - \frac{\mu}{K}\mathrm{V}_D \tag{II-29}$$

Where c_a is the acceleration coefficient tensor that depends sensitively on the geometry of the porous medium [2].

b) Forchheimer's Equation

Darcy's equation (II-24) remains valid when V_D is sufficiently small. In other words, the Reynolds number is of the order of unity or smaller. While V_D increases the form drag due to solid obstacles is now comparable with the Surface drag due to

friction. The appropriate modification to Darcy's equation is to replace Eq. (II-25) by:

$$\nabla P = -\frac{\mu}{K}\mathrm{V}_D - \frac{\mathrm{c}_F}{\sqrt{K}}\rho_f|\mathrm{V}_D|\mathrm{V}_D \qquad \text{(II-30)}$$

where c_F is a dimensionless form-drag constant. Eq. (II-30) is a modification of an equation associated with the names of Dupuit (1863) and Forchheimer (1901) (Nield & Bejan, 2013).

c) Brinkman's Equation

An alternative to Darcy's equation is what is commonly known as Brinkman's equation. It is expressed without the inertial terms. It takes the following form:

$$\nabla P = -\frac{\mu}{K}\mathrm{V}_D + \mu_e\nabla^2\mathrm{V}_D \qquad \text{(II-31)}$$

Where μ_e is the effective viscosity, and P is the intrinsic fluid pressure. As the permeability K approaches zero, the first right term becomes more significant, which makes this equation is equivalent to Darcy's equation. However, for highly permeable porous media, the first right term becomes negligible, then the equation becomes analogous to the Navier-stokes equation.

II.2.4. Energy equation

First, a simple situation is proposed, in which the medium is isotropic and where viscous dissipation, radiative effects, and the work done by pressure changes are negligible. Taking averages over an elemental volume of the medium, and applying the conservation law for the energy, equations for solid and liquid phases are as follow:

$$(1-\varepsilon')(\rho\mathrm{c})_s\frac{\partial \mathrm{T}_s}{\partial t} = (1-\varepsilon')\nabla.(\lambda_s\nabla\mathrm{T}_s) + (1-\varepsilon')q_s^{''} \qquad \text{(II-32)}$$

$$\varepsilon'(\rho c_P)_f \frac{\partial T_f}{\partial t} + (\rho c_P)_f V_D . \nabla T_f = \varepsilon' \nabla . (\lambda_f \nabla T_f) + \varepsilon' q_f^{"} \quad \text{(II-33)}$$

The subscripts s and f refers to solid and fluid phases respectively. c is the specific heat of the solid, c_P is the specific heat at constant pressure of the fluid, λ is the thermal conductivity, $\nabla . (\lambda \nabla T)$ is the net rate of heat conduction, and $q"$ (W/m^3) is the heat production per unit volume. A convective term $(V_D . \nabla T_f)$ appears in Eq. (II-33). Assuming that there is local thermal equilibrium so that $T_s = T_f = T$, where T_s and T_f are the temperatures of the solid and fluid phases, respectively. Here we also assume that heat conduction in the solid and fluid phases takes place in parallel so that there is no net heat transfer from one phase to the other, we have [2]:

$$(\rho c)_e \frac{\partial T}{\partial t} + (\rho c_P)_f V_D . \nabla T_f = \nabla . (\lambda_e \nabla T) + q_e^{"} \quad \text{(II-34)}$$

Whith

$$\left.\begin{aligned} (\rho c)_e &= (1-\varepsilon')(\rho c_P)_s + \varepsilon'(\rho c_P)_f \\ \lambda_e &= (1-\varepsilon')\lambda_s + \varepsilon' \lambda_f \\ q_e^{"} &= (1-\varepsilon') q_e^{"} + \varepsilon' q_e^{"} \end{aligned}\right\} \quad \text{(II-35)}$$

Where $(\rho c)_e, \lambda_e$, and $q_e^{"}$ are, respectively, the overall heat capacity per unit volume, overall thermal conductivity, and overall heat production per unit volume of the medium.

II.3. Description of the problem

We propose to study the phenomenon of double-diffusive convection in a confined space. The two-dimensional geometric configuration is shown in Fig. II-1. We consider the case of a rectangular cavity of the following dimensions: length L', and height H', continuing a porous medium saturated with a binary fluid. The active vertical walls of the cavity are subjected to uniform heat, q', and mass, j' fluxes. The other walls are considered adiabatic and impermeable.

In the present study, the cavity is placed in a uniform constant gravity field $\vec{g}$. The interaction between gravity and temperature and solute gradients gives rise to natural convective motions. The latter is essentially due to the non-uniform distribution of the density of the fluid generated by the factors mentioned above. Particular attention will be paid in this work to fractured porous media, where the fracture is considered as a porous media characterized by distinct permeabilities. The heat and mass transfers induced by the thermosolutal convection movements will be determined as well. In this study, some simplifying assumptions will be adopted to alleviate the complexity of the problem.

II.3.1. Simplifying assumptions

During our study, several approximations were adopted in order to simplify the formulation of the mathematical model:

- ✓ The fluid solution is Newtonian and incompressible.
- ✓ The flow generated is assumed to be laminar; Steady Darcy Law is adopted.
- ✓ The porous matrix is isotropic, permeable, and homogeneous.
- ✓ There is no chemical reaction, no source of heat or mass.
- ✓ Radiant heat transfer is negligible
- ✓ Dufour's heat diffusion effect is disregarded.
- ✓ The work induced by viscous and pressure forces is negligible.
- ✓ The thermophysical properties of the fluid are constant and are evaluated at the reference temperature. However, the fluid density in the volume forces terms alters linearly with temperature. This is given by the following Boussinesq relation:

$$\rho = \rho_0[1 - \beta_T(T' - T_0') - \beta_s(C' - C_0')] \quad \text{(II-36)}$$

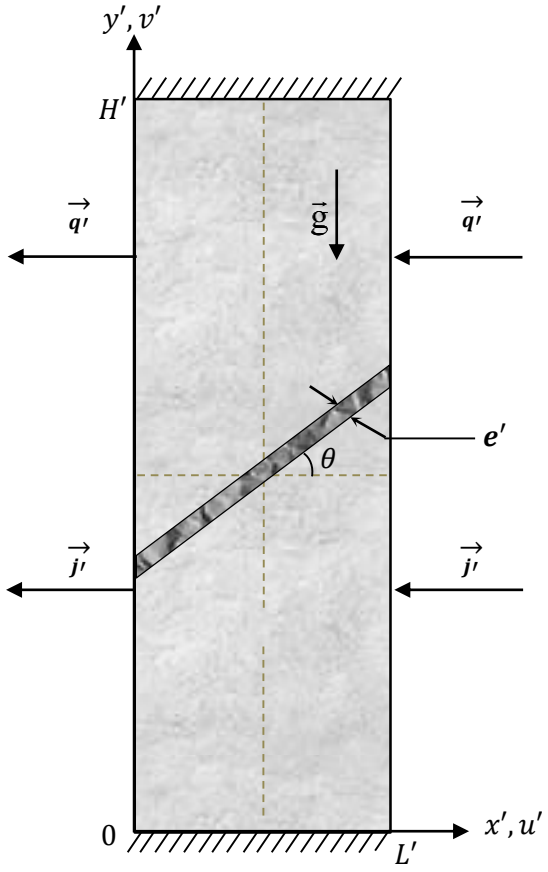

Figure II-1: Geometry of the physical system

$T'$and C' represent the temperature of the fluid mixture and the concentration of the solute at a given point in the system, respectively. T_0', C_0' and ρ_0 are reference quantities which generally represent the average values of the temperature and the concentration in the system.

In equation (II-36), β_T and β_S are the thermal and solutal volume expansion coefficients of the fluid respectively. They are defined by:

$$\beta_T = -\frac{1}{\rho_0}\left(\frac{\partial \rho}{\partial T'}\right)_{P',T'} \quad \beta_S = -\frac{1}{\rho_0}\left(\frac{\partial \rho}{\partial C'}\right)_{P',T'} \tag{II-37}$$

In general, β_T is positive for all fluids, while β_S can be positive or negative depending on the solute considered.

II.3.2. Mathematical formulation

To study the phenomenon of natural convection in porous media, we assume that the porous matrix is solid, permeable, isotropic and saturated with fluid. Darcy's model, which neglects inertial forces, is adopted. These forces can be neglected when:

$$\left.\begin{array}{c} \varepsilon < 0.8 \\ Da \leq 10^{-6} \\ Re < 1 \end{array}\right\} \quad \text{(II.38)}$$

Where ε is the porosity of the porous medium, Da and Re: are the Darcy and Reynolds numbers. These are defined by:

$$\left.\begin{array}{c} Da = \frac{K}{L'} \\ Re = \frac{V_D \overline{d_e}}{\nu} \end{array}\right\} \quad \text{(II-39)}$$

Where V_D is the average velocity of the fluid particles through the solid matrix, K the permeability of the porous medium, ν the kinematic viscosity of the fluid and $\overline{d_e}$ the effective average pores diameter.

In this study, Eq. (II-38) is satisfied. Otherwise, inertial and viscous forces, known as Forchheimer's and Brinkman's, must be taken into account.

The equations relating to heat and mass fluxes in the presence of thermal and solutal gradients are given by De Groot & Mazur [75] :

$$\overrightarrow{q'} = -\lambda \nabla T' \quad \text{(II-40)}$$

$$\overrightarrow{J'} = -\rho D \nabla C' - \rho D_T C_0' (1 - C_0') \nabla T' \quad \text{(II-41)}$$

Where the second term represent the thermodiffusion (Soret) effect, D is the mass diffusivity, D_T is the thermodiffusion coefficient, λ is the thermal conductivity, and C_0' and $\nabla C'$ are the reference solute concentration and the characteristic solute concentration respectively.

The basic equations governing flow, heat and mass transfer are listed below:

a) Continuum equation

The continuity equation expressing the principle of mass conservation for a moving fluid is given by:

$$\frac{\partial u'}{\partial x'} + \frac{\partial v'}{\partial y'} = 0 \tag{II-42}$$

b) Momentum Equation

The formulation of the momentum conservation equation is written as follows:

$$u' = -\frac{K}{\mu}\frac{\partial P'}{\partial x'} \tag{II-43}$$

$$v' = -\frac{K}{\mu}\left[\frac{\partial P'}{\partial y'} + \rho g\right] \tag{II-44}$$

where K is the permeability of the porous medium, μ is the dynamic viscosity, β_T and β_s are the thermal and solutal expansion coefficients and P' is the hydrodynamic pressure. By eliminating the pressure P between Eq. (II-43) and Eq. (II-44) and by invoking the Boussinesq approximation Eq. (II-36) in the body force term ρg of Eq. (II-44), we obtain a single equation for momentum conservation:

$$\frac{\partial u'}{\partial y'} + \frac{\partial v'}{\partial x'} = -\frac{K}{\upsilon} g\left[-\beta_T \frac{\partial T'}{\partial x'} - \beta_s \frac{\partial C'}{\partial x'}\right] \tag{II-45}$$

Where υ is the kinematic viscosity μ/ρ_0. Involving the stream function ψ defined by $u' = \frac{\partial \psi'}{\partial y'}$ and $v' = \frac{\partial \psi'}{\partial x'}$, Eq. (II-43) becomes:

$$\frac{\partial^2 \psi'}{\partial x'^2} + \frac{\partial^2 \psi'}{\partial y'^2} = -\frac{K}{\upsilon} g\left[-\beta_T \frac{\partial T'}{\partial x'} - \beta_s \frac{\partial C'}{\partial x'}\right] \tag{II-46}$$

c) Energy conservation equations

Based on the first law of thermodynamics the energy conservation equation is written as follows:

$$(\rho C_P)_P \frac{\partial T'}{\partial t'} + (\rho C_P)_f \left(u' \frac{\partial T'}{\partial x'} + v' \frac{\partial T'}{\partial y'} \right) = \lambda \nabla^2 T' \qquad \text{(II-47)}$$

where the viscous dissipation terms are neglected. ρC_P is the volumetric heat capacity, and λ is the thermal conductivity of the porous medium.

d) Mass conservation equation

The principle of conservation of mass leads to the following concentration equation:

$$\varepsilon' \frac{\partial C'}{\partial t'} + u' \frac{\partial C'}{\partial x'} + v' \frac{\partial C'}{\partial y'} = D \nabla^2 C' + D_T C'(1 - C') \nabla^2 T' \qquad \text{(II-48)}$$

Where $\bar{u}'$ and $\bar{v}'$ are the components of the velocity vector $\vec{v}'$ in the x' and y' directions, respectively, μ is the dynamic viscosity, λ and ε' are the thermal conductivity and the porosity of the medium porous respectively.

In general, it is assumed that the Soret effect is small, so the expression $C'(1 - C')$ can be taken approximately equal to $C_0'(1 - C_0')$. As we are studying dilute solutions, $C_0' \ll 1$ so $C_0'(1 - C_0') = C_0'$. Equation (II-46) then becomes:

$$\varepsilon' \frac{\partial C'}{\partial t'} + u' \frac{\partial C'}{\partial x'} + v' \frac{\partial C'}{\partial y'} = D \nabla^2 C' + D_T C_0' \nabla^2 T' \qquad \text{(II-49)}$$

To write the equations (II-42), (II-46), (II-47), and (II-49) in the dimensionless form, the following dimensionless variables are introduced:

$$(x, y) = \left(\frac{x'}{H'}, \frac{y'}{H'} \right) \qquad (u, v) = \left(\frac{u' H'}{\alpha}, \frac{v' H'}{\alpha} \right)$$
$$t = \frac{t' \alpha}{H'^2 \sigma} \qquad \varepsilon = \frac{\varepsilon'}{\sigma} \qquad \psi = \frac{\psi'}{\alpha} \qquad \text{(II-50)}$$
$$C = \frac{(C' - C_0')}{\Delta C'} \qquad T = \frac{(T' - T_0')}{\Delta T'}$$

The characteristic parameters are as follow: length $l^* = H'$, time $t^* = \frac{H'^2\sigma}{\alpha}$, velocity $v^* = \frac{\alpha}{H'}$, temperature $\Delta T' = q'H'/\lambda$, and concentration $\Delta C' = j'H'/D$

By introducing the dimensionless variables (II.50) into equations (II-46), (II-47), and (II-49) we obtain the following dimensionless equations:

$$\nabla^2\psi = -aR_T\left(\frac{\partial T}{\partial x} + N\frac{\partial C}{\partial x}\right) \qquad \text{(II-51-A)}$$

$$\frac{\partial T}{\partial t} + \frac{\partial(uT)}{\partial x} + \frac{\partial(vT)}{\partial y} = \nabla^2 T \qquad \text{(II-51-B)}$$

$$\eta\varepsilon\frac{\partial C}{\partial t} + \frac{\partial(uC)}{\partial x} + \frac{\partial(vC)}{\partial y} = \frac{1}{Le}\left(\nabla^2 C + S_P\nabla^2 T\right) \qquad \text{(II-51-C)}$$

The dimensionless velocity components are calculated as follows:

$$u = \frac{\partial\psi}{\partial y}$$
$$v = -\frac{\partial\psi}{\partial x} \qquad \text{(II-52)}$$

Where η is the ratio of the fracture's porosity to the porous medium's porosity $\eta = \varepsilon_F/\varepsilon$. While, a is the ratio of the fracture's Rayleigh number to the porous medium's Rayleigh number $a = R_{TF}/R_T$. We add these two parameters to assign the fracture's permeability, and porosity. For the porous medium $a = \eta = 1$. The non-dimensional governing parameters appearing in the equations are the thermal Darcy-Rayleigh number, R_T, the Lewis number Le, the buoyancy ratio N, the Soret parameter, Sp, and the aspect ratio, A. They are defined in equation (II-53).

$$R_T = \frac{g\beta_T K\Delta T' H'}{\alpha\nu} \quad Le = \frac{\alpha}{D} \quad N = \frac{\beta_S\Delta C'}{\beta_T K\Delta T'}$$
$$Sp = \frac{D_T C_0'\Delta T'}{D\Delta C'} \quad A = \frac{H'}{L'} = 5 \qquad \text{(II-53)}$$

Note, that the classical separation ratio φ is related to S_p and N by the relation $\varphi = S_p N$ [76].

e) boundary conditions

In terms of dimensionless variable, the boundary conditions are defined in equation (II-54):

$$\left.\begin{array}{llllll} \forall y \in [0,\ \ 1]; & x = 0, \frac{1}{A}: & \psi = 0, & \frac{\partial T}{\partial x} = 1, & \frac{\partial C}{\partial x} = 1 - Sp \\ \forall x \in \left[0, \frac{1}{A}\right]; & y = 0,1: & \psi = 0, & \frac{\partial T}{\partial x} = 0, & \frac{\partial C}{\partial x} + Sp\frac{\partial T}{\partial y} = 0 \end{array}\right\} \quad \text{(II-54)}$$

The heat and mass transfer rates, quantified in terms of the Nusselt and Sherwood numbers, can be calculated from the following expressions:

$$\begin{aligned} Nu &= \frac{1}{\nabla T} = \frac{1}{T(L', H'/2) - T(0, H'/2)} \\ Sh &= \frac{1}{\nabla C} = \frac{1}{C(L', H'/2) - C(0, H'/2)} \end{aligned} \quad \text{(II-55)}$$

The mathematical model is applied to the entire cavity. Moreover, a specific permeability is applied to the fracture, which is expressed by a different Rayleigh number (R_{TF}).

II.4. Conclusion

In this second chapter, we have presented different models determining the Soret effect in multicomponent mixtures. Generalities on transport phenomena in porous mediums, the Darcy equation, the chosen physical and the adopted mathematical model as well as the associated boundary conditions, are well detailed.

The obtained dimensionless equations governing flow, heat, and mass transfer are discretized using a central finite difference scheme and solved with the alternate direction implicit (ADI) method. The numerical solving process and the validation of the Fortran code will be the subject of the next chapter.

Chapter III

Numerical Solution

III.1. Introduction

The Nonlinear differential equations system presented in the previous chapter is solved numerically based on the finite difference technique. This method consists in approximating the derivatives of the equations of physics by means of Taylor expansions and is deducted directly from the definition of the derivative. It is due to the work of several 18th-century mathematicians (Euler, Taylor, Leibniz ...). It turns out to be the most suitable and the easiest to use for simple geometry problems. This method consists in discretizing the continuous equations at the nodes of a predefined mesh.

In a Cartesian coordinate system, each node is designated by the pair of indices (i , j) designating the intersection lines of the mesh. Neighboring nodes are implicitly defined by increasing or decreasing one of the indices by a unit increment (see Fig. III-1).

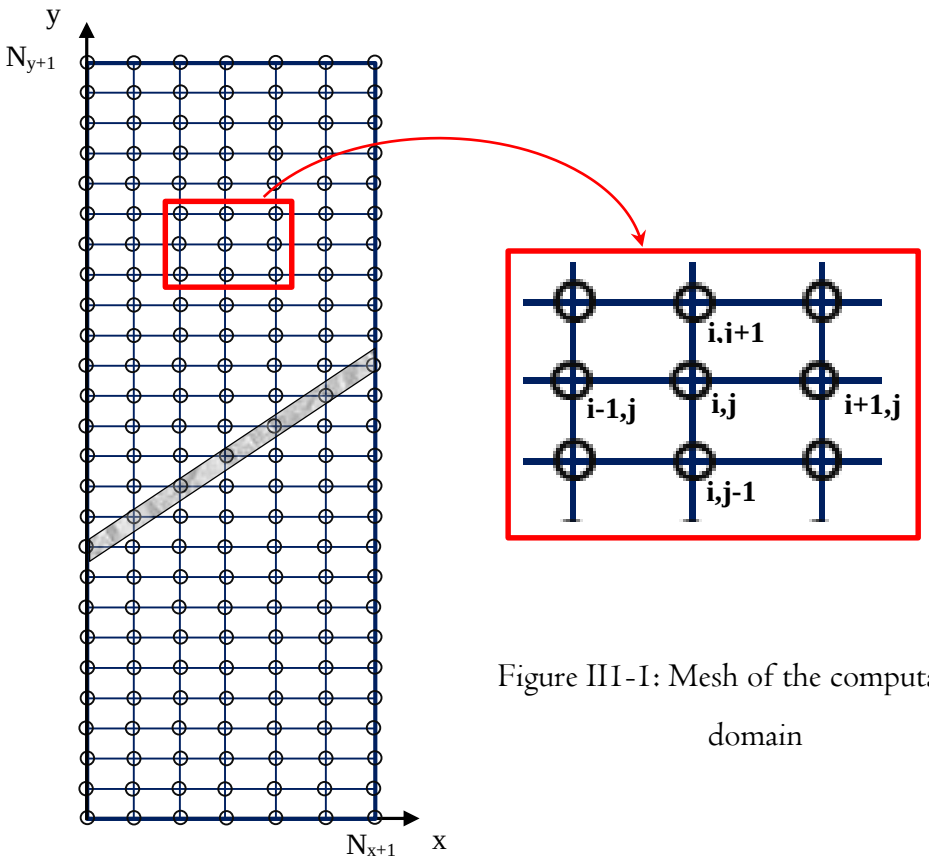

Figure III-1: Mesh of the computational domain

III.2. Methods of Numerical solution

The energy equation (II-51-B) and the concentration equation (II-51-C) are discretized by the finite difference method with a second-order centric scheme. The resolution will be made by the method of alternating directions with the algorithm of Thomas.

The alternating direction implicit method (ADI) consists of dividing the time step into two steps, in the first step is advanced with $\Delta t/2$, and the system is solved implicitly on "X" and explicit on "Y", in the second step We advance with $\Delta t/2$ and the system is resolved explicitly on "X" and implicit on "Y". For each time step the alternating directions implicit method (ADI) gives rise to two tri-diagonal matrix systems to be solved, one resulting from the implicit discretization on X and the other from the implicit discretization on Y.

For each time step, the solution is obtained by scanning the computational domain in the x direction then in that of the y. Knowing the fields of the temperature and of the concentration at the instant (n + 1) Δt, the next step consists of determining the field of the stream function from equation (II-51-A), once discretized with a centered order method and solved with the successive over-relaxation method (SOR) which is an explicit method directly giving the value of Ψ at time (n + 1) Δt, at the node considered, with a sufficient number of iterations so that the desired convergence criterion is satisfied.

III.3. Discretization of the energy equation

The energy equation (II-51-B) can be written in the following form:

$$\frac{\partial T}{\partial t}+\frac{\partial (uT)}{\partial x}+\frac{\partial (vT)}{\partial y}=\frac{\partial^2 T}{\partial x^2}+\frac{\partial^2 T}{\partial y^2} \qquad \text{(III-1)}$$

Implicite in "x" and explicite in "y" directions :

Each term of equation (III-1) is discretized as follows:

$$\frac{\partial T}{\partial t} \approx \frac{T^{k+1/2}(i,j) - T^{k}(i,j)}{\Delta t / 2} = \left[T^{k+1/2}(i,j) - T^{k}(i,j) \right] \times 2 \times DTI \qquad \text{(III-2)}$$

Terms related to x:

$$\left.\frac{\partial (uT)}{\partial x}\right|_{i,j} \approx \left[u(i+1,j)^{k} T(i+1,j)^{k+1/2} - u(i-1,j)^{k} T(i-1,j)^{k+1/2} \right] \times D2XI \qquad \text{(III-3)}$$

$$\frac{\partial^2 T}{\partial x^2} \approx \left[T(i+1,j)^{k+1/2} + T(i-1,j)^{k+1/2} - 2T(i,j)^{k+1/2} \right] \times DX2I \qquad \text{(III-4)}$$

Terms related to y:

$$\frac{\partial (vT)}{\partial y} \approx \left[v(i,j+1)^{k} T(i,j+1)^{k} - v(i,j-1)^{k} T(i,j-1)^{k} \right] \times D2YI \qquad \text{(III-5)}$$

$$\frac{\partial^2 T}{\partial y^2} \approx \left[T(i,j+1)^{k} + T(i,j+1)^{k} - 2T(i,j)^{k} \right] \times DY2I \qquad \text{(III-6)}$$

Where:

$$D2XI = 1/(2\Delta x); \quad D2YI = 1/(2\Delta y); \quad DTI = 1/\Delta t;$$
$$DX2I = 1/\Delta x^2; \quad DY2I = 1/\Delta y^2; \qquad \text{(III-7)}$$

Replacing all the terms eq. (III-2) to eq. (III-6) in the energy equation (III-1), the outcomes can be written as:

$$\mathrm{A(i)}T(i-1,j)^{k+1/2} + B(i)T(i,j)^{k+1/2} + C(i)T(i+1,j)^{k+1/2} = D(i) \qquad \text{(III-8)}$$

Where:

$$\begin{aligned} A(i) &= -DX2I - D2XI \times u(i-1,j)^{k} \\ B(i) &= 2(DX2I + DTI) \\ C(i) &= -DX2I + D2XI \times u(i+1,j)^{k} \\ D(i) = &\left[DY2I + D2YI \times v(i,j-1)^{k} \right] \times T(i,j-1)^{k} \\ &+ 2(-DY2I + DTI) \times T(i,j)^{k} \\ &+ \left[+DY2I - D2YI \times v(i,j+1)^{k} \right] \times T(i,j+1)^{k} \end{aligned} \qquad \text{(III-9)}$$

If we discretize "NX" intervals in the "x" direction with a step of "Δx", we will have "NX + 1" points. Hence, our system will be applied from i = 2 to i = NX for

the interior nodes. Resulting in a Tridiagonal matrix system Eq. (III-10). To solve this system, we can use Thomas' algorithm, It is thus necessary to eliminate the A(2) and the C(NX) to solve the matrix. While, the first and the last nodes, i = 1 and i = NX + 1 will be reserved to the boundary conditions.

$$\begin{bmatrix} b_2 & c_2 & & & 0 \\ a_3 & b_2 & c_3 & & \\ & \ddots & \ddots & \ddots & \\ & & \ddots & \ddots & c_{n-1} \\ 0 & & & a_n & b_n \end{bmatrix} \begin{bmatrix} x_2 \\ x_3 \\ \vdots \\ x_n \end{bmatrix} = \begin{bmatrix} d_2 \\ d_3 \\ \vdots \\ d_n \end{bmatrix} \qquad \text{(III-10)}$$

We discretize the active boundary condition $\partial T / \partial x = 1$, we use a second order upwind scheme for i=1, and a second Order Backward difference scheme for i=N_{x+1} we have:

$$\left.\frac{\partial T}{\partial x}\right|_{i=1} \approx \frac{-3T(1,j)+4T(2,j)-3T(3,j)}{2\Delta x} = 1$$

$$\Rightarrow \quad T(1,j) = \frac{4}{3}T(2,j) - \frac{1}{3}T(3,j) - \frac{2}{3}\Delta x \qquad \text{(III-11)}$$

$$\left.\frac{\partial T}{\partial x}\right|_{i=Nx+1} \approx \frac{3T(N_{x+1},j)-4T(N_x,j)+T(N_{x-1},j)}{2\Delta x} = 1$$

$$\Rightarrow \quad T(N_{x+1},j) = \frac{4}{3}T(N_x,j) - \frac{1}{3}T(N_{x-1},j) + \frac{2}{3}\Delta x \qquad \text{(III-12)}$$

for i = 2 we have:

$$\text{A(2)}T(1,j) + B(2)T(2,j) + C(2)T(3,j) = D(2) \qquad \text{(III-13)}$$

Replacing $T(1,j)$ from eq. (III-11) we find:

$$A(2)\left[\frac{4}{3}T(2,j) - \frac{1}{3}T(3,j) - \frac{2}{3}\Delta x\right] + B(2)T(2,j) + C(2)T(3,j) = D(2) \qquad \text{(III-14)}$$

To eliminate A(2), eq. (III-14) Can be rewritten as:

$$\underbrace{0}_{newA(2)} + \underbrace{\left[B(2)+\frac{4}{3}A(2)\right]}_{newB(2)}T(2,j) + \underbrace{\left[C(2)-\frac{1}{3}A(2)\right]}_{newC(2)}T(3,j) = \underbrace{D(2)+\frac{2}{3}A(2)\Delta x}_{newD(2)} \quad \text{(III-15)}$$

for i = Nx we have:

$$A(N_X)T(N_{X-1},j) + B(N_X)T(N_X,j) + C(N_X)T(N_{X+1},j) = D(N_X) \quad \text{(III-16)}$$

replacing $T(N_{X+1},j)$ from eq. (III-12) we find:

$$A(N_X)T(N_{X-1},j) + B(N_X)T(N_X,j) + C(N_X)\left[\frac{4}{3}T(N_x,j) - \frac{1}{3}T(N_{x-1},j) + \frac{2}{3}\Delta x\right] = D(2) \quad \text{(III-17)}$$

To eliminate C(Nx), eq. (III-17) Can be rewritten as:

$$\underbrace{\left[A(N_X)-\frac{1}{3}C(N_X)\right]}_{newA(N_X)}T(N_{X-1},j) + \underbrace{\left[B(N_X)+\frac{4}{3}C(N_X)\right]}_{newB(N_X)}T(N_X,j) + \underbrace{0}_{newC(N_X)} = \underbrace{D(2)-\frac{2}{3}C(N_X)\Delta x}_{newD(N_X)} \quad \text{(III-18)}$$

Implicite in "y" and explicite in "x" directions :

We proceed the remaining time half step. Terms following "y" will be taken at the time "k + 1" and those following "x" will be taken at the time "k + 1/2". The terms in "k + 1" are unknowns and one seeks to calculate them, those in "k + 1/2" are known since they have already been calculated. The discretization of the energy equation eq. (III-1) terms are given by:

$$\frac{\partial T}{\partial t} \approx \frac{T^{k+1}(i,j) - T^{k+1/2}(i,j)}{\Delta t/2} = \left[T^{k+1}(i,j) - T^{k+1/2}(i,j)\right] \times 2 \times DTI \quad \text{(III-19)}$$

Terms related to x:

$$\left.\frac{\partial^2 T}{\partial x^2}\right|_{i,j} \approx \left[T(i+1,j)^{k+1/2} - 2T(i,j)^{k+1/2} + T(i-1,j)^{k+1/2}\right] \times DX2I \quad \text{(III-20)}$$

$$\left.\frac{\partial (uT)}{\partial x}\right|_{i,j} \approx \left[u(i+1,j)^k T(i+1,j)^{k+1/2} - u(i-1,j)^k T(i-1,j)^{k+1/2}\right] \times D2XI \quad \text{(III-21)}$$

Terms related to y:

$$\left.\frac{\partial^2 T}{\partial y^2}\right|_{i,j} \approx \left[T(i,j+1)^{k+1} - 2T(i,j)^{k+1} + T(i,j-1)^{k+1}\right] \times DY2I \qquad \text{(III-22)}$$

$$\left.\frac{\partial (vT)}{\partial y}\right|_{i,j} \approx \left[v(i,j+1)^k T(i,j+1)^{k+1} - v(i,j-1)^k T(i,j-1)^{k+1}\right] \times D2YI \qquad \text{(III-23)}$$

Where:

$D2XI = 1/(2\Delta x)$; $D2YI = 1/(2\Delta y)$; $DTI = 1/\Delta t$;
$DX2I = 1/\Delta x^2$; $DY2I = 1/\Delta y^2$; are defined in Eq. (III-7)

Replacing all the terms eq. (III-16) to eq. (III-20) in the energy equation (III-1), the outcomes can be written as:

$$A(j)T(i,j-1)^{k+1} + B(j)T(i,j)^{k+1} + C(j)T(i,j+1)^{k+1} = D(j) \qquad \text{(III-24)}$$

Where:

$$\begin{aligned} A(j) &= -DY2I - D2YI \times v(i,j\text{-}1)^k \\ B(j) &= 2(DY2I + DTI) \\ C(j) &= -DY2I + D2YI \times v(i,j\text{+}1)^k \\ D(j) &= \left[DX2I + D2XI \times u(i\text{-}1,j)^k\right] \times T(i\text{-}1,j)^{k+1/2} \\ &\quad + 2(-DX2I + DTI) \times T(i,\ j)^{k+1/2} \\ &\quad + \left[+DX2I - D2XI \times u(i\text{+}1,j)^k\right] \times T(i\text{+}1,j)^{k+1/2} \end{aligned} \qquad \text{(III-25)}$$

We discretize the adiabatic boundary condition $\partial T/\partial y = 0$, we use a second order upwind scheme for j=1, and a second Order Backward difference scheme for j=N_{Y+1} we have:

$$\left.\frac{\partial T}{\partial y}\right|_{j=1} \approx \frac{-3T(i,1) + 4T(i,2) - 3T(i,3)}{2\Delta y} = 0$$

$$\Rightarrow \quad T(i,1) = \frac{4}{3}T(i,2) - \frac{1}{3}T(i,3) \qquad \text{(III-26)}$$

$$\left.\frac{\partial T}{\partial y}\right|_{j=Ny+1} \approx \frac{3T(i,N_{y+1}) - 4T(i,N_y) + T(i,N_{y-1})}{2\Delta y} = 0$$

$$\Rightarrow \quad T(i,N_{y+1}) = \frac{4}{3}T(i,N_y) - \frac{1}{3}T(i,N_{y-1}) \qquad \text{(III-27)}$$

For j = 2 we have:

$$A(2)T(i,1)+B(2)T(i,2)+C(2)T(i,3)=D(2) \tag{III-28}$$

Replacing $T(1,j)$ from eq. (III-23) we find:

$$A(2)\left[\frac{4}{3}T(i,2)-\frac{1}{3}T(i,3)\right]+B(2)T(i,2)+C(2)T(i,3)=D(2) \tag{III-29}$$

To eliminate A(2), eq. (III-26) Can be rewritten as:

$$\underbrace{0}_{newA(2)}+\underbrace{\left[B(2)-\frac{4}{3}A(2)\right]}_{newB(2)}T(i,2)+\underbrace{\left[C(2)+\frac{1}{3}A(2)\right]}_{newC(2)}T(i,3)=\underbrace{D(2)}_{newD(2)} \tag{III-30}$$

For j = Ny we have:

$$A(N_y)T(i,N_{y-1})+B(N_y)T(i,N_y)+C(N_y)T(i,N_{y+1})=D(N_y) \tag{III-31}$$

Replacing $T(i,N_{y+1})$ from eq. (III-27) we find:

$$A(N_y)T(i,N_{y-1})+B(N_y)T(i,N_y)+C(N_y)\left[\frac{4}{3}T(i,N_y)-\frac{1}{3}T(i,N_{y-1})\right]=D(N_y) \tag{III-32}$$

To eliminate C(Ny), eq. (III-32) Can be rewritten as:

$$\underbrace{\left[A(N_y)-\frac{1}{3}C(N_y)\right]}_{newA(N_y)}T(i,N_{y-1})+\underbrace{\left[B(N_y)+\frac{4}{3}C(N_y)\right]}_{newB(N_y)}T(i,N_y)+\underbrace{0}_{newC(N_y)}=\underbrace{D(N_y)}_{newD(N_y)} \tag{III-33}$$

III.4. Discretization of the concentration equation

The concentration equation (II-51-C) can be written in the following form:

$$\eta\varepsilon\frac{\partial C}{\partial t}+\frac{\partial(uC)}{\partial x}+\frac{\partial(vC)}{\partial y}=\frac{1}{Le}\left[\frac{\partial^2 C}{\partial x^2}+\frac{\partial^2 C}{\partial y^2}+S_P\left(\frac{\partial^2 T}{\partial x^2}+\frac{\partial^2 T}{\partial y^2}\right)\right] \qquad \text{(III-34)}$$

As the same as the energy equation, the concentration equation is discretized by the finite difference method with a second-order centric scheme. The resolution will be made by the alternating directions method with the algorithm of Thomas.

Implicite in "x" and explicite in "y" directions :

For i=2, Nx, we have this three-diagonal matrix:

$$a(i)C(i-1,j)^{k+1/2}+b(i)C(i,j)^{k+1/2}+c(i)C(i+1,j)^{k+1/2}=d(i) \qquad \text{(III-35)}$$

Where:

$$\begin{aligned}
a(i) &= -DX2I\times Le - D2XI\times u(i-1,j)^k\\
b(i) &= 2(DX2I\times Le + \eta\varepsilon\times DTI)\\
c(i) &= -DX2I\times Le + D2XI\times u(i+1,j)^k\\
d(i) =&\left[DY2I\times Le + D2YI\times v(i,j-1)^k\right]\times C(i,j-1)^k\\
&+2(-DY2I\times Le + \eta\varepsilon\times DTI)\times C(i,j)^k\\
&+\left[+DY2I\times Le - D2YI\times v(i,j+1)^k\right]\times C(i,j+1)^k\\
&+DX2I\times Le\times Sp\times(T(i+1,j)+T(i-1,j)-2T(i,j))\\
&+DY2I\times Le\times Sp\times(T(i,j+1)+T(i,j-1)-2T(i,j))
\end{aligned} \qquad \text{(III-36)}$$

Discretization of the corresponding active Boundary condition $\frac{\partial C}{\partial x}=1-Sp$ from eq. (II.52), leads to:

$$\begin{aligned}
C(1,j) &= \frac{4}{3}\left[C(2,j)-C(3,j)-2\Delta X(1-Sp)\right]\\
C(N_{X+1},j) &= \frac{4}{3}\left[C(N_X,j)-C(N_{X-1},j)+2\Delta X(1-Sp)\right]
\end{aligned} \qquad \text{(III-37)}$$

Implicite in "y" and explicite in "x" directions :

For j=2, Ny, we have this three-diagonal matrix:

$$a(j)C(i,j-1)^{k+1} + b(j)C(i,j)^{k+1} + c(j)C(i,j+1)^{k+1} = d(j) \qquad \text{(III-38)}$$

Where:

$$\begin{aligned}
a(j) &= +DY2I \times Le + D2YI \times v(i,j-1)^k \\
b(j) &= 2(-DY2I \times Le - \eta\varepsilon \times DTI) \\
c(j) &= +DY2I \times Le - D2YI \times v(i,j+1)^k \\
d(j) &= \left[-DX2I \times Le - D2XI \times u(i-1,j)^k\right] \times C(i-1,j)^k \\
&\quad + 2(DX2I \times Le - \eta\varepsilon \times DTI) \times C(i,j)^k \\
&\quad + \left[-DX2I \times Le + D2XI \times u(i+1,j)^k\right] \times C(i+1,j)^k \\
&\quad - DX2I \times Le \times Sp \times (T(i+1,j) + T(i-1,j) - 2T(i,j)) \\
&\quad - DY2I \times Le \times Sp \times (T(i,j+1) + T(i,j-1) - 2T(i,j))
\end{aligned} \qquad \text{(III-39)}$$

Discretization of the corresponding active Boundary condition $\frac{\partial C}{\partial x} + Sp\frac{\partial T}{\partial y} = 0$ from eq. (II.52), leads to:

$$\begin{aligned}
C(i,1) &= \frac{4}{3}\left[C(i,2) - C(i,3)\right] + \frac{1}{3}(1-Sp)\left[-3T(i,1) + 4T(i,2) - T(i,3)\right] \\
C(i,N_{Y+1}) &= \frac{4}{3}\left[C(i,N_Y) - C(i,N_{Y-1})\right] - \frac{1}{3}(1-Sp)\left[3T(i,N_{Y+1}) - 4T(i,N_Y) + T(i,N_{Y-1})\right]
\end{aligned} \qquad \text{(III-40)}$$

III.5. Discretization of the momentum equation

For a Darcy porous medium, the momentum equation (II-51-A) can be written as:

$$\frac{\partial^2\psi}{\partial x^2} + \frac{\partial^2\psi}{\partial y^2} = -aR_T\left(\frac{\partial T}{\partial x} + N\frac{\partial C}{\partial x}\right) \qquad \text{(III-41)}$$

Once we determined the temperature and concentration fields, the next step consists of determining the field of the stream function from equation (III-41), once discretized with a centered order method and solved with the successive over-relaxation method (SOR) which is an explicit method directly giving the value of the stream function Ψ at time (n+1)Δt, at the node considered. The terms of the above equation can be discretized as:

$$\frac{\partial^2\psi}{\partial x^2} \approx \frac{\psi(i+1,j) + \psi(i-1,j) - 2\psi(i,j)}{\Delta x^2} \qquad \text{(III-42)}$$

$$\frac{\partial^2 \psi}{\partial y^2} \approx \frac{\psi(i, j+1)+\psi(i, j-1)-2\psi(i, j)}{\Delta y^2} \quad \text{(III-43)}$$

$$\frac{\partial T}{\partial x} \approx \frac{T(i+1, j)-T(i-1, j)}{2\Delta x} \quad \text{(III-44)}$$

$$\frac{\partial C}{\partial y} \approx \frac{C(i+1, j)-C(i-1, j)}{2\Delta y} \quad \text{(III-45)}$$

By replacing expressions (III-42) to (III-45) in equation (III-41) we obtain the following equation:

$$\frac{\psi(i+1, j)+\psi(i-1, j)-2\psi(i, j)}{\Delta x^2}+\frac{\psi(i, j+1)+\psi(i, j-1)-2\psi(i, j)}{\Delta y^2}= -aR_T\left[\frac{T(i+1, j)-T(i-1, j)}{2\Delta x}+N\left(\frac{C(i+1, j)-C(i-1, j)}{2\Delta y}\right)\right] \quad \text{(III-46)}$$

This can be rewritten as the following expression:

$$\psi(i, j)=b_1[\psi(i+1, j)+\psi(i-1, j)]+b_2[\psi(i, j+1)+\psi(i, j-1)] +b_3[T(i+1, j)-T(i-1, j)]+b_4[C(i+1, j)-C(i-1, j)] \quad \text{(III-47)}$$

Where

$$\left.\begin{aligned} b_1 &= \frac{\Delta y^2}{2(\Delta x^2+\Delta y^2)} \qquad b_3 = aR_T\frac{\Delta x \Delta y^2}{4(\Delta x^2+\Delta y^2)} \\ b_2 &= \frac{\Delta x^2}{2(\Delta x^2+\Delta y^2)} \qquad b_4 = aR_T N\frac{\Delta x^2 \Delta y}{4(\Delta x^2+\Delta y^2)} \end{aligned}\right\} \quad \text{(III-48)}$$

Applying the SOR method to the equation (III-47) gives:

$$\psi(i, j)^{k+1}=(1-\omega_R)\psi(i, j)^k+\omega_R\left\{\begin{aligned} &b_1[\psi(i+1, j)^k+\psi(i-1, j)^k]+b_2[\psi(i, j+1)^k+\psi(i, j-1)^k] \\ &+b_3[T(i+1, j)^k-T(i-1, j)^k]+b_4[C(i+1, j)^k-C(i-1, j)^k] \end{aligned}\right\} \quad \text{(III-49)}$$

With: k is the iteration and ω_R is the relaxation coefficient, if $\omega_R = 0$ we find equation (III-47). In practice, the choice $\omega_R > 1$ is used to speed up convergence while $\omega_R < 1$ is often used to converge a divergent process.

III.6. Discretization of velocity field

The components of the velocity field are obtained from the stream function according to relations (II.50). The discretization of these equations by a first order centered finite difference scheme gives:

$$u_{i,j}^{k+1} = \frac{\psi_{i,j+1}^{k+1} - \psi_{i,j-1}^{k+1}}{2\Delta y}$$
$$v_{i,j}^{k+1} = \frac{\psi_{i,j+1}^{k+1} - \psi_{i,j-1}^{k+1}}{2\Delta x} \qquad \text{(III-50)}$$

Boundary conditions of the velocity are discretized according to a finite difference scheme decentered to the right and to the left for the active and the adiabatic walls are as follow:

$$v_{1,j} = -\frac{4\psi_{2,j} - \psi_{3,j}}{2\Delta x}$$
$$v_{Nx+1,j} = +\frac{4\psi_{Nx,j} - \psi_{Nx-1,j}}{2\Delta x}$$
$$u_{i,1} = +\frac{4\psi_{i,2} - \psi_{i,3}}{2\Delta y} \qquad \text{(III-51)}$$
$$u_{i,Ny+1} = -\frac{4\psi_{i,Ny} - \psi_{i,Ny-1}}{2\Delta y}$$

III.7. Calculation Algorithm

A FORTRAN program was used to solve the mathematical equation system discretized above. The most important steps of our calculation algorithm are as follow:

1. Data initialization (reading or input).
2. Generation of the mesh.
3. Introduce the fracture (specify the position, slope, aperture, and allocate corresponding nodes).

4. Introduction of the initial distribution of temperature, concentration, and stream function.

5. Initialization of the velocity field, u (i, j) and, v (i, j) for both porous and fractured media.

6. Beginning of the time's loop.

   6.1. Solve the energy equations (III-8) and (III-22) by the ADI method and calculate the temperature field, T (i, j).

   6.2. Solve the concentration equations (III-35) and (III-38) by the ADI method and calculate the whole concentration field, C (i, j).

   6.3. Solve the momentum equation (III-49) by the SOR method and calculate the field of the stream function, Ψ (i, j) for both porous and fractured media.

   6.4. Determination of the velocity field, u (i, j) and v (i, j).

   6.5. Test the convergence (repeat from 6.1 or go to step 7).

7. Evaluate heat and mass transfer rates (calculate Nusselt and Sherwood numbers).

8. Printing of results.

9. End of the program.

The convergence criterion during the resolution of equations (III-49) is given by:

$$\frac{\sum_i \sum_j \left| \psi_{i,j}^{k+1} - \psi_{i,j}^{k} \right|}{\sum_i \sum_j \left| \psi_{i,j}^{k} \right|} \leq 10^{-9} \qquad \text{(III-52)}$$

III.8. Conclusion

In this chapter, we have delivered the discretization process for heat, concentration, and stream function equations and the chosen solving method for each equation. Thermal, concentration, as well as velocity boundary conditions, are likewise discretized for both active and adiabatic cavity walls. The calculation algorithm steps stand at the end of this chapter.

During the course of this research, a FORTRAN program was adopted and adjusted to solve the discretized numerical equations. where the concentration equation (mass equation) was changed and the Soret effect term was added; The boundary conditions were extended to tackle both Neumann and Dirichlet conditions; A fracture characterized by specific porosity "ε" and permeability "K_F" was introduced to the medium, appointing its position, slope, aperture, with corresponding ε and R_{TF}; The data transfer between each subroutine was improved; any unnecessary statement was removed.

This FORTRAN code was tested and compared with known results. The outcomes are so conformable. The results of the validation of the code take part in the next chapter.

Chapter IV

Results and discussion

IV.1. Introduction

This study intends to understand the effects of a discrete fracture on heat and mass transfer in porous media, where the Soret effect has been considered. In the first place, aiming to present the effect of the thermodiffusion for a binary fluid mixture, we will investigate the thermosolutal flow, and compare both cases, where the Soret effect is or is not considered. Secondly, depending on governing parameters, the permeability corresponds to the optimal contribution between the Soret effect and convection forces- that provide a maximum separation- will be determined. Finally, and more importantly, a discussion is made on how the heterogeneity of a porous medium influencing separation. In this logic, we propose to insert a fracture that can be filled with another distinct porous media. The fracture's permeability, position, thickness, and orientation are well deliberated for different cases, to understand its impact on heat and mass transfer, and to define the optimal parameters that provide a higher separation.

The fracture passes across the center of the cavity as shown in Fig. III-1. The latter is characterized by an angle θ define the tilt, an aperture e, and a specific Rayleigh number R_{TF} determined by the permeability of the fracture. Furthermore, the ratio of the fracture Rayleigh number R_{TF} over the porous medium Rayleigh number R_T is calculated and denoted a, as $a = R_{TF}/R_T$. For this study, the aspect form of the cavity and the buoyancy ratio is fixed to A=5, and N=0.4 respectively. For all simulations, a mono-cellular flow occurred in the cavity.

IV.2. Validation

The mathematical model and resolution process need to be validated using a known case. For this purpose, the boundary conditions were modified to reproduce the work performed by [77] using our own calculation code. In his simulation, the author examined the thermosolutal convection in a square porous cavity heated and

salted form the vertical sides, where the Soret effect was neglected. Table IV-1 presents comparative results, where a good agreement can be seen. Our code was also conformed to [76] results, who studied the Soret effect on double-diffusive convection in a square porous cavity heated and salted from below, Fig. V-1. Shows the concentration profiles in the mid-width of the cavity corresponding to a bi-cellular flow obtained with different values of Soret parameter Sr. Good conformity can be seen. Note that at Y=0.18 the concentration remains unchanged when Sr is varied; this behavior was denominated by Khadiri, et al., [76] as a neutral position and has not been explained. However, using a small Rayleigh number R_T=50 (for example) allows the Soret effect to become more important and dominates convection forces. For such situation, these neutral positions will have no existence anymore. This outcome is shown in Figure IV-2. Even though it was not presented by [76].

Table IV-1: Validation of the numerical code, (a square porous cavity heated and salted from the side, for N=0, Sp=0).

		Present code		Khadiri et al., [76]		Goyeau et al., [77]	
Ra	Le	Nu	Sh	Nu	Sh	Nu	Sh
50	10	1.982	8.966	/	/	1.98	8.79
100	20	3.118	19.50	3.11	19.02	3.11	18.89
200	10	5.007	20.22	4.96	20.02	4.96	19.86
	20	5.007	27.90	4.96	28.37	4.96	28.17
500	10	9.061	34.27	9.075	33.27	8.93	33.27
	20	9.061	47.37	9.075	45.91	8.93	46.77
1000	10	13.77	48.20	13.76	47.4	13.47	48.32
	20	13.77	66.55	13.76	66.95	13.47	67.45

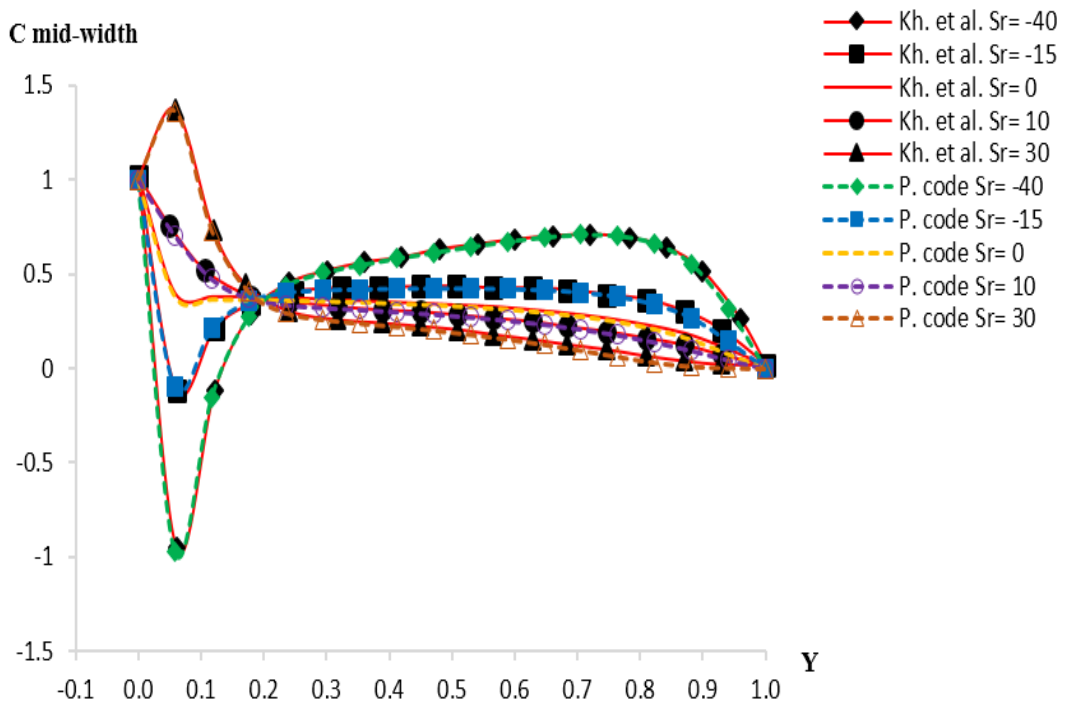

Figure IV-12: Vertical profiles of concentration at x=0.5 for A=1, R_T=200, Le=10, N=0.1, and various values of Sp

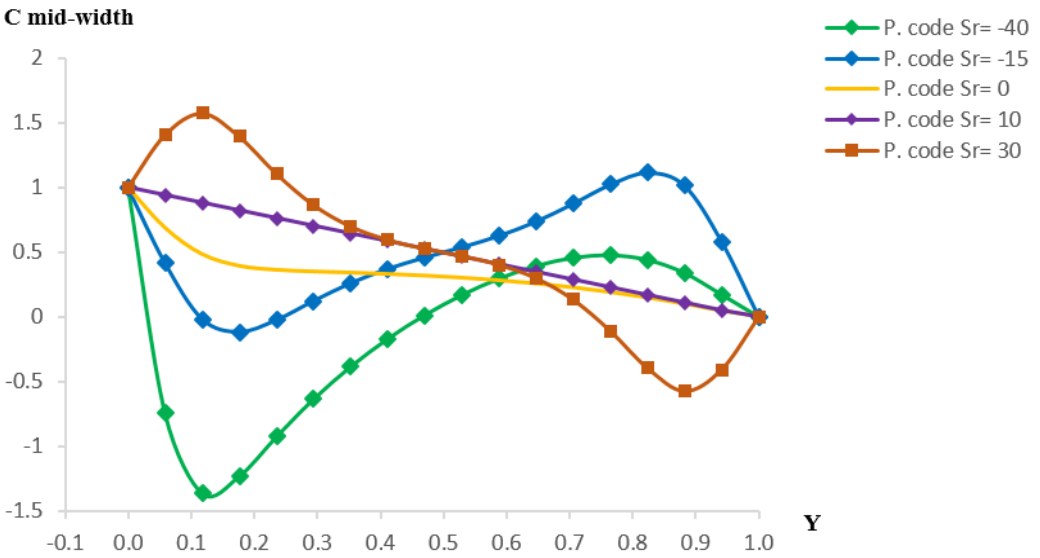

Figure IV-2: Vertical profiles of concentration at x=0.5 for A=1, R_T=50, Le=10, N=0.1, and various values of Sp.

Key parameters considered for the described problem are the thermal Darcy-Rayleigh number, R_T, the Lewis number Le, the buoyancy ratio N, the Soret parameter Sp and the aspect ratio of the cavity A. After ensuring the precision and the accuracy of the program's outputs, we will present the Soret effect contribution on the thermosolutal convection in a porous medium. However, a presentation of key parameters governing the mathematical problem is necessary to comprehend their effect from a physical point of view.

IV.3. Grid size effect

In order to determine the best compromise between precision of the results and calculation time, the effect of the grid size on the results was analyzed using different uniform rectangular mesh sizes for the same conditions. Figures IV-3-a, IV-3-b, and IV-3-c show the grid size effect on Nusselt and Sherwood numbers and the separation S respectively. Table IV-2 indicates satisfying results when using at least 171*171 nodes. Where the maximum relative error for Nu, Sh, and S do not exceed 1.5%.

Table IV-2: Effect of the grid size for R_T =50, R_{TF} =150, Le=10, Sp*=0.5, and. θ=70.*

Grids	Nu	Sh	*S*	Relative error %
71*71	2.5400	11.59	0.3837	4.93
101*101	2.5430	11.8	0.3916	2.97
131*131	2.5480	11.91	0.3956	1.98
171*171	2.5510	11.97	0.3976	1.48
301*301	2.5540	12.05	0.4015	0.52
501*501	2.5548	12.09	0.4035	0.02
601*601	2.5549	12.09	0.4036	0

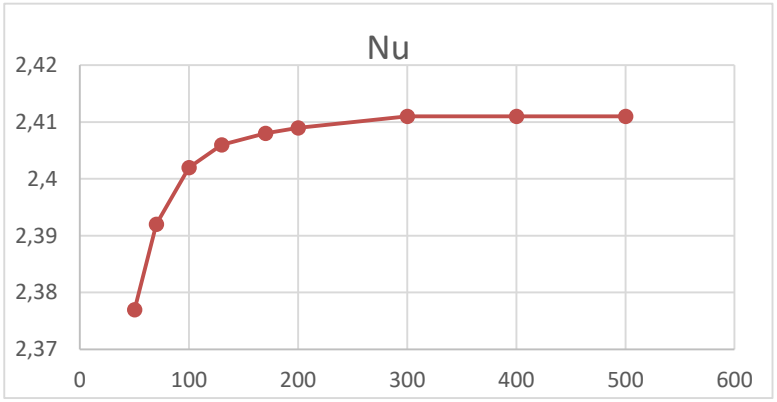

a

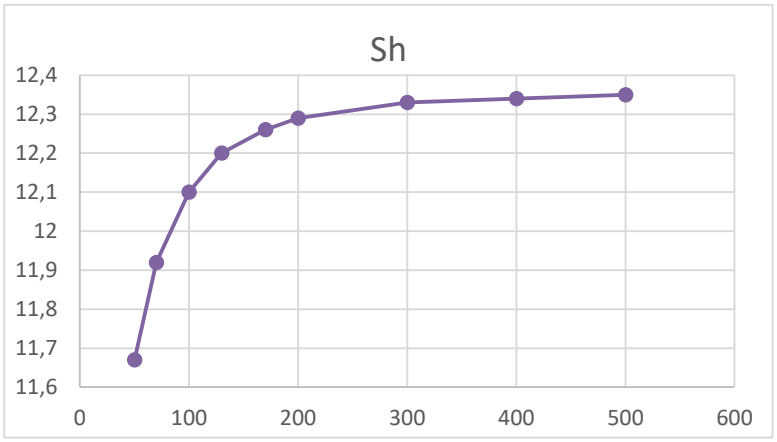

b

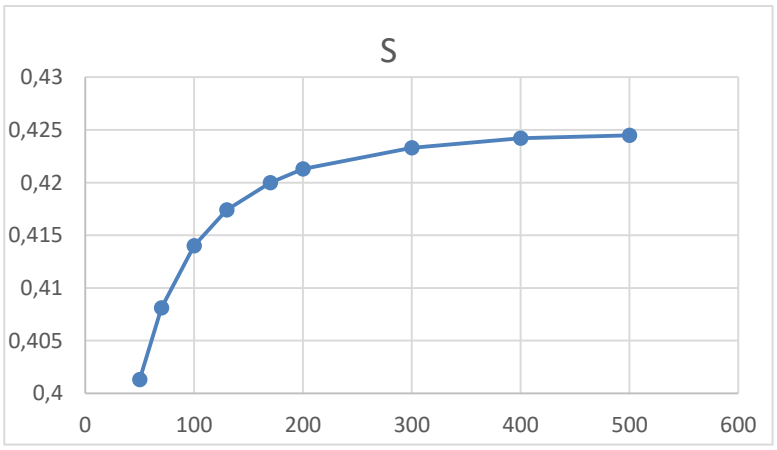

c

Figure IV-3: The grid size effect on (a) Nusselt and (b) Sherwood numbers and (c) the separation S, for R_T =50, R_{TF} =150, Le=10, Sp=0.5, and. θ=70.

IV.4. Analysis of the Soret effect in a homogeneous porous medium

IV.4.1. *Effect of the aspect ratio (A):*

Figure IV-4 shows a distinctive numerical results for R_T = 45, Le = 10, N=0.4, and A = 1, 5 and 8. Streamlines, isotherms, and iso-concentrates are presented from

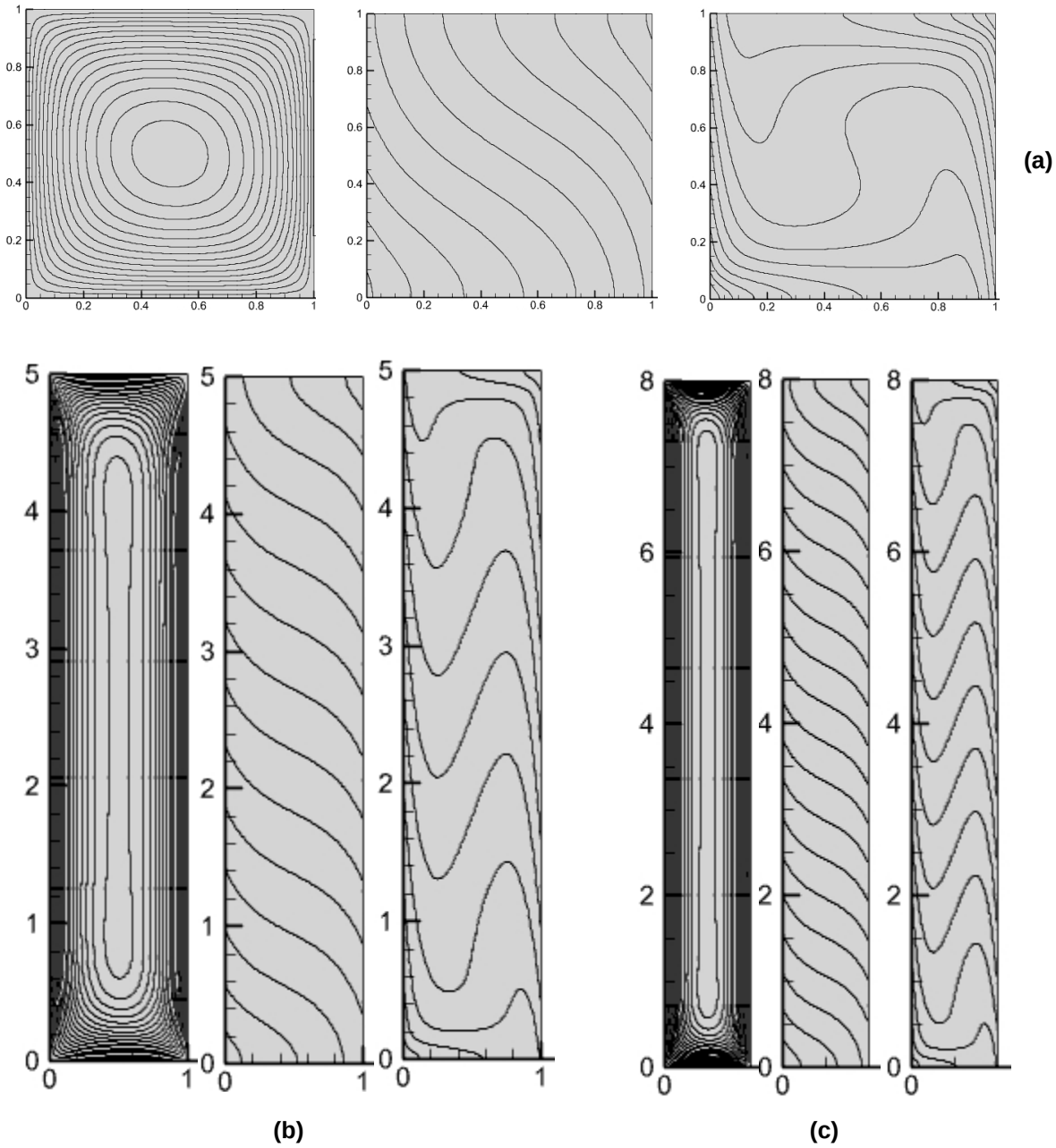

Figure IV-4: Streamlines, isotherms and iso-concentrates for R_T = 45, Le = 10, N=0.4, for (a) A = 1, (b) A=5 and (c) A= 8.

left to right, respectively. Figure IV-4 clearly shows that the current problem depends on the aspect ratio A. The results illustrate that the temperature and concentration are stratified linearly in the vertical direction of the cavity. While the flow in the central region of the cavity is basically parallel when A is large enough: A=5,8 (Figure IV-4-b, c), which is not the case for A=1 (Figure IV-4-a). In general, it has been confirmed that the numerical results can be considered independent of the aspect ratio, and the flow distribution becomes parallel when A> 4 [32]. For this current study the aspect ratio has been chosen to be A = 5.

IV.4.2. *Soret parameter effects (Sp):*

As shown in Fig. IV-1, and Fig. IV-2, the Soret effect greatly changes the species concentration distribution in the cavity. Depending on the permeability of the porous

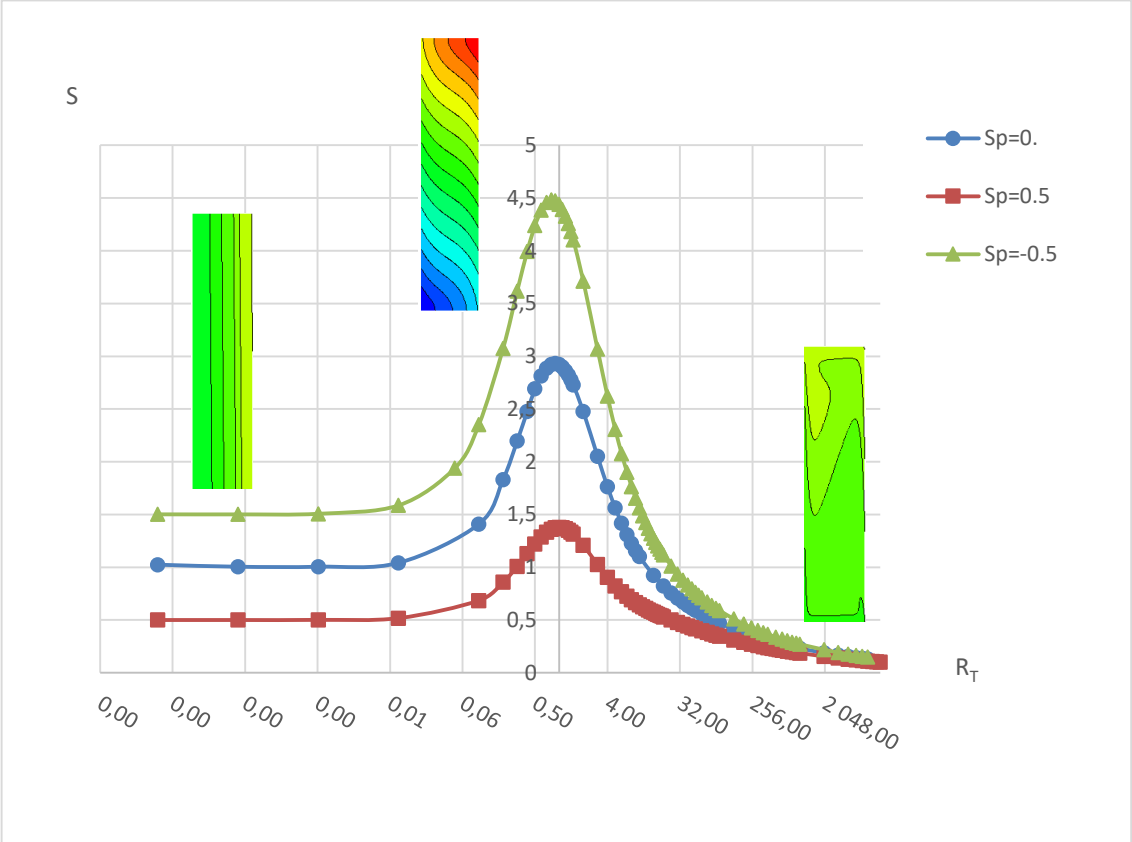

Figure IV-5: Separation (S) as function of R_T for Le=10, N=0.4, and various values of Sp.

medium, the contribution of the convection forces with the Soret coefficient effect can lead to a higher separation of the mixture constituents.

The effect of Soret parameter is investigated for an extent Rayleigh number scope. Figure IV-5 shows that the separation curves for all Soret parameters (Sp = -0.5; 0; 0.5) presents evident similarities in the behavior; in which three different zones are distinguished: at low Rayleigh number (R_T<0.01) the porous medium is less permeable, Hence, a purely diffusive regime overcomes the situation in this case, where the mass transfer is caused by only diffusion and thermodiffusion effects (there are no convection forces). Augmenting R_T leads to the onset and progressive growth of the convection forces. The contribution of the convection forces with the Soret effect performs the peak of the separation at an optimal Rayleigh number R_{Topt} that creates a diagonal concentration gradient in the cavity. At high values of Rayleigh number (R_T>50), convection forces dominate the process, mixing the constituent of the binary fluid, where the thermodiffusion is considered as a secondary phenomenon displays no significant effect. For all Soret parameters (Sp = -0.5; 0; 0.5), the separation in this zone is less than that of the purely diffusive regime (first zone).

Furthermore, the separation is also affected by the Soret parameter sign. Generally, for positive Soret coefficient values, the bigger and heavier components migrate to the cold wall of the cavity (left end) and might give a negative Sherwood number. However, for a cavity heated and salted from the same side (as in our case), for negative value of Soret parameter, thermodiffusion effect is opposing diffusion effect, where the heavier component moves towards the hot wall of the cavity (right end) and withhold the gradient of concentration, which explains the higher separation value. The value and the sign of the Soret parameter have a slight impact on the peak occurrence performed by the contribution of convection forces and Soret effect. For Soret parameter values (Sp) equals to -0.5, 0, 0.5 the peak appearance corresponds to an optimal Rayleigh number (R_{Topt}) of 0.8, 0.9, 1.0 respectively (Figure V-5).

Table IV-3: Effect of Soret parameter (Sp) sign for N=0.4, and Le=10.

R_T	Sp	ψ_{Min}	ψ_{Max}	Nu	Sh	$\nabla C = \frac{1}{Sh}$	S
0.01	-5	0.0E+00	4.2E-04	1.000	0.167	5.995	6.792
	-2	0.0E+00	2.7E-04	1.000	0.335	2.985	3.253
	0	0.0E+00	1.7E-04	1.000	1.000	1.000	1.005
	2	0.0E+00	7.5E-04	1.000	-1.000	-1.000	1.024
	5	-7.5E-04	0.0E+00	1.000	-0.250	-4.000	4.093
1	-5	0.0E+00	1.9E-01	1.018	0.446	2.242	17.139
	-2	0.0E+00	1.7E-01	1.013	0.748	1.337	8.859
	0	0.0E+00	1.5E-01	1.009	1.803	0.555	2.923
	2	0.0E+00	9.4E-02	1.004	-1.470	-0.680	3.121
	5	-4.9E-02	0.0E+00	1.001	-0.281	-3.559	9.691
450	-5	0.0E+00	2.6E+00	4.884	6.336	0.158	0.818
	-2	0.0E+00	3.0E+00	5.523	7.703	0.130	0.515
	0	0.0E+00	3.4E+00	5.809	14.870	0.067	0.296
	2	0.0E+00	3.8E+00	5.611	-13.990	-0.071	0.110
	5	-3.2E-01	5.9E+00	5.008	-2.191	-0.456	1.542

These results support the earlier explanation of the contribution of convection forces with Soret parameter. More results are shown in Table IV-3. For R_T = 0.01, the gradient of concentration is settled horizontally, and the difference of concentration ∇c measured at the middle of the two vertical walls of the cavity is almost the same as the separation (which is defined as the deference of the maximum and the minimum concentration between the two vertical walls). Whereas, the concentration gradient is diagonal for R_T = 1, and the separation becomes more important. Note that depending on the reference value in the dimensionless process, the separation can be higher than 1.

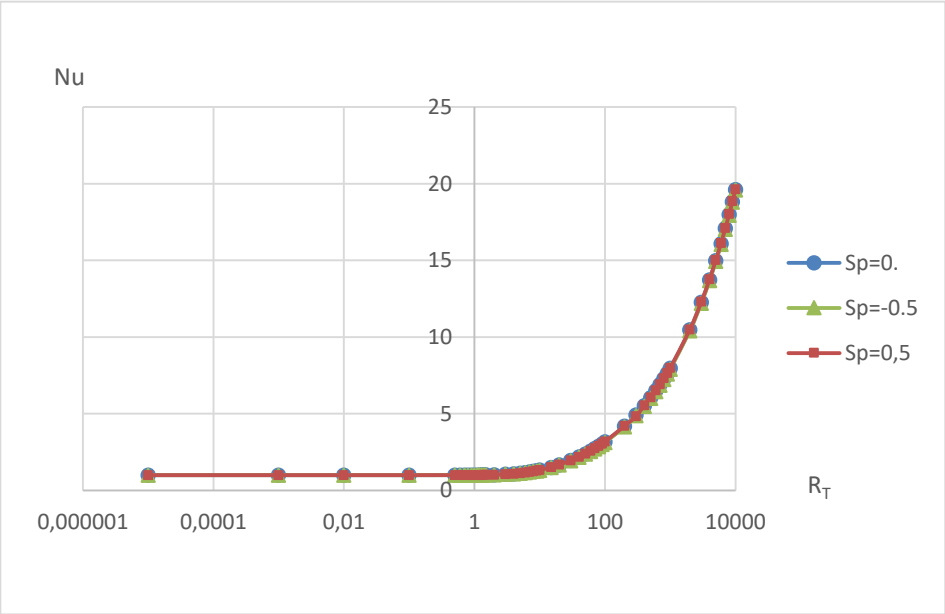

Figure IV-6: Nusselt num. as function of R_T for Le=10, N=0.4, and various values of Sp.

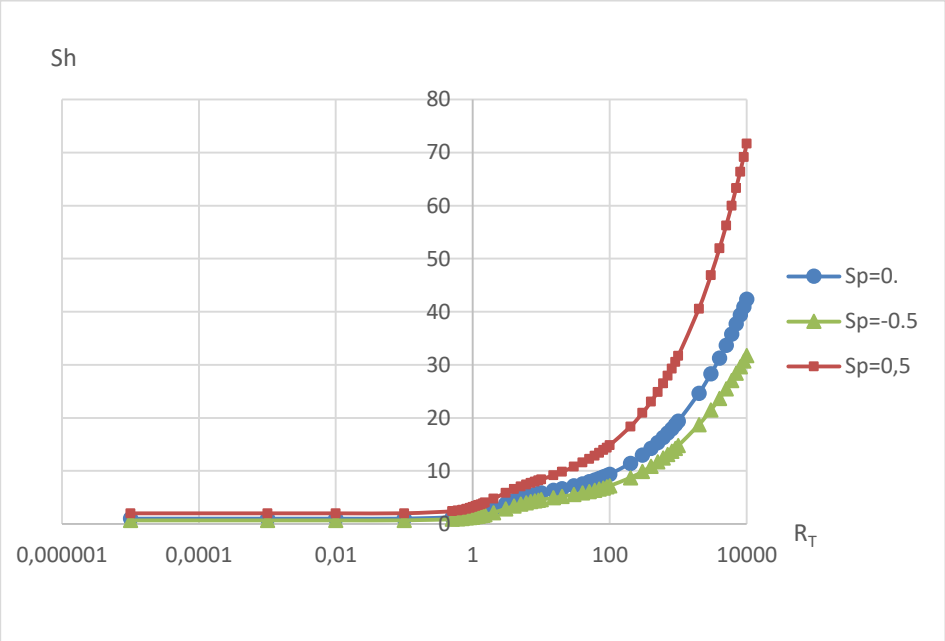

Figure IV-7: Sherwood num. as function of R_T for Le=10, N=0.4, and various values of Sp.

In order to evaluate the Soret effect on heat and mass transfer, Nusselt and Sherwood numbers representing respectively heat and mass transfers are traced in Figure IV-6 and Figure IV-7. Comparison between the variations of Nu and Sh with

R_T shows evident similarities in the behavior, even though Sh is clearly higher than Nu since the Lewis number is larger than unity (Le = 10). The Soret effect has unremarkable role on the heat transfer (Figure IV-6). However, for positive values of the Soret parameter, the Thermodiffusion effect contributes with diffusion force to transfer the bigger component toward the cold wall (left end) which increases Sherwood number. Otherwise, for negative values of the Soret parameter, the mass transfer generated by thermodiffusion opposes applied mass flux on the cavity, which maintains the concentration gradient, and results in fewer mass transfers and a higher separation.

In fact, the Soret effect is not the only parameter impacting mass transfer and Sherwood number. The buoyancy forces exemplified by the parameter N, has also a significant effect which will be highlighted by the following.

IV.4.3. *The buoyancy ratio effect (N):*

The buoyancy coefficient N characterizes the external concentration gradient applied to the medium. It is known that for most fluids β_T is positive, while β_S can be positive or negative depending on the contribution of the diffusing components to the density of the fluid. In the present study, β_S is assumed to be positive, which leads to having a positive N for adding flows and a negative N for opposing flows.

Table IV-4: The buoyancy coefficient effect (N) for R_T =100, and Le=10.

N	*Sp*	ψ_{min}	ψ_{max}	*Nu*	*Sh*	*S*
-0.5	-5	-0.3492	1.33	1.116	0.515	15.1518
0	-5	0	2.356	3.138	1.655	1.8363
0.5	-5	0	1.571	2.562	4.887	1.7121
-0.5	0	0	2.503	3.041	7.202	0.5222
0	0	0	2.356	3.138	8.387	0.4883
0.5	0	0	2.249	3.169	9.623	0.4704
-0.5	5	0	1.683	2.641	-8.098	0.7377
0	5	0	2.356	3.138	-2.733	0.8596
0.5	5	-4.029	2.252	1.083	-4.288	5.11

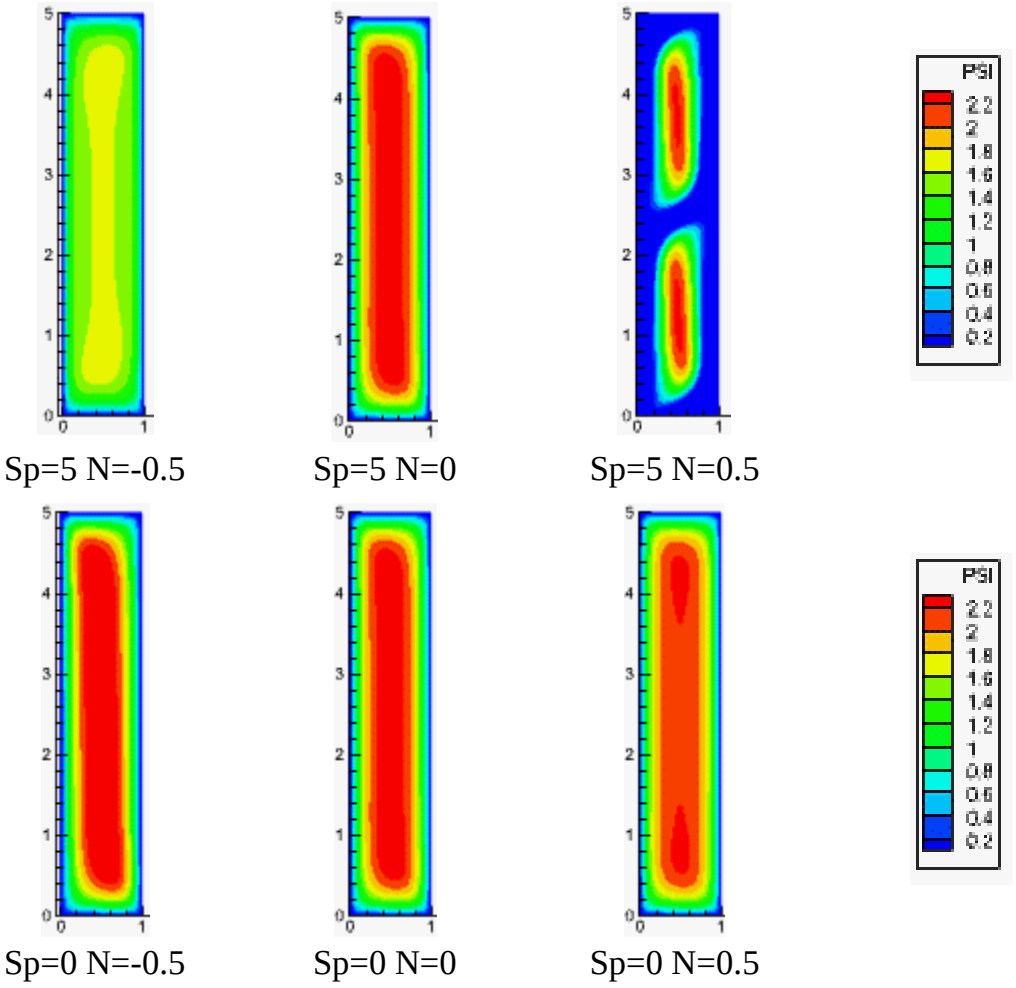

Figure IV-8: The buoyancy coefficient effect (N) for R_T =100, and Le=10.

Table IV-4 present the effect of the buoyancy factor N and its contribution with the Soret effect for R_T=100, Le=10. Thus, Figure IV-8 illustrate the stream function for some cases. As discussed earlier (Figure IV-5), a positive Soret parameter might give a negative Sherwood number. While, for a negative value of Soret parameter, thermodiffusion effect is opposing diffusion effect, which slightly increases the separation, knowing that for R_T =100, the convection forces are considerable.

It is found that for a negative buoyancy parameter N<0, the convection flows direction is reversed, and become counterclockwise. While for N=0 a thermal driven buoyancy forces occurs. In this study, the buoyancy forces parameter was set to N=0.4 for most cases.

IV.5. Analysis of the Soret effect in a hoterogeneous porous medium

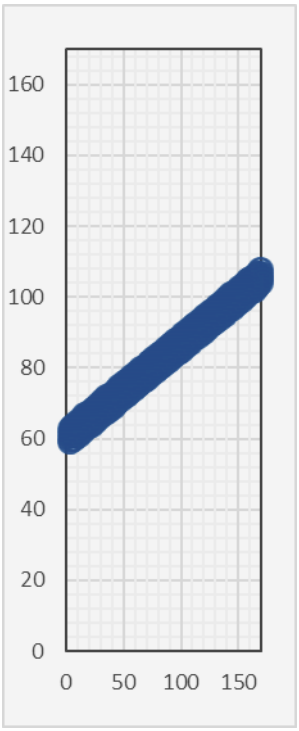

(a)

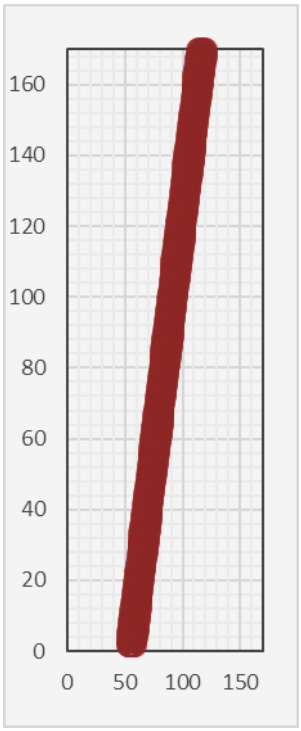

(b)

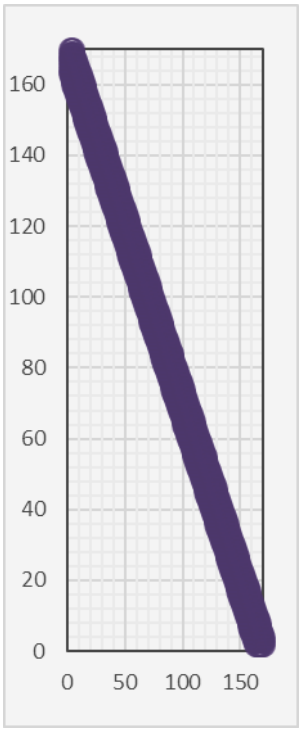

(c)

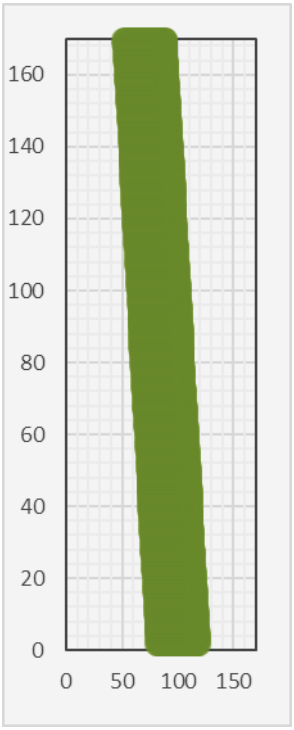

(d)

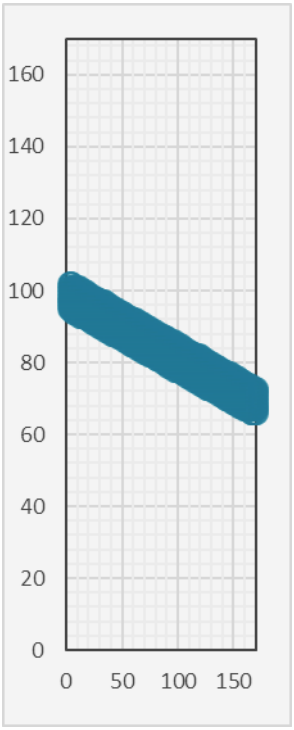

(e)

a) $\theta = 15$, $e = 0.038$, 845 nodes

b) $\theta = 70$, $e = 0.038$, 1230 nodes

c) $\theta = 135$, $e = 0.038$, 1659 nodes

d) $\theta = 100$, $e = 0.19$, 6465 nodes

e) $\theta = 170$, $e = 0.055$, 1352 nodes

Figure IV-9: Typical inclinations and apertures of the fracture

Heterogeneity is truly something essential in natural porous mediums. For this study, we propose to introduce a linear discrete fracture to the cavity. The fracture passes from the center of the cavity and could be filled with another porous medium. Which means it has a different porosity ε_F, and different permeability k_F. The fracture is also characterized by an aperture e and an inclination θ. Depending on the slope and the aperture of the fracture, the upper and the lower limits of the fracture are defined. Hence a tensor F(i,j) determining the fracture nodes was generated to introduce the assigned physical properties of the fracture ε_F, and R_{TF} defined by η and a to the concentration and the momentum equations (III-35 , III-38), and (III-49) respectively. Where η is the ratio of the fracture's porosity to the porous medium's porosity, $\eta = \varepsilon_F/\varepsilon$. While, a is the ratio of the fracture's Rayleigh number to the porous medium's Rayleigh number, a = $R_{TF}/\ R_T$. Tracing the fracture nodes tensor F(i,j) allows us to present the position of the fracture in the cavity. Typical inclinations and apertures of the fracture are presented in Figure IV-9. Note that, the total nodes of the cavity are about 29,241 (171*171) nodes. Modeling of the fracture with the finite difference method is actually closer to reality. Thus, it enables us to retain the fracture roughness, which is something inevitable in nature.

IV.5.1. *Effect of Lewis number*

Figure IV-10 shows the separation S for different values of Le for an inclined fracture of θ=70°, e=0.038, and a Rayleigh ratio a =30. Solid lines correspond to homogeneous porous medium, and doted ones correspond to heterogeneous (fractured) porous medium. It is clearly demonstrated that the more the Lewis number is increasing (Le), the convection forces become more effective, which provide an earlier peak of separation (at low Rayleigh number R_T), and also a more pointed one. Similar results were found by [78] in a horizontal cavity. The fracture behavior towards different Le values is almost the same. Thus, similar pattern are obtained.

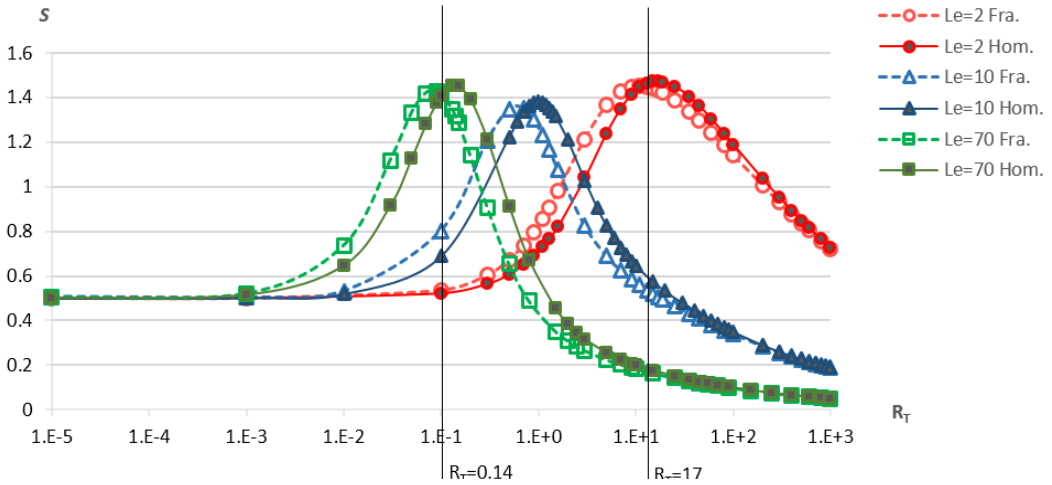

Figure IV-130: Separation in fractured PM vs. Homogeneous PM for θ =70°, Sp =0.5, a=30, and different values of Le.

Adding a fracture (characterized by a higher permeability) to the porous medium leads to improve the entire permeability of the medium. Consequently, the convection forces become more important, which gives a better separation S while the Rayleigh number R_T is less than the optimal R_{Topt}, and thereafter it decreases. However, when the Rayleigh number is more than the optimal (R_T>R_{Topt}) the fracture has slight negative effects on the separation. This observation is more remarkable for higher Lewis numbers (Le =10,70) compared with lower ones (Le=2). This difference could be related to the nature of the fluid, in literature Le =2 refers to a gas (El-Hajjar, 2008), and Le =10,70 refers to liquids [77]

Figure IV-11 shows the concentration profiles at the diagonal for homogenous and fractured porous media for a fracture of θ =70°, e=0.038, and Rayleigh ratio a=30. At the center of the cavity, the mixture persists homogeneous for different Rayleigh and Lewis numbers, deviation is more observed in the cavity extremes. The optimal Rayleigh number for Le =70 is R_T=0.14, what explains a higher concentration gradient for Le = 70 as seen in Figure IV-11 (a), for Le =10, the fracture plays a positive role, raising the total permeability of the medium and augmenting the separation S by 19.2%.

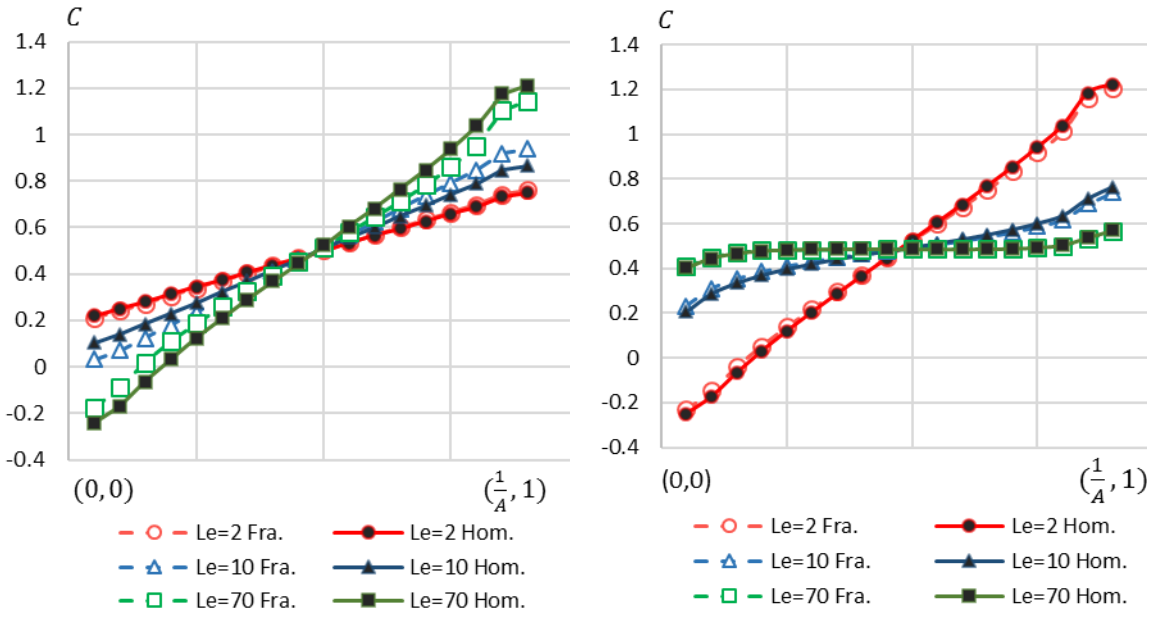

Figure IV-141: Diagonal profiles of concentration (with & without Fracture) for Le 2, 10, 70 at (a) R_T= 0.14, (b) R_T= 17. Solid and dotted lines represent homogeneous and fractured porous medium respectively

However, for Le = 2, R_T=0.14, there is no convection forces in the cavity, the fracture has no significance effect, and the concentration profiles represent the boundary conditions effect. Figure IV-11 (b) shows a higher concentration gradient for Le=2, since R_T=17 corresponds to the optimum. However, for Le=10, and 70, R_T=17 is higher than the optimal. Thus, the convection forces induce a homogeneous mixture.

IV.5.2. *The fracture's permeability effects (R_{TF})*

In order to better understand and confirm the effect of the fracture's permeability on the separation, different Rayleigh number were set to the fracture R_{TF}, for a given value of porous medium's Rayleigh number R_T. Three different value of porous medium's Rayleigh number R_T were investigated viz a viz; less than, equal, and higher than the optimum correspond to (a), (b), and (c) respectively (Figure IV-12). Comparing the separation caused by the fracture with that caused by the homogeneous porous medium, the following remarks are observed: when the porous

medium permeability is less than the optimal (a), the fracture plays an important role, raising the separation by 93% at its peak $R_T = 3$, then it starts decreasing. However, when the porous medium's permeability is equal or higher than the optimal as in (b) and (c), the fracture can apply a negative effect on the separation. The fracture existence strongly affects the behavior at the optimal Rayleigh number R_{Topt}. For a heterogeneous porous media, it was stated by Jiang, [39] -who investigated the separation of a mixture of methane and n-butane in dual permeability cavity- that due to heterogeneity condition of the problem, the separation ratio in heterogeneous porous media is always higher than that in homogeneous porous media. However, throughout these results, their statement is valid only when the total porous medium permeability is less than the optimal, and this does not contradict with their results.

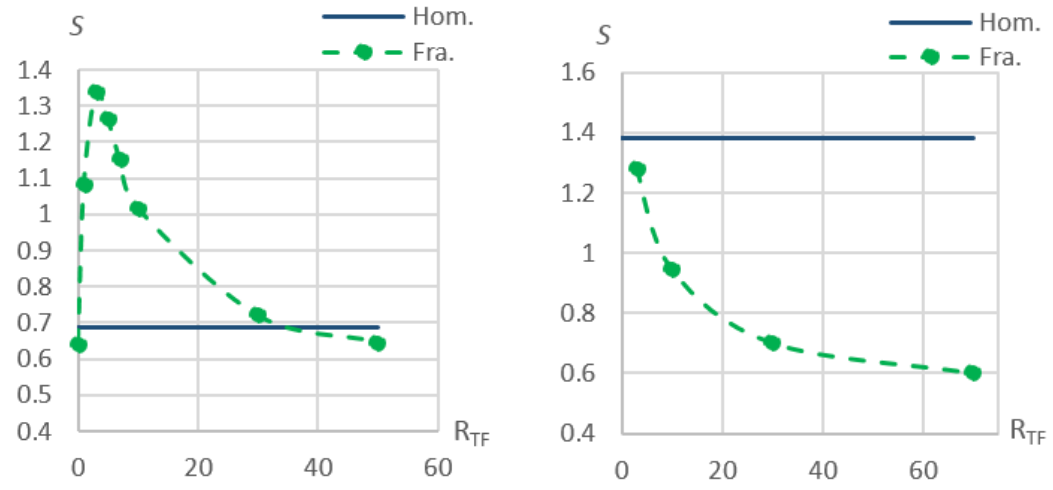

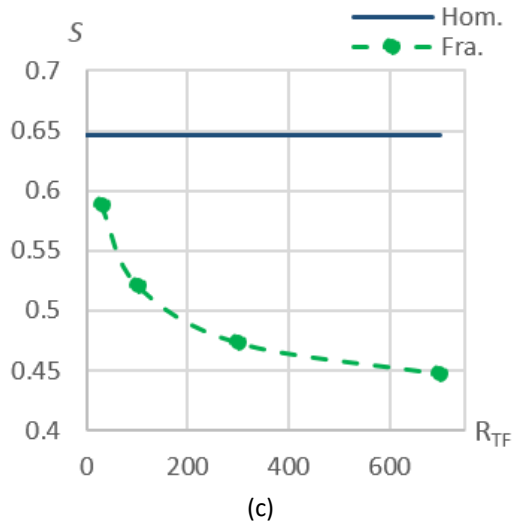

Figure IV-152: Effect of the fracture's permeability on the separation for Le=10, θ =90°, e=0.038, and different Rayleigh numbers (a) R_T= 0.1, (b) R_T= 1, (c) R_T= 10. Solid and dotted lines represent homogeneous and fractured porous medium respectively.

IV.5.3. *The fracture's orientation (θ) effect*

Altering the inclination angle of the fracture causes a change in the length and the area of the fracture, so in the number of the fracture nodes. For a valid comparison, aiming to reduce the variation in the fracture nodes when switching the angle, various numerical attempts were carried out. A recap is presented in Figure IV-13. Where "b" is the number of nodes resulting from the difference between the two fracture limits at the left side end of the cavity, and "e" represent the aperture of the cavity (dimensionless length). Using a fixed value of e, b can be calculated using the following expression: $b = (e/cos\,\theta) * NY$. In general, working with an approaching number of the fracture nodes for different inclinations will changes the aperture: tights it when the slope absolute value approaches one ($|slope\ \theta| \sim 1$), and enlarge it otherwise. Therefore, we choose to work with a fixed aperture (e=constant) and compare vertically symmetric fractures.

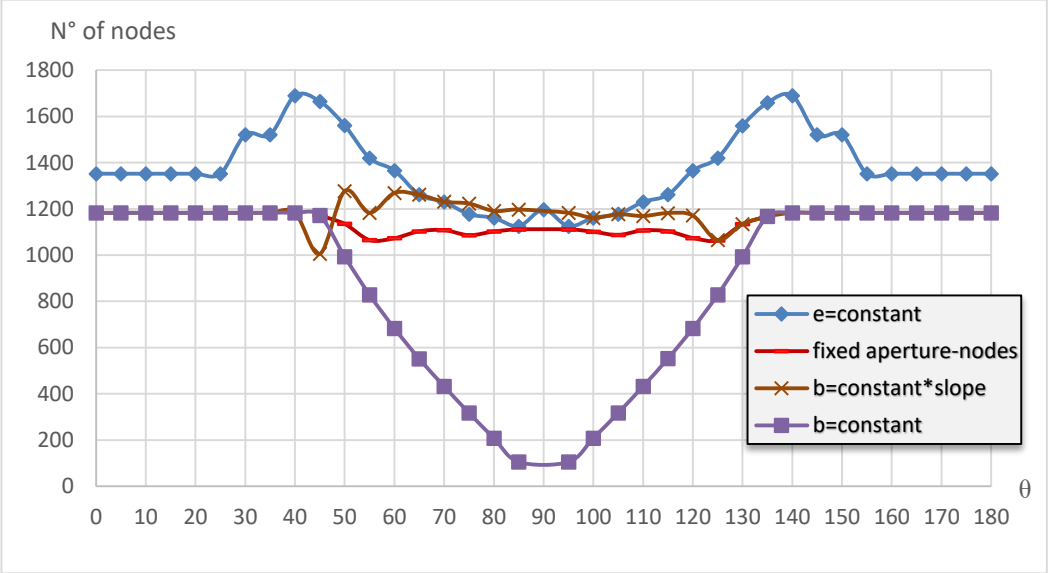

Figure IV-13: number of nodes for different expressions of b and e.

The separation of components by the Soret effect becomes more important when low convection forces accompany it. For a better perception of how these two effects contribute together, special attention is given to the region associated with the onset of the convection forces. We traced the separation at low Rayleigh number (R_T) for

e = 0.038, Sp=0.5, Le=10, and a =30 for different fracture's angles (Figure IV-14). The results show that for R_T less than 0.5, the separation in fractured porous media is always higher than that for homogeneous ones. As predicted, fractures cause to hasten the optimal R_T for the separation whatever the angle. However, comparing vertically symmetrical fractures, curves are identical for θ =70° and θ =110°, but they become less identical for angles near the horizontal. In order to understand the main cause of this variance, the heat and mass transfer represented by Nusselt and Sherwood numbers are presented in Figure IV-15 (a) and (b) respectively.

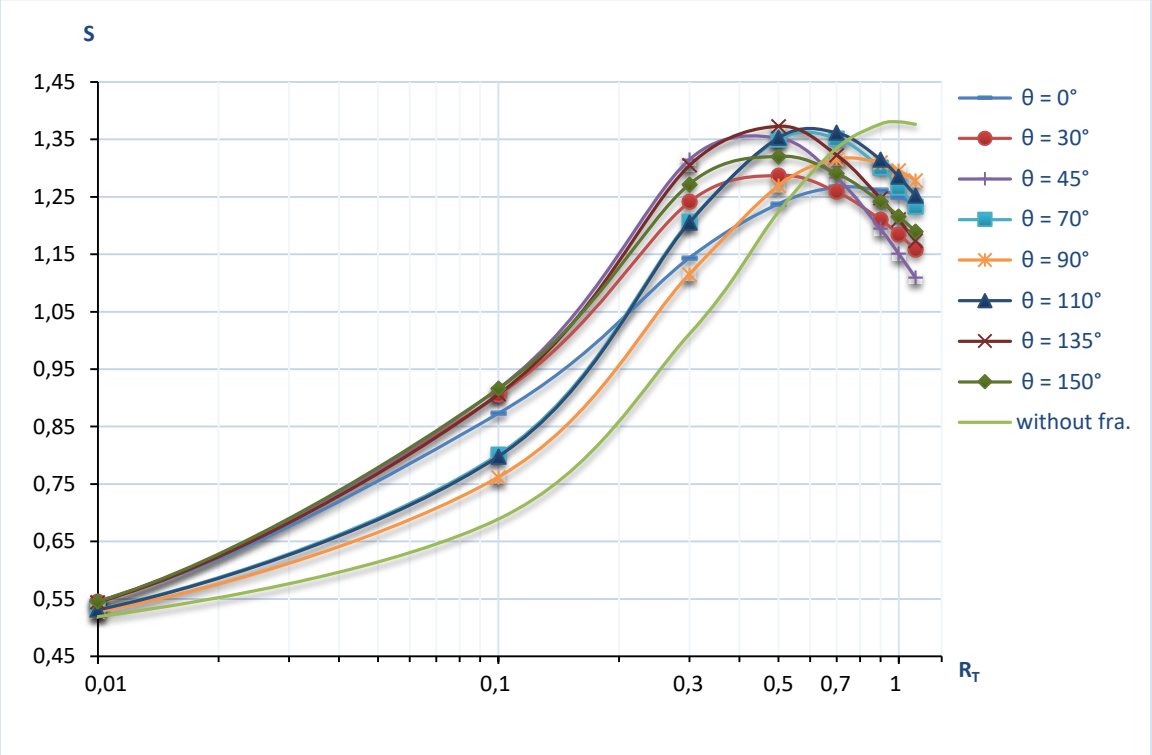

Figure IV-14: Effect of the fracture's orientation (θ) on the separation for Le=10, e=0.038, Sp=0.5, and a =30 at low Rayleigh numbers

For a vertical fracture, the mass transfer is almost the same as for a homogeneous porous medium (without fracture), with some slight decrease, while the horizontal fracture significantly increases it. As explained by Clusius and Dickel [79], the horizontal dynamics in a thermogravitational column are governed by the Soret effect. At low Rayleigh number R_T weak convection forces exist, thus, the mass

transfer is made horizontally by only diffusion and thermodiffusion effects. Therefore, the more the fracture is inclined towards the horizontal, the higher mass transfer is. The same observation can be seen for the Nusselt number (Figure IV-15 (a)) since the applied boundary conditions are the same for both heat and mass transfer.

Heat and mass transfer made by vertically symmetric fractures of an inclination of θ and $(\pi-\theta)$ is the same in most cases, but it becomes more differentiated for small θ (closely horizontal fracture). Note that the length of the fracture is variable with the angle, but it is the same for vertically symmetric fractures.

The difference between the behavior of vertically symmetric fractures towards heat and mass transfer is a result of a combination of several effects, including the direction of convection circulation, the gravity acceleration, boundary conditions, and the Soret parameter sign. In our case, at the onset of the convection region, low convection forces occur. For positive Soret parameters, the mass transfer of the heavier component is made towards the cold wall (left end) by both diffusion and thermodiffusion effects. However, with the same counterclockwise convection flow direction, fractures inclined towards the cold wall (left-end) are heated from the bottom. Consequently, they have more important convection forces than the ones inclined toward the hot wall (right-end) and heated from the top. Thus, the mass transfer produced within an inclined fracture toward the cold wall is more important than the one produced within an inclined fracture toward the hot wall (Sh for $\theta=150° >$ Sh for $\theta=30°$).

The gravity role in this regard is either enhancing or diminishing heat and mass transfer rates. Its contribution is more advantageous for fractures that are inclined to the hot walls. It facilitates the migration of the heavier component toward the cold region (left-end). Thus, for a fracture of $\theta=45°$, -due to the gravity effect- even though it's heated from the top, the resulting mass transfer rates is almost the same as for an inclined fracture of $\theta=135°$ (Sh for $\theta=45°$ = Sh for $\theta=135°$).

For inclined symmetric fractures near the vertical, the difference is no longer persists, fractures – in this case – doesn't connect between the right and left ends (both are heated from the bottom), and the gravity has the same effect on both of them. Resulting in the same mass transfer (Sh for θ=70° = Sh for θ=110°).

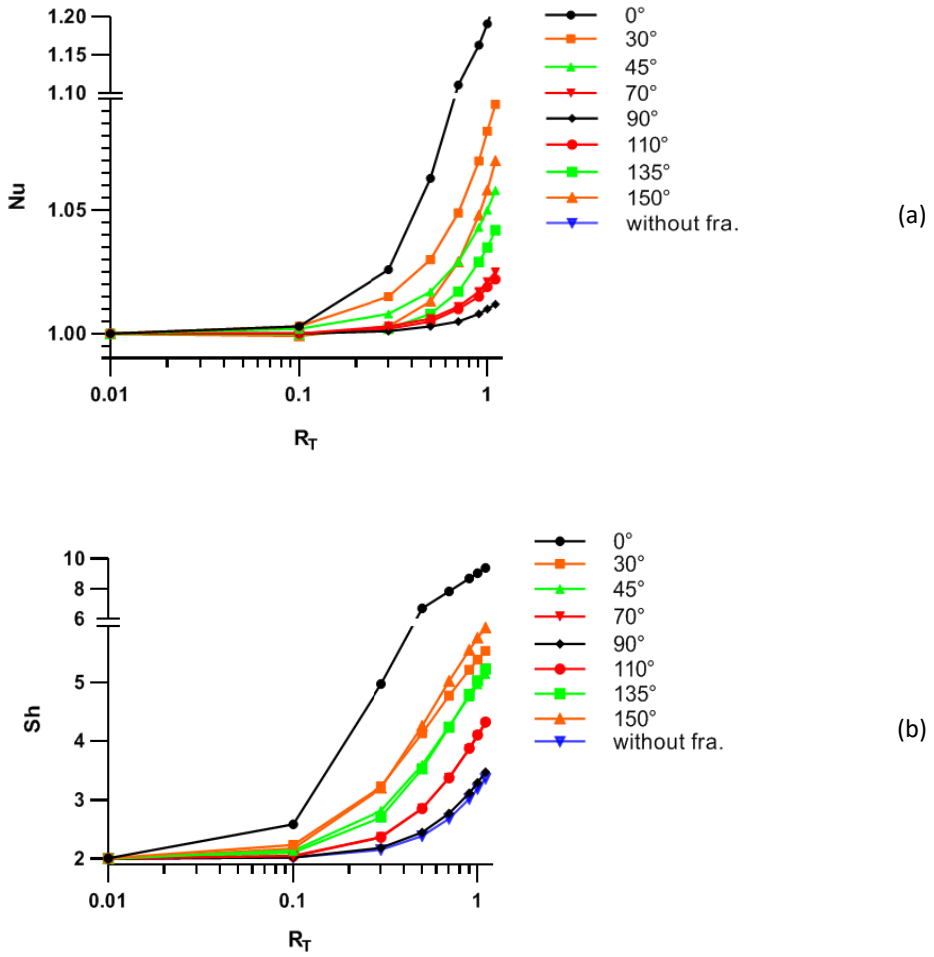

Figure IV-15: Nusselt (a) and Sherwood (b) numbers for Le=10, e=0.038, Sp=0.5, and a=30 at low Rayleigh numbers.

Previous explanations of the fracture's orientation effect are more based on the mass transfer rates presented by Sherwood number (Figure IV-15 (b)). However, while examining the Nusselt number (Figure IV-15 (a)) which represents the heat transfer rates, the same remarks could be availed, thought Nu and Sh number are arbitrary evaluated at the geometrical center of the cavity. Note that, for this study,

the Soret parameter is assumed constant. In addition, the negligible effect of the mass concentration variation on the heat transfer (Dufour effect) is not considered.

IV.6. Conclusion

Thermo-solutal convection in porous media is significantly affected by the contribution of Soret effect and convection forces, where the permeability of the medium is the dominant parameter. The fracture effect on the thermo-solutal convection, considering the Soret effect is rarely studied before. In this investigation, a fractured porous medium from the center of the cavity is considered and characterized by slightly higher permeability in purpose of understanding the thermosolutal convection coupled with the Soret effect in heterogeneous and fractured porous media.

Deducing from the analysis carried out in this study, we conclude that the fracture in the porous medium strongly influences the behavior of the thermo-gravitational flow and the corresponding heat and mass transfer performance in the cavity, which has effects on the separation.

At low Rayleigh number $R_{T,}$ Soret effect dominate the mass transfer process, and the addition of a fracture to the porous medium plays an important role in enhancing convective forces, which leads to increase heat and mass transfer and promotes better separations (depending on its permeability and position). However, the fracture can cause a negative effect on the separation when the Rayleigh number of the porous medium is higher or equal to the optimal value.

Particular attention is given to the orientation of the fracture. It comes from the analysis, that at low Rayleigh number R_T, the more inclination of the fracture is close to the horizontal; the more it favors the heat and mass transfer. Furthermore, due to the heating source, fractures inclined towards the cold wall have higher convection forces than the ones inclined towards the hot wall. This could increase or decrease the separation depending on R_T and a.

General Conclusion

At the end of this study, several analyzes were developed in order to quantify the effect of thermodiffusion or Soret effect -in a monophasic binary mixture- on natural convection in a heterogeneous porous medium. The mathematical model has been solved numerically with the finite difference method. A FORTRAN program was adopted and adjusted to solve the discretized numerical equations. Where the concentration equation (mass equation) was changed and the Soret effect term was added; A fracture characterized by specific porosity "ε" and permeability "K_F" was introduced to the medium, appointing its position, slope, aperture, with corresponding ε and R_{TF}.

The developed FORTRAN code is tested and compared with the results of Khadiri et al. [76] and Goyeau et al. [77].

Key parameters considered for the described problem are the thermal Rayleigh number, R_T, the Lewis number Le, the buoyancy ratio N, the Soret parameter Sp and the aspect ratio of the cavity A. The behavior of the thermo-solutal convection flow is analyzed based on: the rate of heat and mass transfer quantified by Nusselt and Sherwood numbers respectively; distributions of the concentration in the porous cavity, the separation parameter, S, and the fracture characteristics (permeability, position, and thickness). The results showed consistent coupled phenomena.

The main conclusion of this study is that the effect of thermodiffusion on convection in a binary system is controlled by a key parameter that is the permeability of the porous medium K. The existence of a fracture in the porous medium strongly changes the behavior of the thermogravitational flow. For permeabilities of porous media k, lower than the optimal permeability k_{opt} the fracture can contribute to the increase of the separation (according to its permeability, position, size …). However, for permeabilities of porous media greater than or equal to k_{opt}, the fracture existence could exert a negative effect on the separation.

The outcome of this thesis is important to predict a distribution of a hydrocarbon reservoir, or to improve the thermogravitational column technique, which is the base of the separation process industries. We believe, as well that the thermosolutal convection in heterogeneous porous media coupled with the Soret effect has a lack of knowledge. Our contribution to the phenomena explanation is just as a droplet of water in the ocean. Thus, this subject is still missing a lot to be accomplished.

Bibliography

[1] T. Radko, Double-diffusive convection, Cambridge university press, 2013.

[2] D. A. Nield and A. Bejan, Convection in Porous Media, 4th ed., New York Heidelberg Dordrecht London: Springer Science+Business Media, 2013.

[3] D. B. Ingham and I. Pop, Transport phenomena in porous media, 1st ed., Pergamon: Oxford, 1998.

[4] V. Kambiz, Handbook of porous media, Taylor & Francis Group, 2005.

[5] M. Abdelkader, Charrier-Mojtabi, Marie-Catherine, B. Elhajjar and Y. P. and Razi, "Thermogravitational Diffusion in a Porous Medium Saturated by a Binary Fluid," in *Handbook of porous media*, 3rd edition, Taylor & Francis Group, 2015, pp. 269-320.

[6] C. Ludwig, "Diffusion zwischen ungleich erwarmten Orten gleich zusammengesetzer," *Akad. Wien. Math. Naturwiss.,* vol. 20, p. 539, 1856.

[7] C. Soret, "Sur l'état d'équilibre que prend au point de vue de sa concentration une dissolution saline primitivement homogène dont deux parties sont portées à des températures différentes," *Arch. Sci. Phys. Nat.,* vol. 2, p. 187, 1879.

[8] P. Costesèque, A. Mojtabi and J. K. Platten, "Thermodiffusion phenomena," *Comptes Rendus Mécanique,* no. 339, p. 275–279, 2011.

[9] S. R. De Groot, "L'Effet Soret-Diffusion thermique dans les phases condensées," Amsterdam, 1945.

[10] W. Köhler and K. I. Morozov, "The Soret Effect in Liquid Mixtures – A Review," *Journal of Non-Equilibrium Thermodynamics,* pp. 151-197, 2016.

[11] A. Leahy-Dios, *Experimental and Theoretical Investigation of Fickian and GThermal Diffusion coefficients in hydrocarbon Mixtures,* yale : yale university, 2008.

[12] E. W. LeMaster, *Separation of the isotopes of neon by thermal diffusion,* Texas: Texas Technological College, 1966.

[13] M. Rahman and M. Saghir, "Thermodiffusion or Soret effect: Historical review," *International Journal of Heat and Mass Transfer,* pp. 693-705, 2014.

[14] K. Clusius and G. Dickel, "New Process for separation of gas mixtures and isotopes,," *Naturwissenschaften,* vol. 26, p. 546, 1938.

[15] W. Fury, R. Jones and L. Onsager, "On the theory of isotope separation by thermal diffusion," *Phys Rev,* vol. 55, no. 11, p. 1083–1095, 1939.

[16] S. R. De Groot, "Theorie phénoménologique du procédé thermo-gravitationnel de séparation dans un liquide," *Physica IX,* no. 8, pp. 801-816, 1942.

[17] G. G. Philomena and F. Barbara, "Clusius-Dickel Separation: A New Look at an Old Technique.," *Separation Science,* vol. 12, no. 2, pp. 103-169, 1977.

[18] M. Lorenz and A. H. J. Emery, "The packed thermal diffusion column," *Chemical Engineering Science,* vol. 11, pp. 16-23, 1959.

[19] J. K. Platten, "Enhanced molecular separation in inclined thermogravitational columns," *The Journal of Physical Chemistry B,* vol. 107, no. 42, p. 11763–11767, 2003.

[20] Z. Alloui, R. Rebhi, M. Mamou and P. Vasseur, "Effects of quadratic drag on natural convection in a tilted porous layer with uniform heat flux from the side," *International Journal of Heat and Mass Transfer,* vol. 115, pp. 314-325, 2017.

[21] B. El Hajjar, A. Mojtabi, P. Costesèque and M. C. Charrier-Mojtabi, "Separation in an inclined porous thermogravitational cell," *International Journal of Heat and Mass Transfer,* vol. 53, p. 4844 – 4851, 2010.

[22] J. Lee, I. Shivakumara and A. Mamatha, "Effect of Non-uniform Temperature Gradients on Thermo-gravitational Convection in a porous layer Using a Thermal Non-equilibrium Model," *Journal of Porous Media,* vol. 14, pp. 659-669, 2011.

[23] O. Abahri, D. Sadaoui, K. Mansouri and A. M. M. Mojtabi, "Thermogravitational Separation in Horizontal Annular Porous Cell," *Mechanics & Industry,* vol. 18, no. 1, pp. 106-116, 2017.

[24] V. Grigor'ev and E. Rivin, "Determination of the Soret Coefficient Based on the Separation of Mixtures of Organic Liquids in a Thermogravitational Column," *Theoretical Foundations of Chemical Engineering,* vol. 51, no. 4, pp. 464-467, 2017.

[25] D. Mutschler, M. A. Larabi and A. Mojtabi, "Theoretical Models for the Thermo-Gravitational Separation Process in Porous Media Filled by N-Component Mixtures," *The European Physical Journal E,* vol. 40, no. 4, pp. 49-56, 2017.

[26] A. Mojtabi, B. Ouattara, D. A. S. Rees and M. -C. Charrier-Mojtabi, "The Effect of Conducting Bounding Horizontal Plates on Species Separation in Porous Cavity Saturated by a Binary Mixture," *International Journal of Heat and Mass Transfer. 126: 479-48,* vol. 126, pp. 479-488, 2018.

[27] S. Kozlova and I. Ryzhkov, "The Transient Separation of Multicomponent Mixtures in a Cylindrical Thermo-gravitational Column," *International Journal of Heat and Mass Transfer,* vol. 126, pp. 660-669, 2018.

[28] N. Hashemipour, J. Karimi-sabet, K. Motahari, S. M. Monfared and Y. M. M. A. Amini, "Experimental and Simulation Investigation on Separation of Binary Hydrocarbon Mixture by Thermogravitational Column," *Journal of Molecular Liquids,* vol. 268, p. 791–806, 2018.

[29] M. L. Benano, J. Caltagirone, B. Faissat, F. Montel and P. Costeseque, "Modelling Soret coefficient measurement experiments in porous media considering thermal and solutal convection," *Internat. J. Heat Mass Transfer,* vol. 44, pp. 1285-1285, 2001.

[30] M. Marcoux and P. Costeseque, " Study of transversal dimension influence on species separation in thermogravitational diffusion columns," *Journal of Non-Equilibrium Thermodynamics,* vol. 32, no. 3, p. 289–298, 2007.

[31] N. Boutana, A. Bahloul, P. Vasseur and F. Joly, "Soret and double diffusive convection in a porous cavity," *Journal of Porous Media,* vol. 7, no. 1, pp. 41-57, 2004.

[32] Z. Alloui, A. Merabtine and P. Vasseur, "Soret and thermosolutal effects on natural convection in a vertical cavity filled with a binary mixture," *The Canadian Journal of Chemical Engineering,* vol. 88, pp. 718-727, 2010.

[33] A. Amahmid, M. Hasnaoui, M. Mamou and P. and Vasseur, "On the transition between aiding and opposing double diffusive flows in a vertical porous matrix," *J. Porous Media,* vol. 3, pp. 123-137, 2000.

[34] H. Ben Niche, S. Bouabdallah, B. Ghernaout and M. Teggar, "Unsteady double diffusive natural convection with Dufour and Soret effects," *International Journal of Heat and Technology,* vol. 34, no. 1, pp. 39-46, 2016.

[35] M. Er-Raki, M. Hasnaoui, A. Amahmid, M. Mamou and M. Bourich, "Soret effect on double-diffusive boundary layer flows in a vertical porous cavity," *Journal of Porous Media,* vol. 10, pp. 783-795, 2007.

[36] B. S. Bhadauria, "Double-diffusive convection in a saturated anisotropic porous layer with internal heat source," *Transport in porous media,* vol. 92, no. 2, pp. 299-320, 2012.

[37] K. Raju, "Effect of temperature dependent viscosity on ferrothermohaline convection saturating ananisotropic porous medium with Soret effect using the Galerkin technique," *International Journal of Heat and Technology,* vol. 36, no. 2, pp. 439-446, 2018.

[38] C. G. Jiang, M. Z. Saghir, M. Kawaji and K. Ghorayeb, "Two-dimensional numerical simulation of thermo-gravitational convection in a vertical porous column filled with a binary fluid mixture," *International Journal of Thermal Sciences,* vol. 43, p. 1057–1065, 2004.

[39] C. G. Jiang, "modeling of thermo-solutal convection in porous media," Toronto, 2005.

[40] T. J. Jaber, "Numerical study of permeability effect on convection in fractured porous media filled with hydrocarbon ternary mixture. Proceedings of CHT-08 ICHMT International Symposium on Advances in Computational Heat Transfer. Marrakesh, Mo," 2008.

[41] Z. Aouf and C. Seladji, "Thermosolutal Convection in a Porous Medium Cavity Subjected to Heat and Mass Flux: A Discrete Fracture Effect," *Acta Universitatis Sapientiae Electrical and Mechanical Engineering,* vol. 12, pp. 86-104, 2020.

[42] M. M. C. Charrier, B. El Hajjar, B. Ouattara, A. Mojtabi and P. Costesèque, "Soret-driven convection and separation of binary mixtures in a porous horizontal slot submitted to a heat flux," vol. 339, pp. 303-309, 2011.

[43] H. Ben AHMED , *Étude de la convection mixte d'origine thermosolutale sous l'influence de l'effet SORET dans un milieu poreux : analyse de stabilité linéaire et simulations 3D,* Tunis, 2008.

[44] S. Srinivasan and M. Z. Saghir, "Thermodiffusion in Multicomponent Mixtures Thermodynamic, Algebraic, and Neuro-Computing Models," in *SpringerBriefs in Applied Sciences and Technology Thermal Engineering and Applied Science*, USA, 2013, p. 114.

[45] M. Paszkuta, *Phénomènes de transport couples dans les argiles du callovo-oxfordien,* Paris, 2005.

[46] a. Leahy-Dios, *experimental and theoretical investigation of fickian and thermal diffusion coefficients in hydrocarbon mixtures,* yale, 2008.

[47] R. Peuhkuri, C. Rode and K. Hansen, "Non-isothermal moisture transport through insulation materials," *Building and Environment,* vol. 43, no. 5, p. 811–822, 2008.

[48] M. Chacha, D. Faruque, M. Saghir and J. Legros, "Solutal thermodiffusion in binary mixture in the presence of g-jitter," *Int. J. Thermal Sci,* vol. 41, pp. 899-911, 2002.

[49] K. Ghorayeb, A. Firoozabadi and T. Anraku, "Interpretation of the unusual fluid distribution in the Yufutsu gas-condensate field," *SPEJ,* vol. 8, pp. 114-123, 2003.

[50] H. Kramers and J. Broeder, "Thermal diffusion as a method for the analysis of hydrocarbon oils," *Anal. Chim. Acta.,* vol. 2, pp. 687-692, 1948.

[51] K. H. and J. Broeder, "Thermal diffusion as a method for the analysis of hydrocarbon oils," *Analytica Chimica Acta,* vol. 2, pp. 687-692, 1948.

[52] G. Galliéro, "thermodiffusion dans les fluides de LENNARD-JONES par dynamique moleculaire," 2003.

[53] S. Srinivasan and M. Z. Saghir, "Experimental approaches to study thermodiffusion - Areview," *InternationalJournalofThermalSciences,* vol. 50, pp. 1125-1137, 2011.

[54] H. Davarzani, "Déterminations Théorique et Expérimentale des Coefficients de Diffusion et de Thermodiffusion en Milieu Poreux," Toulouse, 2010.

[55] K. Kokugan, N. Ishizaka and M. Shimizu, *A new method for measuring thermal diffusion factor of gas mixtures,* vol. 7, Tokyo, 1974, pp. 467-469.

[56] M. Lorenz and A. H. Emery, "The packed thermodiffusion column," *Chemical Engineering Science,* vol. 11, p. 16–23, 1959.

[57] W. Furry, R. Jones and L. Onsager, "On the theory of isotope separation by thermal diffusion," *Phys Rev,* vol. 55, no. 11, p. 1083–1095, 1939.

[58] V. Shevtsovaa, D. Melnikov, . J. C. Legros, Y. Yan, Z. Saghir, T. Lyubimova, G. Sedelnikov and B. Roux, "Influence of vibrations on thermodiffusion in binary mixture: A benchmark of numerical solutions," *Physics of Fluids,* vol. 19, no. 1, pp. 017111/1-15, 2007.

[59] S. Wiegand, "Thermal diffusion in liquid mixtures and polymer solutions," *J. Phys: Cond. Matter,* vol. 16, pp. 357-379, 2004.

[60] M. Sahimi, Flow and Transport in Porous Media and Fractured Rock, Second Edition ed., University of Southern California: WILEY-VCH, 2011, p. 701.

[61] P. W. J. Glover, "Petrophysics MSc Course Notes, Permeability," university of Aberdeen , UK, 2000.

[62] M. Kaviany, principles of heat transfer in porous media, Springer, 1995.

[63] S. Ergun, "Fluid flow through packed columns," *Chem. Eng. Progr.,* vol. 48, pp. 88-94, 1952.

[64] S. A. Bories, Fragment de description de la physique des transferts thermiques dans le sous – sol, vol. 3, La Houille Blanche, 1985, pp. 312-219.

[65] D. Sangare, J.-F. Thovert and P. Adler, "Macroscopic properties of fractured porous media," *Physica A: Statistical Mechanics and its Applications,* vol. 398, no. 5, p. 921–935, 2010.

[66] P. M. Adler, J.-F. Thovert and V. V. Mourzenko, "The geometry of a single fracture," in *Fractured Porous Media*, P. M. Adler, J. Thovert and V. V. Mourzenko, Eds., Oxford University Press, 2012.

[67] I. Berre, F. Doster and E. Keilegavlen, "Flow in Fractured Porous Media: A Review of Conceptual Models and Discretization Approaches," *Transport in Porous Media,* vol. 130, p. 215–236, 2019.

[68] R. Haase, "Thermodynamics of Irreversible processes, Chapter 4," Addison Wesley, London, 1969.

[69] W. M. Rutherford and j. G. Roof, "thermal diffusion in methane-n-butane mixture in the critical region," *Chem,* no. 63, p. 1506, 1959.

[70] K. Shukla and A. Firoozabadi , "A New Model of Thermal Diffusion Coefficients in Binary Hydrocarbon Mixtures," *Ind. Engrg. Chem. Res.,* vol. 37, pp. 3331-3342, 1998.

[71] L. J. Kempers, "A thermodynamic theory of the Soret effect in a multicomponent liquid," *The Journal of Chemical Physics,* vol. 90, no. 11, pp. 6541-6548, 1989.

[72] M. Khawaja, *Molecular and Thermal Diffusion Coefficients Of n-Dodecane, Isobutylbenzene and Tetrahydronaphtalene Hydrocarbon Mixtures in Porous Media.,* Toronto: Ryerson University, 2005.

[73] J. Charles-Guobing, "modeling of thermo-solutal convection in porous media," Toronto, 2005.

[74] A. Firoozabadi, K. Ghorayeb and k. Shukla, "Theoretical Model of Thermal Diffusion Factors in Multicomponent Mixtures," *AIChE,* vol. 46, no. 5, pp. 892-900, 2000.

[75] S. R. De Groot and P. Mazur, Non-equilibrium thermodynamics, North Holland, 1962.

[76] A. Khadiri, A. Amahmid, M. Hasnaoui and A. and Rtibi, "Soret Effect on Double-Diffusive Convection in a Square Cavity Heated and Salted from Below," *Numerical Heat Transfer, Part A,* vol. 57, pp. 848-868, 2010.

[77] B. Goyeau, J. P. Songbe and D. Gobin, "Numerical Study of Double-Diffusive Natural Convection in a Porous Cavity using the Darcy–Brinkman Formulation," *Int. J. Heat Mass Transfer,* vol. 39, p. 1363–1378, 1996.

[78] B. El Hajjar, "sur le couplage thermodiffusion-convection: séparation et instabilités induites par de nouvelles configurations géométriques et thermiques," (IMFT) Toulouse, 2008.

[79] P. Costesèque, D. Fargue and P. Jamet, "Thermodiffusion in Porous Media and Its Consequences," in *Thermal Nonequilibrium Phenomena in Fluid Mixtures. Lecture Notes in Physics*, vol. 584, Berlin, Heidelberg, Springer, 2002, p. 389–427.

[80] Z. Wang and a. Xuzhou, *Thermophoresis of synthetic and biological systems,* University of Cologne, 2014.

ملخص

في هذه الدراسة، تم تحليل تأثير الكسر المنفرد على الحمل الحراري المتداخل مع تأثير Soret في تجويف مسامي عمودي ثنائي الأبعاد، مشبع بمزيج ثنائي تم تسخينه وتغذيته من الجهة اليمنى.

أظهرت النتائج الرئيسية أن الصدع يمكن أن يؤثر بشكل كبير على التدفق الجاذبي-الحراري وقد يلعب دورًا إيجابيًا في الفصل الناجم عن تأثير Soret، خاصةً عندما تكون السماحية **k** أقل من السماحية المثالية $\mathbf{k_{opt}}$. أما عندما تكون السماحية **k** أكبر أو تساوي $\mathbf{k_{opt}}$، فإن تأثير الصدع يكون سلبي على عملية الفصل. علاوة على ذلك، فإن الصدع المائل إلى الجدار البارد يسبب انفصالًا كبيرًا مقارنةً بالحالة عندما يتم إمالة الصدع إلى الجدار الساخن بنفس الزاوية. نتيجة لذلك، يمكن تحسين عملية الفصل بشكل كبير.

الكلمات المفتاحية: تأثير Soret ، الحمل الحراري ، وسائط مسامية ، صدع ، غير متجانس، فصل.

Abstract

In this study, the effect of a single discrete fracture on the thermo-solutal convection coupled with Soret effect in a two-dimensional vertical porous cavity, saturated by a binary mixture, heated and salted from the right-end have been analyzed.

The main results show that the fracture can greatly affect the behavior of the thermo-gravitational flow and might play a positive role to the separation caused by the Soret effect, especially when the permeability **k** is below the optimal permeability $\mathbf{k_{opt}}$. However, when the permeability **k** is greater or equal to the optimal $\mathbf{k_{opt}}$, the fracture affects negatively the separation process. Furthermore, the fracture tilted to the cold wall causes a large separation compared to the case when the fracture is tilted to the hot wall with the same angle. As a result, the separation process could be greatly improved.

Keywords: Soret effect, thermodiffusion, porous media, fracture, heteroginious, separation.

Résumé

Dans cette étude, nous avons analysé l'effet d'une fracture discrète sur la convection thermo-solutale, associé à l'effet Soret, dans une cavité poreuse verticale bidimensional, saturée par un mélange binaire, chauffée et alimentée du côté droit.

Les principaux résultats montrent que la fracture peut grandement affecter le comportement du flux thermo-gravitationnel et peut jouer un rôle positif dans la séparation provoquée par l'effet Soret, notamment lorsque la perméabilité **k** est inférieure à la perméabilité optimale **kopt**. Cependant, lorsque la perméabilité **k** est supérieure ou égale au **kopt** optimal, la fracture affecte négativement le processus de séparation. En outre, la fracture inclinée à la paroi froide provoque une séparation importante par rapport au cas où la fracture est inclinée à la paroi chaude avec le même angle. En conséquence, le processus de séparation pourrait être grandement amélioré.

Mots clés: Effet Soret, thermodiffusion, milieux poreux, fracture, hétérogène, séparation.